ABSTRACT

Title of Dissertation: NONLINEAR SPIN DYNAMICS AND

ULTRA-FAST PRECESSIONAL SWITCHING

Mihai Dimian, Doctor of Philosophy, 2005

Dissertation directed by: Professor Isaak D. Mayergoyz
Department of Electrical and Computer Engineering

This thesis is intended to provide a theoretical analysis of magnetization dynamics in nanometer scale structures over picosecond time scales. This research has been motivated by promising technological applications in the area of magnetic data storage, as well as by pure scientific quest for ultra-fast spin dynamics in nanostructures.

The present paradigm of magnetic data storage is approaching its fundamental limits for areal storage density, as well as for speed in data processing. As a result, there is an urgent need for reliable alternatives to current magnetic recording media, which are based on longitudinal thin film, and to the conventional mechanism of magnetization reversal, based on damping switching. In this dissertation, faster modes of magnetization reversals, using precessional magnetization motion, are analyzed in traditional longitudinal media and in its promising alternatives: perpendicular and patterned media. This analysis uses multi-spin description of

magnetic nanoparticles and continuum micromagnetics for thin film media. The spins dynamics in both discrete and continuum versions is modeled by Landau Lifshitz type equations. These models are introduced in Chapter 2, subsequent to an overview of magnetic recording media offered in Chapter 1.

The analytical study of precessional switching in perpendicular thin film media is presented in Chapter 3. The features of precessional magnetization switching and conventional magnetization reversal are compared, and the design of magnetic field pulses that guarantee precessional switching is discussed. In Chapter 4, the study of precessional magnetization switching in longitudinal thin film media is undertaken. After a short summary of the research studies on this topic, the inverse problem approach to the analysis of precessional switching in these media is presented. This approach leads to explicit expressions for the magnetic field pulses that guarantee the precessional switching.

The study of surface anisotropy effects on magnetization reversals in nanoparticles is presented in Chapter 5. The expressions for critical magnetic fields that guarantee the quasi-static and precessional reversals are analytically derived for the case of very strong exchange and weak surface anisotropy. These analytical results are also used to test the numerical approach, which is applied to the general case of the problem.

NONLINEAR SPIN DYNAMICS AND

ULTRA-FAST PRECESSIONAL SWITCHING

by

Mihai Dimian

Dissertation submitted to the Faculty of the Graduate School of the
University of Maryland, College Park in partial fulfillment
of the requirements for the degree of
Doctor of Philosophy
2005

Advisory Committee:

Professor Isaak D. Mayergoyz, Chair
Professor Edward Ott
Professor Perinkulam S. Krishnaprasad
Professor Howard C. Elman
Professor Raymond L. Johnson

DEDICATION

To my loving parents

and

to my lovely fiancée

ACKNOWLEDGEMENTS

I would like to thank Professor Isaak D. Mayergoyz for being my guarding angel on the road to discovery, as well as for helping me understand the subtle relation between research and teaching, as two perspectives on the same educational unit.

I am thankful to my collaborators, Doctors Giorgio Bertotti, Claudio Serpico, and Hamid Kachkachi for sharing their experiences and ideas, as well as for encouraging me during this project.

I would also like to thank the members of my dissertation defense committee, Professors Isaak D. Mayergoyz, Edward Ott, Perinkulam S. Krishnaprasad, Howard C. Elman, and Raymond L. Johnson for their time and effort spent in reviewing my dissertation.

I feel very fortunate to have great friends who are a permanent source of extraordinary enjoyment and inestimable help. I am grateful to all of them and express my regrets to those with whom I could not share the same sunny sky.

I also express my gratitude to the faculty members of the University of Maryland and the University of Romania who directly contributed to my scientific and engineering education.

After these years of doctoral studies, I rather think of myself as "infested" with science than a potential doctor of it.

College Park, March 2005

Mihai Dimian

TABLE OF CONTENTS

LIST OF TABLES

LIST OF FIGURES

1. Introduction

"To see a world in a grain of sand,

And a heaven in a wild flower,

Hold infinity in the palm of your hand,

And eternity in an hour."

Auguries of Innocence, William Blake

This thesis is intended to provide a theoretical analysis of magnetization dynamics in nanometer scale magnetic structures over picosecond time scales. This research has been motivated by promising technological applications in the area of magnetic data storage, as well as by pure scientific quest for ultra-fast spin dynamics in nanostructures.

The prevalent objectives in data storage technology are to increase the storage capacity in memory devices and to decrease the access time to any given bit inside the device. It is apparent that these two objectives cannot be optimized simultaneously, and for any specific application a trade-off should be accepted. For example, terabit capacities are correlated with millisecond access times in hard-disk drives (HDD) [1-4], while megabit capacities are correlated with ten-nanosecond access times in magnetoresitive random access memories (MRAM) [5-8].

The evolution of data storage technology has been impressive since 1955, when IBM built the first hard disk drive featuring a storage capacity of 5MB with areal recording density of 2 kbit/in^2. The barrier of 100 Gbit/in^2 has already been passed in 2002 and demonstrations with area recording densities as high as 1 Tbit/in^2 are

expected. It is apparent from these data that the storage of an information bit is related to nanometer scale magnetic thin film structures. Moreover, magnetic patterned media with a single-bit-per-island recording methodology have also been considered as recording media and have successfully passed preliminary tests [9-10]. These patterned media use nanoparticles with diameters from 3 to 12 nanometers. In addition to the interest in the areal storage densities, a special emphasis is placed on the data rate of the disk drive, which is also continuously increasing at a fast pace. The current disk drives operate at a maximum internal data transfer rate of approximately 130 MB/s, which corresponds to a channel data rate of 1.17 Gbit/s (using an 8/9 modulation code). Therefore, the writing time for a single bit, or equivalently the magnetization reversal time in a bit nanostructure cell, is below 1 ns.

Another tremendous research effort in the magnetic data storage has been devoted in the recent years to magnetoresistive random access memory. MRAM has the potential to store data at a high density, to access them with a high speed, and to be a low power consumer [6]. Once the performances in these directions become comparable with the ones of the semiconductors based memory, the nonvolatility property could determine the use of MRAM as a 'universal memory'. In 2004, Infineon Technology and IBM have produced the first 16 MB MRAM chip with read and write cycles less than 30 ns. The most common design for MRAM uses a magnetic tunnel junction: two ferromagnetic thin films play the role of electrodes and a thin tunneling barrier separates them. The resistance of the tunneling junction is significantly modified as the magnetic moments of the ferromagnetic layers change their relative orientation. The difference in junction resistances corresponding to the

stable parallel and anti-parallel orientations, respectively, makes possible the definition of the binary memory states (see Section 1.1). The ferromagnetic thin films electrodes have nanometer dimensions and the magnetization reversal time in these devices is in nanosecond regime. In conclusion, the understanding and controlling the behavior of magnetic nanoparticles and nanostructures over picosecond time scales are of great present and future interest in the hard disk drive area, as well as in MRAM technology.

The traditional mechanism of magnetization reversal (so called *damping* switching) is in nanosecond regime. In principle, this reversal time can be reduced to picosecond regime by applying higher writing magnetic fields. However, the modern write poles are approaching their maximum achievable writing field. In addition, the increase of storage density is done with the cost of increasing the anisotropy field in order to meet the requirements for long-term stability of the stored bit (see Section 1.1). Since the reversal time is actually proportional with the difference between the writing field and the anisotropy field, a trade-off problem appears between the storage density and the reversal time. In conclusion, there is an urgent need for much faster modes of reversals in order to match the demand for speed in data processing, both in HDD and MRAM. A promising idea in this direction is to exploit fast precessional magnetization dynamics, which belongs to picosecond regime (*precessional* switching) [11-13].

In this thesis, the study of precessional switching is the *Ariadne's thread* that will guide us through the labyrinth of nonlinear spin dynamics in magnetic nanostructures.

1.1. Overview of the magnetic recording media: present and promises

In this section, we review a few fundamental aspects of the traditional magnetic recording media and analyze novel architectures that are or promise to become alternative solutions to the current media. Some of these discussions will be extended in the next chapters according to the specific topic of each chapter.

The evolution of the data storage technology in the last fifty years can be framed into one paradigm, namely the longitudinal recording. In the longitudinal recording, the magnetization lies in the plane of the recording media and it is flipped between the two stable orientations along the head-medium motion. The recording process is sketched in Figure 1.1. The writing head is composed of a soft magnetic circuit (yoke) and a wire winding around it connected to a signal current source. When a current passes through the wire, the yoke is magnetized and a fringing magnetic field appears from the gap. The appropriate choice of the current leads to a magnetic field orientated opposite to the cell magnetization, high enough to switch the magnetization orientation. Afterward, either the recoding medium (in tape, floppy disk) or the write-head (in HDD) is moving, and another layer cell is written, if necessary. The reading process in the longitudinal recording is based on sensing the gradient of the magnetic field created by the recording layer at the transition between two opposite magnetized cells. Thus, the existence of opposite magnetization states in two adjacent cells is translated into digit 1, while the absence of such transition is interpreted as 0. The read-head is either similar to the description of the write-head, or it has a spin valves sensor based on giant magnetoresistive effect [14].
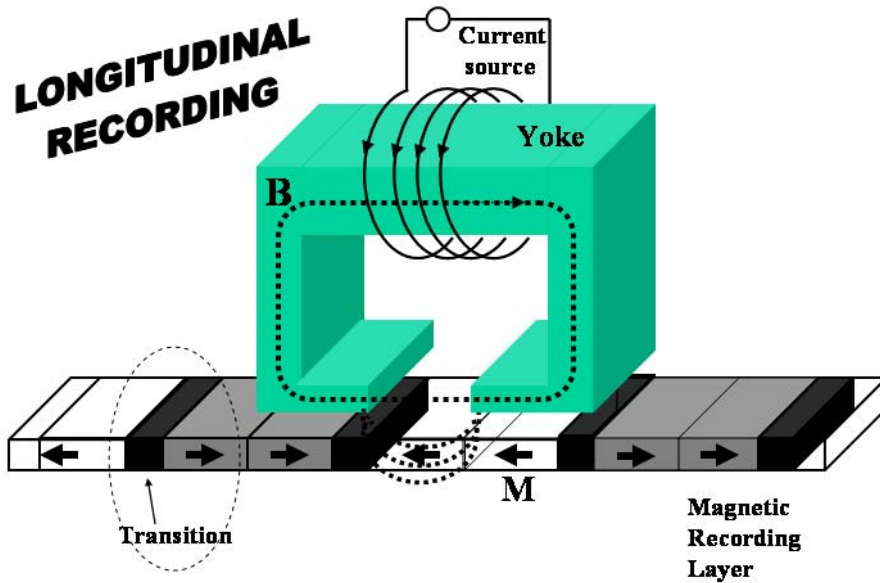
Figure 1.1: Schematic representation of a typical longitudinal recording system, including a ring head and a magnetic recording layer.

(a)

(b)
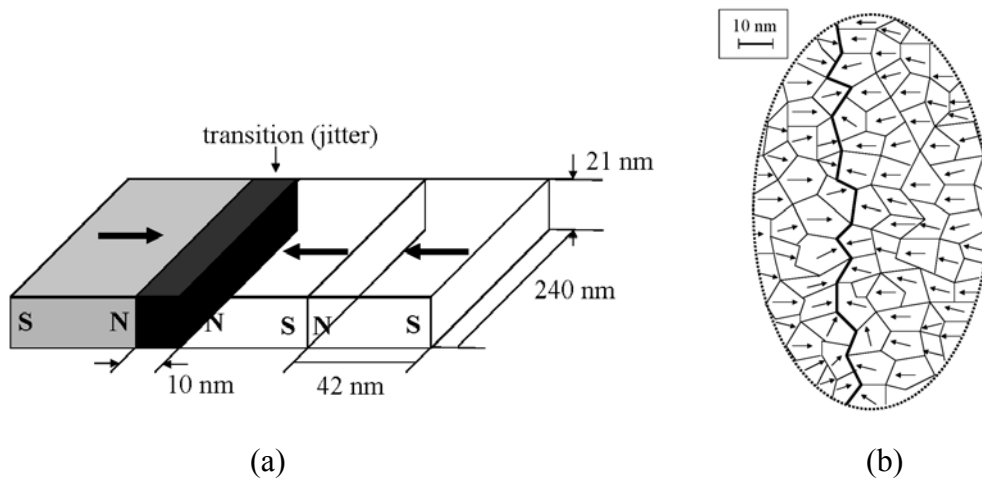
Figure 1.2: (a) Schematic representation of written tracks in a thin film media with 63 Gb/in^2 storage density. (b) A typical zigzag shape transition between cells magnetized in opposite directions.

Regarding the magnetic layers used in the previously described recording process, there are two possible structures: particulate and thin film media. The former have a discrete structure and are generally composed of ferri or ferromagnetic oxide particles deposited on a rigid or flexible substrate. The particles are usually aciculate (which leads to a pronounced shape anisotropy), with the length between 200 and 700 nm and a thickness 5-7 times smaller, and have uniaxial magnetocrystaline anisotropy constant K_u varying from 1-100 kJ/m^3 depending on the chemical composition. The particulate media are used in tapes, floppy disks, and zip disks. The thin film medium has a continuous granular structure (see Figure 1.2 (b)) and consists of Co-alloy sputtered on a suitable growth enhancing underlayer. The *grain* diameter can go as low as a few nanometers and the magnetic anisotropy is mainly of crystalline origin with anisotropy constant K_u varying from 0.1-10 MJ/m^3. The small grain size and the continuous structure (packing factor is almost 100%, while in particulate media it is between 25 and 40%) make them appropriate to high density storage. Thin film media replaced the particulate media in hard disk drives in early 1990's and had been the main contributor to the swift increase in the hard disk drives performances over the last decade.

The basic physical principle along this evolutionary path was the scaling law of the magnetostatic problems: Maxwell equations for magnetostatic case are invariant to the scaling of spatial dimensions by a factor f, as long as current densities are scaled by $1/f$ (or equivalently, the current intensities are scaled by f). Thus, the magnetic field configuration and magnitudes remain unchanged, and the main challenge is to maintain the magnetic properties of the materials at smaller

dimensions. It is clear that this principle is only an ideal representation of the real situation and consequently, there are many other technological or scientific problems to be solved for a successful scaling procedure [15]. Nevertheless, this principle has been successfully implemented for the last fifty years without fundamental changes of magnetic recording paradigm. Next, we intend to analyze if this development process can be successfully continued or it is obstructed by some fundamental limits related to the preservation of the magnetic properties of the materials at smaller scales.

It is probably common to imagine a recording layer as a collection of magnetic particles or grains, each one of them containing a bit of information. However, the reality is far more complicated: a single memory cell has to contain a few hundreds particles or grains and the bit of information is actually stored in the magnetic field gradient at the transition between two adjacent cells. This situation is mostly due to the limited technological capabilities of creating uniform size magnetic particles and assembling them in a periodic structure. Nevertheless, with the recent advances in nanotechnology, these limitations might be overcome and it is most likely that data storage will be based on a single bit per nanoparticle technology in the future. The costs of manufacturing them on a large scale and implementing new write-read technologies are still much higher than the ones in particulate and thin film magnetic media [16], and consequently, the latter will still be dominating the magnetic data storage industry in the next few years.

The existing HDDs provide a recording areal density of 20-40 Gb/in^2 and, as we mentioned above, 100-200 Gb/in^2 have been achieved in various research laboratories [17-19]. In Figure 1.2 we present a schematic geometrical configuration for a thin

film used in Read-Rite Corporation Laboratories to obtain a density of 63 Gb/in^2 [17]. Each cell contains about 200 grains, with an average grain diameter of approximately 10 nm. The nonuniformity of the grains, as well as their random locations with respect to cell boundaries lead to the zigzag shape of the transition between the cells, as it is illustrated in Figure 1.2 (b). This nonuniform transition between cells leads to nonuniformities in the field gradient, which generates disturbances in the signal produced by the reading sensor. This is the main source of noise due to the magnetic layer in the magnetic recording. An acceptable signal-to-noise ratio requires at least hundreds of grains in a memory cell. It is now clear that the scaling procedure for higher storage densities also requires scaling the magnetic grains forming the memory cell. As we will see in a subsequent discussion, the further decrease in the grains dimension encounters fundamental limitations due to the thermal perturbations that affect the stability of the grain magnetization orientation.

The behavior of the grains magnetic moments under the applied magnetic field is affected by: exchange interactions, which favor the parallel alignment of the neighboring moments; dipole-dipole interactions, which lead to a demagnetizing field that forces the magnetic moments of the grains to lie in the thin film plane; and the magnetocrystalline uniaxial anisotropy that favors the magnetization orientation along easy anisotropy axis. By using a nonmagnetic alloy to separate the grains, the exchange interactions between the grains are significantly reduced. As a result, the thin film medium acts as a collection of partially independent magnetic particles with random easy anisotropy axes subject to a strong demagnetizing field that forces magnetic moments to lie in the thin film plane. Although the randomness of the easy

axes is not a desirable property of the recording media, it is technologically difficult to grow thin films with grains magnetic anisotropy axis tangent to the circular track. The qualitative behavior of a memory cell magnetization during the reversal process produced by a *slowly* varying applied field is illustrated in Figure 1.3 (the external field varies "slowly" as compared to the magnetization relaxation). The characteristic quantities of the magnetization curve are: remanent magnetization M_r (the cell magnetization after the field is switched off), coercive field H_c (the value of the applied field at which magnetization crosses zero), and saturation magnetization M_s (the maximum value of the magnetization cell, which corresponds to the perfect alignment of the grains magnetic moments along the applied field direction).
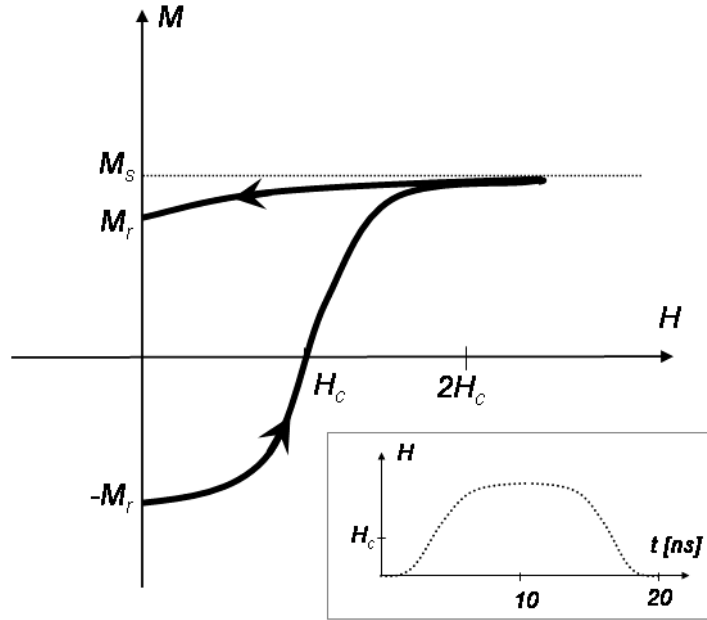
Figure 1.3: Conventional magnetization reversal curve produced by a *slowly* varying applied magnetic field. A typical variation of the external applied field is presented in the lower right corner.

9

Let us remark that if all easy axes of the grains were oriented along the track then the corresponding magnetic curve would have a rectangular shape with $M_r=M_s$, while in the case of non-interacting grains with randomly oriented easy axis the magnetization evolution would have a more curved shape with $M_r=(1/2)M_s$. The compromise between the randomness of the anisotropy axis and the interactions between grains leads to the behavior presented in the Figure with the remanent magnetization usually related to the saturation magnetization be a factor of 0.8-0.85. On the other hand, coercive field H_c of the magnetic layer is related to the magnetocrytalline anisotropy field ($=2K_u/\mu_0 M_s$) and the shape anisotropy of the grains, but it is also greatly affected by extrinsic effects such as film stress or thin film surface. The relation between coercive and anisotropy fields varies from one case to another and raises many controversies due to the discrepancy between the experimental results and theoretical predictions [20].

Next, we will focus on the behavior of a single grain inside the assembly, rather than the assembly as a whole. For the sake of discussion, let us consider a magnetic nanoparticle of spherical shape. According to the fundamental theorem of fine-ferromagnetic-particle theory proved by Brown [21], there is a critical diameter, below which the nanoparticle is uniformly magnetized and the magnetization reversal occurs by uniform mode. For somewhat larger ones, nonlinear reversal modes (such as curling mode and buckling mode) are expected but the particle can still be considered as a monodomain; for even larger samples the magnetization has a multi-domain structure and magnetization reversal may occur via domain wall propagation process [21, 22]. The numerical and experimental results published over the last

decade in this area [23]-[25] have partially confirmed this scenario. The large majority of grains in magnetic layers with storage densities above 20 Gb/in^2 have diameters below 20nm. Since the critical diameter for a cobalt sphere is above 20nm (analytical calculations [26] lead to a critical diameter equal to 23.4 nm), we can conclude that each grain behaves as a magnetic monodomain and the magnetization rotates in unison across the grain.

The basic principles of the quasi-static magnetization reversals in single magnetic domain particles can be found in the seminal works of Stoner and Wohlfarth [27], and Neel [28] in late 1940's. This physical system exhibits multiple metastable states. The magnetization can persist in a metastable state for some time, but thermal perturbations may drive it to other metastable states. As it is presented in Figure 1.4, the energy of uniaxial anisotropy magnetic particle has two minima and the magnetization orientation lies initially into one energy minimum.
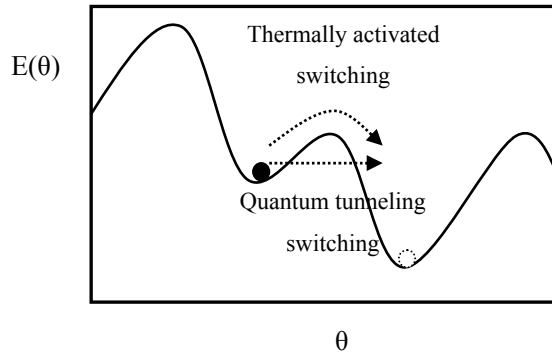
Figure 1.4: Energy variation as a function of angle θ between the direction of magnetization and easy anisotropy axis. The dotted lines represent different mechanisms of switching in the presence of an energy barrier.

The energy barrier for the magnetization reversal of an isolated spherical grain in the absence of the applied field is simply given by:

$$\Delta E = K_u V, \tag{1.1}$$

where K_u is the magnetocrystalline anisotropy constant, and V is the volume of the nanoparticle. According to the Arrhennius-Neel law [3, 28], the mean time for the thermally activated magnetization reversal (so called *superparamagnetic effect*) to occur can be expressed in the following form:

$$\tau = \tau_0 \exp\left(\frac{\Delta E}{k_B T}\right), \tag{1.2}$$

where $k_B \sim 1.38 \times 10^{-23}$ m²kg/(s²K) is the Boltzmann's constant, T is the absolute temperature of the system, and the constant τ_0 is on the order of nanosecond. It is apparent now that the condition of the stability for the recording media can be translated in a condition for the energy barrier between the energy minima. Consequently, in order to assure the magnetization orientation stability for a longer time than τ, the diameter of the nanoparticle should satisfy the following condition:

$$d > \sqrt[3]{\frac{6 k_B T \ln(\tau/\tau_0)}{\pi K_u}}. \tag{1.3}$$

Since the reliability of the hard disk drives requires a time τ larger than 10 years, the previous condition gives $d>9$nm, when the anisotropy constant K_u=0.5 MJ/m³ (for cobalt) and temperature T=350 K are considered. As we mentioned above and it is represented in Figure 1.2, the average nanoparticle diameter in thin film layer with 63Gb/in² storage density is approximately 10 nm. In conclusion, the superparamagnetic effect imposes a fundamental limit to the scaling principle.

The previous analysis of superparamagnetic limit was done for an isolated spherical grain. As we mentioned above, the grain is actually part of a thin film medium and consequently, it senses the interactions with other grains of the assembly. In addition, variations from the spherical shape, as well as from the chemical composition of the grain are involved in a real thin film. These facts make the study of thermal effects a much more complex problem. There exist a few recent attempts to offer a more appropriate description of these limits (see [29-31]). However, the final results are not essentially different from the ones computed using formula (1.3), and the corrections mainly contribute to the increase in the critical diameter making the superparamagnetic problem even more critical. In conclusion, the traditional magnetic recording procedures, as well as the improving principle, seem to reach their own saturation. In spite of these fundamental difficulties, it is too early to predict the "death" of magnetic recording as it has been suggested in the last years. There exist numerous less-explored paths that can provide alternative solutions to overcome these limitations.

One of the simplest ideas to overcome the current superparamagnetic limit is revealed in formula (1.3). By using magnetic materials with higher anisotropy constant K_u, the critical radius can be reduced. It has been showed in [9] and [32] that a specially prepared FePt and CoPt alloys, respectively, possess anisotropy constants up to one order of magnitude higher than the ones currently in use. Another direction is to improve the signal-to-noise characteristics of the recording media and, consequently, the total number of grains required in each memory cell can be decreased. A solution in this direction is to grow thin film with grains anisotropy axis

oriented as close as possible along the track. A measure of this feature is given by the orientation ratio $OR = M_r / M_{r\perp}$, where M_r and $M_{r\perp}$ represent the remanent magnetization along and perpendicular to the track, respectively. The current media have a random distribution of the easy axis that leads to an orientation factor close to one. Highly oriented media have been reported in the last three years and used to achieve recording densities of 100-200 Gb/in^2 [19, 33].

The solutions for further improving storage density can also be found outside the current paradigm of magnetic storage that uses longitudinal recording. Thus, the perpendicular oriented media have been introduced in HDDs since 2004, and they are expected to push areal densities beyond 1Tb/in^2 in the next few years. Although these media have been studied for more than thirty years, the cost of implementing them was not justified as long as the longitudinal media were developing at a very fast pace and a low cost. A perpendicular recording system is sketched in Figure 1.5.

As opposed to the longitudinal recording, the magnetization stands perpendicular to the thin film plane. This situation is realized using materials with high anisotropy constants K_u (such as cobalt) in combination with other metals (for example, chromium) that reduce the saturation magnetization M_s while keeping relatively stables the easy-axis and the anisotropy constant. As a result, the anisotropy field (proportional to K_s) becomes greater than the demagnetizing field (proportional to M_s) and consequently, the orientation perpendicular to the thin film plane is favorable for the magnetization [34-36]. The write field is generated by a single pole head and a soft magnetic underlayer located below the recording layer. The soft magnetic underlayer "creates" a mirror image of the recording head.

14
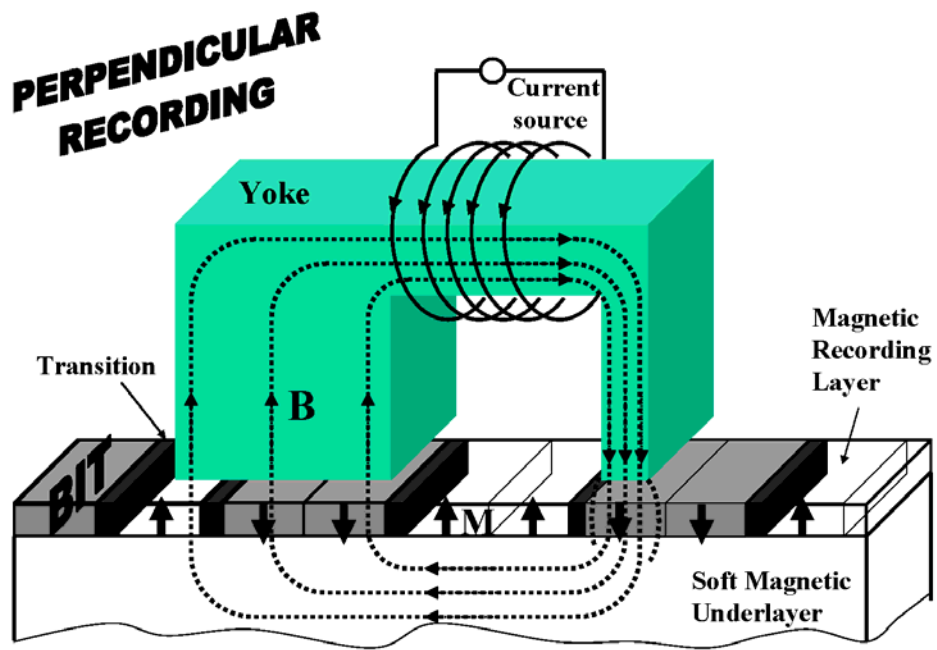
Figure 1.5: Schematic representation of a typical perpendicular recording system, including a single-pole head, a magnetic recording layer, and a soft magnetic underlayer.
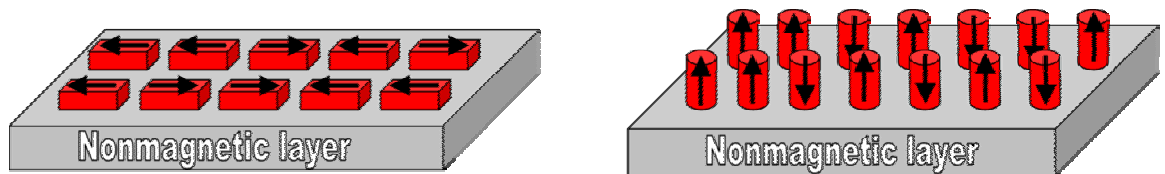
Figure 1.6: Schematic representation of longitudinal (left) and perpendicular (right) patterned media.

Consequently, the magnetic recording layer is situated in the gap formed by the real pole and its mirror image. As opposed to longitudinal recording, which is performed by the fringing fields emanating from the gap region between the write-poles of a conventional ring-type head (see Figure 1.1), the writing field for perpendicular recording is the magnetic field created in the gap. This observation reveals an immediate advantage of the perpendicular recording over the longitudinal one: the upper limit of the writing gap field (given by $4\pi M_s$) is two times higher than the highest achievable with fringing field (given by $2\pi M_s$). As a consequence, higher write fields allow using magnetic materials with higher anisotropy constants, which decrease the critical diameter (1.3) required for thermal stability. Moreover, the perpendicular recording also benefits from its naturally high orientation ratio, which allows reliable signal-to-noise ratio in the condition of a smaller number of grains per memory cell (recall the previous discussion of the orientation ratio for the case of longitudinal media). In addition, a key advantage of perpendicular over the longitudinal one is the behavior of the demagnetizing field at high density. While in longitudinal media the demagnetizing fields destabilize the domain structures at high densities, in perpendicular media the demagnetizing field improves the bit pattern stability. In conclusion, the perpendicular recording offers many advantages over traditional longitudinal recording but, in order to fully benefit from this potential, further improvements are needed.

Magnetic patterned media with a single-bit-per-island recording methodology have also been considered as possible solutions to overcome the superparamagnetic limit encountered by the current longitudinal thin film media. A schematic

representation of these media is presented in Figure 1.6. These patterned media use nanoparticles with diameters from 3 to 12 nanometers. In contrast to thin film media that use hundreds of nanograins to store a bit of information, the patterned media use only one nanoparticle for this purpose. However, there exist many technological challenges to manufacture uniformly size magnetic particles and assemble them in a periodic structure, at a low cost [16]. Apart from the fabrication problem, there is a major difficulty of synchronizing the write pulse to the bit pattern, as compared to the thin film media, where slight variations in write head speed are permissible [37].

In addition to the strong interest in the hard disk drive development, a tremendous research effort in magnetic data storage industry has been devoted to the magnetoresistive random access memory over the last five years. A schematic representation of a memory cell in the MRAM is presented in Figure 1.7. Each memory cell has a submicron multilayer magnetic structure formed by: an antiferomagnetic layer at the bottom, an artificial antiferromagnetic layer in the middle with the direction of magnetization fixed (so-called pined layer), a soft ferromagnetic layer on the top that has the magnetization moving freely (so called free layer), and a tunneling insulating barrier between the free and pined layer. This magnetic structure is connected to two electrodes (top and bottom electrodes) used for read process. In addition, another electric track is located at the bottom (write word line) and it is used for the writing process. The free magnetic layer has two equilibrium positions ("left" and "right"), which correspond to the data values "1" and "0". The writing and reading processes are quite different from the one in HDD and are described in the next paragraph.
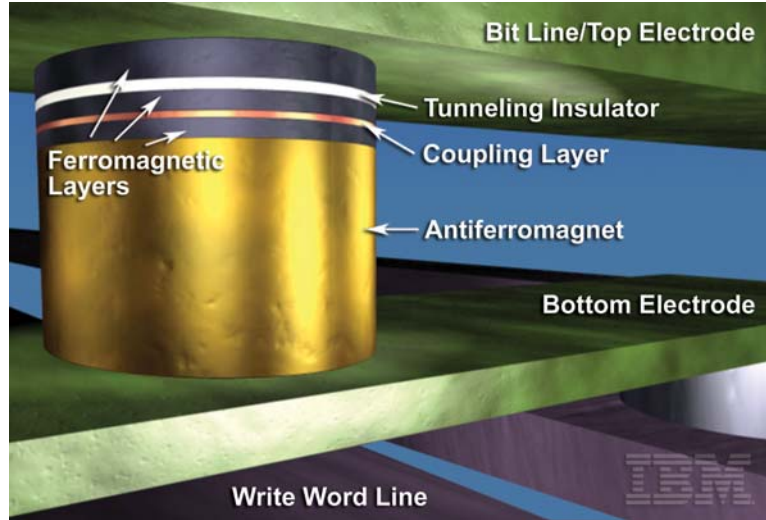
Figure 1.7: Schematic representation of a MRAM cell: the magnetic multilayer structure, the top and bottom electrodes, and the write word line.

In order to explain the writing process, let us denote by y the direction of write word line and by x the bit line direction. When a current is flowing through the write word line a magnetic field is created in the x direction. This field is sensed by all magnetic cells situated on that word line, but is not high enough to switch the magnetization of the free layer in any one of them. An analog situation occurs when an additional current is sent trough the bit line creating a magnetic field in the y direction. However, the superposition of these two fields, mainly concentrated on the cell located at the intersection of the bit and write-word lines, has enough amplitude to switch the magnetization of the free layer belonging to the discussed cell. The resistance of the tunneling junction is significantly modified as the magnetic moments of the ferromagnetic layers change their relative orientation. The difference in junction resistances corresponding to the stable parallel and anti-parallel orientations,

respectively, makes possible the definition of the binary memory states. In the reading process, a current is sent from the bottom to the top electrode and a low or high resistance is thus detected, corresponding to the data value "1" or "0", respectively.

The magnetic memory combines high-speed data processing and high storage density with nonvolatility property. The immediate goal of MRAM industry is to replace the current nonvolatile flash memory, which has a much lower operational speed and a higher fabrication cost. The long-term objective is to approach the processing speed of the static random access memory (SRAM) and the density of the dynamic random access memory (DRAM). Once the performances in these directions become comparable with the ones of the semiconductors based memory, the nonvolatility property could determine the use of MRAM as a 'universal memory'. However, both density and speed improvements face fundamental limits similar to the ones discussed in HDD case. Consequently, there is an urgent need for new recording and storage techniques to overcome these limitations.

In this section, a few basic aspects of the traditional magnetic recording media were reviewed and the fundamental limitations to this approach were presented. In addition, novel architectures that are or promise to become alternative solutions to the current longitudinal recording were discussed. In this thesis, the conventional, as well as the alternative recording media are analyzed on ultra-short (picosecond) time scales complementing the traditional studies focused on larger time scales.

1.2. Outline of the ultra-fast magnetization reversal studies

The experimental research in the magnetization dynamics has been essentially limited to the quasi-static range until recently. The situation has been substantially changed by the ongoing development of femtosecond laser technologies that made stroboscopic imaging of the magnetization dynamics in microscopic structures very convenient. In addition, this development has offered the opportunity to create ultrashort magnetic pulses needed for the study of magnetization dynamics on the picosecond time scale.

Freeman *et al.*, from the IBM Research Division, have presented the basic ideas of these techniques and some preliminary results in early 1990's [38-41]. However, the possibility of writing a magnetic pattern into magnetic recording media using ultrashort magnetic pulses was demonstrated using a completely different experimental set-up designed by Siegmann *et al.*, at the Stanford University in 1995 [11]. In this method, the field was produced by an electron beam focused on a few square microns of a perpendicularly oriented film of CoPt. Doyle and He presented a numerical description of these experiments using Landau-Lifshitz equation approach and clarified the precessional origin of this ultrafast magnetization switching [42-43]. In the late 1990's, new experimental results were published and proved to be in quantitative agreement with Landau-Lifshitz equation in macrospin approximation [44-45]. Although beautifully conceived, the method of Siegmann *et al.* requires a special current source, namely the Stanford Linear Accelerator, which rather limits the technological applicability.

In the last five years, many experimental techniques [46-49] have emerged in this area, impelled by the promising applications in HDD and MRAM technologies, each of them having its own advantages and disadvantages (see also monographs [12-13] for extensive discussions). A common idea in these recent developments is to use soft magnetic materials (such as permalloy) for this study. These thin film media are susceptible to switch at much smaller applied magnetic fields as compared to the hard magnetic materials used in the experiments of Siegmann *et al.* Consequently, it is much easier to design technologically realizable magnetic field pulses with reasonable high amplitude and short time duration. However, this condition limits the applicability of these techniques to magnetoresistive random access memories, and do not offer any alternative to the Stanford Linear Accelerator source for the case of hard magnetic materials used in hard disk drives.

The present state of the art in the magnetization reversal area could be best described by the following words: "The foregoing types of pulsed experiments have been the basis of a large proportion of the advances in understanding magnetization reversal, but nevertheless carry with them the sense that one is missing the complete picture." (M.R. Freeman and W.K. Hiebert [13])

In conclusion, a theoretical analysis of spin dynamics in nanometer scale magnetic structure over picosecond time scale is motivated by promising technological applications in the area of magnetic data storage, as well as by pure scientific interest in filling the gaps that exist in understanding ultrafast magnetization reversals in nanostructures.

21

1.3. Dissertation Organization

The remaining part of this dissertation is organized as follows:

In Chapter 2, two phenomenological models of spin dynamics in magnetic materials are presented. In the first section of this chapter, some insights in the origin of the precessional spin motion are offered, and various relaxation mechanisms are discussed. These considerations may suggest some justifications for the Landau-Lifshitz-type equations of multi-spin dynamics and continuum micromagnetics dynamics introduced in the second and third sections, respectively.

The analytical study of precessional switching in perpendicular thin film media is presented in Chapter 3. This study is based on the Landau-Lifshitz equation to describe the magnetization dynamics in these media. The case of the perpendicular media subject to rectangular magnetic field pulses is first analyzed. The features of the precessional magnetization switching and the conventional mechanism of magnetization reversal are compared in the first section. By using integrals of motions and the "unit disk representation" of undamped magnetization dynamics, the expressions for critical field and pulse durations that guarantee precessional magnetization reversals are derived in the second section. This study is extended to non-rectangular magnetic field pulses in the third section, where the inverse problem approach is used to design magnetic field pulses that guarantee precessional switching. This chapter partially replicates the materials published in following forms:

- I. D. Mayergoyz, <u>M. Dimian</u>, G. Bertotti, and C. Serpico, "Critical fields and pulse durations for precessional switching of perpendicular media," to appear in *J. Appl. Phys.*, May 2005.

- I. D. Mayergoyz**,** <u>M. Dimian</u>, G. Bertotti, and C. Serpico, "Inverse problem approach to precessional switching in perpendicular media," to appear in *J. Appl. Phys.*, May 2005.

- G. Bertotti, I. D. Mayergoyz, C. Serpico, and <u>M. Dimian</u>, "Comparison of analytical solutions of Landau-Lifshitz equation for damping and precessional switching," *J. Appl. Phys.*, vol. 93, no. 10, 2003, pp. 6811-6813..

In Chapter 4, the precessional magnetization switching in longitudinal thin film media is discussed. After a short summary of the research studies existent on this topic, the inverse problem approach to the analysis of precessional switching in these media is presented. This approach leads to explicit expressions for the magnetic field pulses that guarantee the precessional switching. The effectiveness of the developed technique is illustrated by examples. This chapter partially replicates the materials published in the following form:

- I. D. Mayergoyz, <u>M. Dimian</u>, G. Bertotti and C. Serpico, "Inverse problem approach to the design of magnetic field pulses for precessional switching," *J. Appl. Phys.*, vol. 95, no. 11, 2004, pp. 7004-7006.

The study of surface anisotropy effects on magnetization reversals in nanoparticles is presented in Chapter 5. The multi-spin dynamics in magnetic

nanoparticles is found by using Landau-Lifshitz equation with the effective field derived from Heisenberg-type Hamiltonian. The expressions for critical magnetic fields that guarantee the quasi-static and precessional reversals are analytically derived for the case of very strong exchange and weak surface anisotropy. These analytical results are also used to test the numerical approach, which is applied to the general case of the problem. The distinct features of the quasi-static and precessional reversals in nanoparticles are examined and their dependence on various parameters of the problem is discussed. This chapter partially replicates the materials published in following forms:

- M. Dimian and I. D. Mayergoyz, "Influence of surface anisotropy on magnetization precessional switching in nanoparticles," to appear in *J. Appl. Phys.*, May 2005.

- H. Kachkachi and M. Dimian, "Hysteretic properties of a magnetic particle with strong surface anisotropy," *Phys. Rev. B*, vol. 66, no. 17, 2002, art. no. 174419.

- M. Dimian and H. Kachkachi, "Effect of surface anisotropy on the hysteretic properties of a magnetic particle" *J. Appl. Phys.*, vol. 91, no 10, 2002, pp. 7625-7627.

Finally, conclusions are drawn in Chapter 6.

2. Landau-Lifshitz equation approach to spin dynamics

> "My work always tried to unite the truth
> with the beautiful, but when I had to choose
> one or the other, I usually chose the
> beautiful."   Herman Weyl [50]

In this chapter, two phenomenological models of spin dynamics in magnetic materials are presented. In the first section, some insights in the origin of the precessional spin motion are offered, and various relaxation mechanisms are discussed. These considerations may suggest some justifications for the Landau-Lifshitz-type equations of multi-spin dynamics and continuum micromagnetics dynamics introduced in the second and third sections, respectively.

The origin of the magnetic properties in various materials has been a fascinating and intense studied topic in the last two centuries. Nevertheless, there is no unitary theory to completely explain the magnetic phenomena in a fundamental manner. On the one hand, the famous theorem of Bohr and van Leeuwen eliminates any possibility of elucidating the magnetic properties of the materials in pure classical terms [51]. On the other hand, the pure quantum theory may offer some qualitative explanations, but its quantitative descriptions of the magnetic experiments fail beyond "simple" cases. Thus, a semi-classical theory of magnetism was constructed, a theory that offers quantitative descriptions of the magnetic materials behavior with the price of some inconsistency. Although it seems discreditable, the situation is somehow similar to the largely accepted case of the Cantor theory of sets used as a foundation

of modern mathematics. Quantum mechanics and Zermelo-Fraenkel system, respectively, are certainly preferable from the consistency point of view, but they are almost impractical for the above mentioned purposes. These circumstances may explain our preference for postulating Landau-Lifshitz-type equations rather than offering long and inconsistent derivations of them starting from fundamental principles.

2.1. Magnetic moment dynamics in uniform magnetic fields

In this section, some insights in the origin of the precessional spin motion are offered and various relaxation dynamics are discussed.

The motion of magnetic moment **M** in a uniform magnetic field, described by its intensity **H,** can be intuitively decomposed into two components: a precessional motion about the direction of the magnetic field and a relaxation motion that tends to orient the magnetic moment along the direction of the field.

First, let us consider the precessional motion, which can be mathematically expressed in the following form:

$$\frac{d\mathbf{M}}{dt} = -\gamma \mathbf{M} \times \mathbf{H} , \qquad (2.1)$$

where $\gamma = \mu_0 \gamma_0$, with $\mu_0 = 4\pi 10^{-7} [H/m]$ is the permeability of the vacuum and γ_0 is a quantity characteristic to the magnetic moment that can be either regarded as a parameter whose value should be found from experiments, or computed considering the physical origin of the magnetic moment. Thus, when the magnetic moment originates from the orbital motion of a particle with mass m_0 and charge q_0 the

absolute value of gyromagnetic ratio $\gamma_0 = g|q_0|/2m_0$, where g is the gyromagnetic factor (g~2 for a free electron).

The equation for the precessional motion can be theoretically justified either on quantum or classical grounds. By considering a "static" particle with spin in a uniform magnetic field, the time evolution for the mean value of the spin operator can be derived using either Schrödinger equation (see [52]) or equivalently, Von Neumann equation (see [53]). On the classical ground, Equation (2.1) can be justified assuming that the magnetic moment arises from a "circular" motion of an electron and using Newton's law for the angular momentum, as well as the relation between the magnetic moment and angular momentum (see [54]). The idea of this classical explanation was first given by Sir Joseph Larmor, and that is why the precessional motion of the magnetic moment about the magnetic field is often called Larmor precession. One may also think of deriving Equation (2.1) from a variational principle. The magnetic moment **M** can be regarded as a "classical top" with principal moments of inertia (0, 0, C), and the Lagrangian formulation of this top case leads to Equation (2.1) (see [22]). However, each one of these derivations contains assumptions (indicated by quotation marks), which are physically inconsistent. Consequently, they cannot be considered as derivations of Equation (2.1), but rather as justifications of this equation. In spite of these difficulties, Larmor precession offers accurate explanations of numerous experiments involving the magnetic moment behavior in a uniform magnetic field, such as nuclear magnetic resonance, paramagnetic and ferromagnetic resonance [54], and magnetization reversals [12-13].

Next, we consider the relaxation motion of the magnetic moment, which can be quantitatively described by adding a dissipative (damping) correction term to Equation (2.1). The "dissipated" energy is actually transformed by various mechanisms into the thermal energy of a system. Although these mechanisms are partially known [55-56], they are too complex to be taken into account in an explicit derivation of the damping correction term at a macroscopic level. In order to describe the experimental results, various phenomenological expressions are employed. Most notable ones were given by Landau and Lifshitz for the description of energy losses in the magnetic domain wall motion in ferromagnetic materials [57], and by Bloch for the description of nuclear magnetic relaxation [58]. Since then, these expressions have been successfully applied to various physical phenomena involving dissipation of the magnetic energy. The Landau-Lifshitz expression is mostly used for the description of various dissipative processes in which the norm of the magnetic moment is conserved, while the Bloch expression is appropriate to complementary cases.

The Landau-Lifshitz expression for the damping term reads:

$$-\frac{\gamma\alpha_L}{M^2}\mathbf{M}\times(\mathbf{M}\times\mathbf{H})\,, \tag{2.2}$$

where α_L is a damping parameter with the dimensionality of the magnetic field, and M is the norm of the magnetic moment $\mathbf{M}$. Nowadays, it is preferred to call dimensionless parameter $\alpha = \alpha_L / M$ as the damping parameter, and this convention is used throughout this thesis. This damping parameter may take a large interval of values depending on the various types of magnetic materials and experiments involved. The experiments involving magnetization reversals in ferromagnetic thin

films and nanoparticles used in magnetic data storage indicate rather small values for the damping parameter on the order of 10^{-3} up to 10^{-1}.

Bloch used the following expression for the damping term:

$$\left(-\frac{m_x}{\tau_2}, -\frac{m_y}{\tau_2}, \frac{m_s - m_z}{\tau_1} \right),$$

(2.3)

where z is the direction of the applied magnetic field, m_s is the magnetization saturation value in the equilibrium state, and the parameters τ_1 and τ_2 account for the relaxation times in the longitudinal (z) and transverse directions, respectively. Since our interest is in magnetization dynamics that conserves the norm of the magnetic moment, we do not extend further the discussion of Bloch equation.

The dissipative term given by formula (2.2) is somehow atypical, in the sense that it cannot be derived in terms of the standard Rayleigh dissipation function. By using the standard Rayleigh function to introduce the dissipative effects in the Lagrangian formulation for the conservative precessional motion, Gilbert [59] derived the following damping term:

$$-\frac{\gamma \alpha_G}{M} \mathbf{M} \times \frac{d\mathbf{M}}{dt},$$

(2.4)

where $\alpha_G > 0$ denotes the Gilbert dimensionless damping parameter.

In conclusion, the general equation of motion for a magnetic moment in homogeneous applied field can be written as:

$$\frac{d\mathbf{M}}{dt} = -\gamma_G \mathbf{M} \times \mathbf{H} - \frac{\gamma_G \alpha_G}{M} \mathbf{M} \times \frac{d\mathbf{M}}{dt},$$

(2.5)

in the Gilbert form, known as Landau-Lifshitz-Gilbert equation. Here, γ_G is identical to γ, but the G index is used for the clarity of future considerations. By using the damping term given by formula (2.2), the equation of motion has the following form:

$$\frac{d\mathbf{M}}{dt} = -\gamma \mathbf{M} \times \mathbf{H} - \frac{\gamma\alpha}{M} \mathbf{M} \times (\mathbf{M} \times \mathbf{H}). \tag{2.6}$$

This equation is known as Landau-Lifshitz equation. It turns out that Equations (2.5) and (2.6) are mathematically equivalent. This fact can be simply proved by evaluating the expression $\mathbf{M} \times \dfrac{d\mathbf{M}}{dt}$ using Equation (2.6). Thus,

$$\begin{aligned}
\mathbf{M} \times \frac{d\mathbf{M}}{dt} &= -\gamma \mathbf{M} \times (\mathbf{M} \times \mathbf{H}) - \frac{\gamma\alpha}{M} \mathbf{M} \times (\mathbf{M} \times (\mathbf{M} \times \mathbf{H})) \\
&= \frac{M}{\alpha} \left[\frac{d\mathbf{M}}{dt} + \gamma \mathbf{M} \times \mathbf{H} \right] + (\gamma\alpha M) \mathbf{M} \times \mathbf{H}
\end{aligned}, \tag{2.7}$$

and by rearranging the terms, one finds:

$$\frac{d\mathbf{M}}{dt} = -\gamma(1+\alpha^2) \mathbf{M} \times \mathbf{H} - \frac{\alpha}{M} \mathbf{M} \times \frac{d\mathbf{M}}{dt} \tag{2.8}$$

It is clear now that substitutions $\gamma(1+\alpha^2) \to \gamma_G$ and $\dfrac{\alpha}{\gamma(1+\alpha^2)} \to \alpha_G$ transform the Landau-Lifshitz equation exactly into the Landau-Lifshitz-Gilbert equation. However, there is some physical discrepancy between them if one thinks of γ as a physical constant with its value given by the physical origin of the magnetic moment. Nevertheless, this discrepancy is considerable diminished when α is a small parameter, as it is considered in this thesis. Recently, it was found that dissipation terms can also be introduced into a variational formalism by using generalized Rayleigh functions and the Landau-Lifshitz damping term was proved to be of this type [60]. Another notable result is given in [61], where the Landau-Lifshitz equation

30

is derived as a dynamic equation compatible with micromagnetics constraints (the preservation of the magnetization norm and the equilibrium condition given by equation $\mathbf{M} \times \mathbf{H} = 0$).

The Landau-Lifshitz equation can be easily generalized to describe the behavior of the magnetic moment in complex environments substituting in equation (2.6) the magnetic field $\mathbf{H}$ by the effective field $\mathbf{H}_{eff}$, which is derived from the potential energy $U(\mathbf{M})$ associated with the environment.

2.2. Landau-Lifshitz type equations for multi-spin dynamics

In this section, the Landau-Lifshitz equations for multi-spin dynamics are presented. A simplified version of these semi-classical multi-spin equations was first used to study spin wave modes in ferromagnetic materials [62]. We used these equations in order to investigate surface anisotropy effects on quasi-static and dynamic magnetization reversals in nanoparticles (See Chapter 5).

Consider a set of n three-component vectors $\mathbf{S}_i$ (representing the spin moment), each one located at the fixed point i of a three-dimensional lattice. The total energy of interaction for this system is given by:

$$U = -\frac{1}{2}\sum_{i,j} J_{ij}\mathbf{S}_i \cdot \mathbf{S}_j - (g\mu_B\mu_0)\sum_{i=1}^{n}\mathbf{H}_i \cdot \mathbf{S}_i - \sum_{i=1}^{n}K_i\left(\mathbf{s}_i \cdot \mathbf{u}_i\right)^2 +$$
$$\frac{\mu_0}{8\pi}(g\mu_B)^2\sum_{i,j}\frac{\mathbf{S}_i \cdot \mathbf{S}_j - 3(\mathbf{S}_i \cdot \mathbf{e}_{ij})(\mathbf{S}_j \cdot \mathbf{e}_{ij})}{\left\|\mathbf{r}_i - \mathbf{r}_j\right\|^3} \qquad (2.9)$$

Here, $\mathbf{r}_i$ denotes the position vector of the point i, $\mathbf{e}_{ij}$ is the unit vector of the direction $\mathbf{r}_i$-$\mathbf{r}_j$, constants J_{ij} (>0, for ferromagnetic materials) accounts for the strength of the exchange interactions between spins, $\mu_B \sim 9.27 \times 10^{-24}\, A \cdot m^2$ is the Bohr magneton. The

constants g and μ_0 are defined in the previous section. The vector $\mathbf{H}_i$ denotes the magnetic field at the site i, and the magnetocrystalline uniaxial anisotropy is described by easy axis $\mathbf{u}_i$ and anisotropy constants K_i. The $\mathbf{s}_i$ denotes the unit vector along the direction $\mathbf{S}_i$, and it is usually preferred to $\mathbf{S}_i$ for the definition of the anisotropy energy. The first term in energy expression (2.9):

$$U_{ex} = -\frac{1}{2}\sum_{i,j} J_{ij} \mathbf{S}_i \cdot \mathbf{S}_j \,, \tag{2.10}$$

is known as the exchange energy. This expression was proposed by Heisenberg and Dirac, independently, in the context of quantum mechanics and its physical origin is the overlap of electronic wave functions. Although these interactions are short-ranged, they are very strong compared to the other interactions considered in this problem. As a consequence, they favor long-ranged spin ordering and represent the main ingredient for explaining the existence of the spontaneous magnetization in ferromagnetic materials. The second term in the energy expression:

$$U_z = -(g\mu_B\mu_0)\sum_{i=1}^{n} \mathbf{H}_i \cdot \mathbf{S}_i \,, \tag{2.11}$$

is identified as Zeeman energy and originates from the classical interaction of the magnetic moment associated to the spin, $i.\ e.\ \mathbf{M}_i = -g\mu_B\mathbf{S}_i$, with the external magnetic field $\mathbf{H}_i$. Its effect on the magnetic moment was discussed in the previous section. The third term:

$$U_{an} = -\sum_{i=1}^{n} K_i \left(\mathbf{s}_i \cdot \mathbf{u}_i\right)^2 \,, \tag{2.12}$$

is related to the spin interaction with the physical hosting lattice, and it is known as magneto-crystalline anisotropy energy. This term may have various expressions

depending on the symmetry of the corresponding physical system, but we restrict our discussion to the uniaxial anisotropy case. This interaction favors the spin orientation along the easy axis (for $K_i>0$) or along the plane perpendicular to the easy axis (for $K_i<0$). Finally, the last term in equation (2.9):

$$U_d = \frac{\mu_0}{8\pi}(g\mu_B)^2 \sum_{i,j} \frac{\mathbf{S}_i \cdot \mathbf{S}_j - 3(\mathbf{S}_i \cdot \mathbf{e}_{ij})(\mathbf{S}_j \cdot \mathbf{e}_{ij})}{\|\mathbf{r}_i - \mathbf{r}_j\|^3} , \qquad (2.13)$$

accounts for dipole interactions between the magnetic moments associated with the spins. The individual dipole-dipole interaction is typically much smaller than the exchange interaction between neighboring spins. However, their range of interaction is much longer than the one of the exchange interaction. Therefore, the cumulative effect of dipole-dipole interactions becomes comparable to the exchange influence in systems with a large number of spins. The competition between these two energies results in the appearance of well-known magnetization domain structures in ferromagnetic materials.

The Landau-Lifshitz equation of motion for each spin $\mathbf{S}_i$ reads:

$$\hbar\frac{d\mathbf{S}_i}{dt} = -\mathbf{S}_i \times \mathbf{H}_i^{eff} - \alpha\,\mathbf{S}_i \times \mathbf{S}_i \times \mathbf{H}_i^{eff} , \qquad (2.14)$$

where $\mathbf{H}_i^{eff}$ is the effective field acting on the spin $\mathbf{S}_i$ and it is given by:

$$\mathbf{H}_i^{eff} = -\frac{1}{\mu_0}\nabla_{\mathbf{S}_i} U . \qquad (2.15)$$

By giving the exchange constants, as well as the anisotropy axes and constants for the spin system, we arrive at $3n$ coupled nonlinear differential equations that describe the multi-spin dynamics of the magnetic system with the appropriate initial conditions $\mathbf{S}_i(0) = \mathbf{S}_0^i$ chosen for each spin. *Ab initio* evaluations of exchange constants [63-65],

as well as anisotropy constants [66-67], are possible, but the accuracy of these calculations is still inadequate. However, the continuous improvement of computational capabilities may lead to acceptable results in the near future. In this thesis, the exchange and anisotropy constants are treated as parameters of the model. This model is applied in Chapter 5 for the study of surface anisotropy effects on hysteretic and dynamical properties of magnetic nanoparticles.

2.3. Landau-Lifshitz type equations for continuum magnetic media

In this section, the framework of the continuum-magnetization dynamics is presented. The multi-spin description of magnetic nanoparticles presented in the previous section leads to complex many-body problems, which are normally tractable only by numerical methods. Due to the computer limitations, the investigations are restricted to very small systems with diameters of a few nanometers. Therefore, the only way to approach larger magnetic systems is to ignore the atomic nature of matter and to use a continuum approximation.

The continuum-mechanics approach to the spin dynamics can be traced back to the works of Landau and Lifshitz, Brown, and Aharoni, and it is known as *micromagnetics*. A general presentation of the micromagnetics can be found in the classical book of Brown [22] and in the one edited by Rado and Suhl [68]. An up-to-date critical analysis of this domain is presented in the book of Aharoni [20], while the most recent reviews of analytic and numerical micromagnetics, compared to experimental results, can be found in the books of Kronmuller and Fahnle [24], and Hubert and Schafer [23].

Micromagnetics theory has been mainly applied to the calculation of quasi-static magnetization processes. The classical approach was based on the analytical and numerical study of the static Brown equation and its linearized form. The increasing computational capabilities made possible a new approach based on the dynamic Landau-Lifshitz type equation. However, the complexity of the dynamic approach may generate unacceptable large errors in describing long-time scale processes. For example, a standard problem proposed by the National Institute for Standards and Technology (NIST) was simulated by various computational groups and the numerical results had been submitted during 1997-1998 [69]. The wide distribution of these results raised many doubts concerning the reliability of the numerical methods applied to solve this complex problem. As a consequence, NIST proposed simpler standard problems related to the short time scale processes. In this case, the submitted numerical results tend to agree with each other on a time scale below 1 ns [69]. A large number of research articles and PhD theses (see, for example, [12-13], [70-76] and references therein) concentrate nowadays in this area, providing valuable numerical algorithms to approach Landau-Lifshitz type equations for continuum media. On the other hand, the recent developments in experimental magnetization dynamics (recall Section 1.2) made also possible the experimental confirmation of the computational micromagnetics dynamics, as far as short-time scale phenomena are concerned. In conclusion, the micromagnetics dynamics offers a valuable tool for describing the magnetization motion in magnetic materials, but the robustness of the numerical methods applied to this dynamics is still limited to short-time scale processes.

Chapters 3 and 4 of this dissertation will focus on analytical rather than computational approach to magnetization dynamics on short time scale, but members of our group are also involved in developing computational methods for this problem [75, 76].

Next, let us postulate Landau-Lifshitz type equations for magnetization dynamics in continuum media. Consider a time-dependent continuous vector field $\mathbf{M}(\mathbf{r},t)$ defined over the volume V. This vector field represents the magnetization field understood as a magnetic moment per unit volume. Let us assume that magnetization norm M_s is constant over the volume as well as in time, and consequently $\mathbf{M}(\mathbf{r},t)$ can be written as $M_s\mathbf{m}(\mathbf{r},t)$, where $\mathbf{m}(\mathbf{r},t)$ is the unit vector field along the magnetization vector field. The total energy of interaction of the system is given by the following sum:

$$G\big(\mathbf{M}(\cdot);t\big) = G_Z\big(\mathbf{M}(\cdot);t\big) + G_{an}\big(\mathbf{M}(\cdot)\big) + G_{ex}\big(\mathbf{M}(\cdot)\big) + G_{dem}\big(\mathbf{M}(\cdot)\big). \qquad (2.16)$$

It is more appropriate to call this energy as *free energy* (or even more precisely *Gibbs function*) since it represents the thermodynamic potential associated to the problem under study (the temperature, volume and density are considered invariable in the physical process associated to this model).

The first term reads:

$$G_Z\big(\mathbf{M}(\cdot);t\big) = -\mu_0 \int_V \mathbf{M}(\mathbf{r},t) \cdot \mathbf{H}_{app}(\mathbf{r},t)d\tau , \qquad (2.17)$$

where $\mathbf{H}_{app}$ is the external applied magnetic field. This term is known as Zeeman energy, and it can be seen as a straightforward generalization to the continuum case of the Zeeman energy for a discrete spin system given by formula (2.11). The second

term accounts for the magnetocrystalline anisotropy energy and is given by the following formula:

$$G_{an}\left(\mathbf{M}(\cdot)\right)=-\int_V K_u\left(\mathbf{r}\right)\left(\mathbf{m}(\mathbf{r},t)\cdot\mathbf{u}\left(\mathbf{r}\right)\right)^2 d\tau , \qquad (2.18)$$

with $K_u(\mathbf{r})$ being the magnetocrystalline anisotropy distribution function. It is apparent that this formula is a generalization for the continuum case of the magnetocrystalline energy for a discrete system of spins given by formula (2.12). The next term in energy formula (2.16) is:

$$G_{ex}\left(\mathbf{M}(\cdot)\right)=\int_V A\left(\left\|\left(\nabla M_x\right)(\mathbf{r},t)\right\|^2+\left\|\left(\nabla M_y\right)(\mathbf{r},t)\right\|^2+\left\|\left(\nabla M_z\right)(\mathbf{r},t)\right\|^2\right)d\tau , \qquad (2.19)$$

where A is the exchange constant, and $\|\ \|$ simply denotes the Euclidian norm. This expression for exchange energy seems somehow intrigued if one tries to relate it to the exchange energy for a discrete system given by formula (2.10). A straight generalization of the discrete case would give:

$$\tilde{G}_{ex}=-\frac{1}{2(g\mu_B)^2}\iint_{V V} J\left(\left\|\mathbf{r}-\mathbf{r}'\right\|\right)\mathbf{M}(\mathbf{r})\cdot\mathbf{M}(\mathbf{r}')d\tau d\tau' , \qquad (2.20)$$

if one consider that constants J_{ij} are actually only dependent on the relative distance of the spin vectors. Because the exchange is a short range interaction, the function $J(\|\mathbf{r}\text{-}\mathbf{r}'\|)$ can also be considered negligible outside a sphere $S(\mathbf{r},\varepsilon)$ of center $\mathbf{r}$ and small radius ε. Inside this sphere we can expand the magnetization $\mathbf{M}(\mathbf{r}')$ about the center point $\mathbf{r}$ in a Taylor series:

$$\mathbf{M}(\mathbf{r}')=\mathbf{M}(\mathbf{r})+\left((\mathbf{r}'-\mathbf{r})\cdot\nabla_\mathbf{r}\right)\mathbf{M}(\mathbf{r})+\frac{1}{2}\left((\mathbf{r}'-\mathbf{r})\cdot\nabla_\mathbf{r}\right)^2\mathbf{M}(\mathbf{r})+... \qquad (2.21)$$

By retaining only terms up to the second order, and introduce them in formula (2.20) the exchange energy $\tilde{G}_{ex}$ can be written as:

$$\tilde{G}_{ex} \approx -\frac{1}{2(g\mu_B)^2} \left\{ \frac{M_s^2 V}{\langle J \rangle} + \sum_{i,j} \lambda_{ij} \int_V \frac{\partial \mathbf{M}}{\partial r_i}(\mathbf{r}) \cdot \frac{\partial \mathbf{M}}{\partial r_j}(\mathbf{r}) d\tau \right\}, \qquad (2.22)$$

where $\langle J \rangle = \int\limits_{S(0,\varepsilon)} J(\|\mathbf{x}\|)d\tau$ and $\lambda_{ij} = \frac{1}{2} \int\limits_{S(0,\varepsilon)} J(\|\mathbf{x}\|)x_i x_j d\tau$. The second term from

expansion (2.21) does not lead to any contribution since its scalar product with $\mathbf{M}$ can

be written as the derivative of M_s, which is zero. The third term in (2.21) leads to the

second term in (2.22), when the integration by parts and uniformity of the norm are

used. For the points close to the surface, the $S(\mathbf{r}, \varepsilon)$ may not be completely inside the

volume V. These effects are neglected here, but they are included in the boundary

conditions of the problem. By using symmetry arguments, the off-diagonal elements

of λ_{ij} are proved to be zero and the diagonal ones equal. Since a constant term is

irrelevant to an energy formula, expression (2.19) for the exchange energy can be

now seen as a generalization of the exchange formula for discrete spin systems. The

justification presented here uses similar arguments to the one presented in classical

micromagnetics books [20, 22], but we hope it is improving the clarity and rigor of

the above mentioned ones. Nevertheless, this derivation may be considered as a

simple remark to the postulation of the exchange energy term given by (2.19).

To complete the description of energy formula (2.16), the last term, known as

the demagnetizing (or magnetostatic) energy, is given by:

$$G_{dem}\left(\mathbf{M}(\cdot)\right) = -\frac{1}{2}\mu_0 \int_V \mathbf{M}(\mathbf{r},t) \cdot \mathbf{H}_{dem}\left(\mathbf{M}(\cdot)\right)d\tau, \qquad (2.23)$$

where:

$$\left\{\mathbf{H}_{dem}\left(\mathbf{M}(\cdot)\right)\right\}(\mathbf{r},t) = \frac{1}{4\pi}\left\{ \oint_S \frac{\mathbf{n}_{\mathbf{r}'} \cdot \mathbf{M}(\mathbf{r}',t)(\mathbf{r}-\mathbf{r}')}{\|\mathbf{r}-\mathbf{r}'\|^3}ds' - \int_V \frac{\nabla_{\mathbf{r}'} \cdot \mathbf{M}(\mathbf{r}',t)(\mathbf{r}-\mathbf{r}')}{\|\mathbf{r}-\mathbf{r}'\|^3}d\tau' \right\}, \quad (2.24)$$

where S is the surface embedding the volume V and $\mathbf{n_{r'}}$ is unit vector normal to the surface S at the point $\mathbf{r'}$. This term is related to the dipole-dipole interactions considered in the discrete case, but this justification is much more complicated than the one given for the exchange case. However, this term is well-known from classical magnetostatic problems based on Maxwell equations, and consequently, it is usually tacitly accepted.

The Landau-Lifshitz equations for the magnetization vector field dynamics can be written in the following form:

$$\frac{\partial \mathbf{M}}{\partial t} = -\gamma \mathbf{M} \times \mathbf{H}_{eff}(\mathbf{M},t) - \frac{\gamma\alpha}{M_s}\mathbf{M} \times \left(\mathbf{M} \times \mathbf{H}_{eff}(\mathbf{M},t)\right), \tag{2.25}$$

where the effective field is given by the Fréchet derivatives of the energy functional:

$$\mathbf{H}_{eff} = -\frac{1}{\mu_0}\frac{\delta G}{\delta \mathbf{M}(\cdot)} = \mathbf{H}_Z + \mathbf{H}_{an} + \mathbf{H}_{ex} + \mathbf{H}_{dem}. \tag{2.26}$$

The constants γ and α coincide with the ones defined in the Section 2.1. The boundary conditions associated with this problem are:

$$(\mathbf{n} \cdot \nabla)\mathbf{M}(\mathbf{r},t) = 0, \quad \mathbf{r} \in S, \tag{2.27}$$

and the initial conditions read:

$$\mathbf{M}(\mathbf{r},0) = \mathbf{M}_0(\mathbf{r}). \tag{2.28}$$

with $\mathbf{M}_0(.)$ being a given vector function that has to satisfy the time-independent boundary condition associated to (2.27).

The effective field terms have the following explicit forms:

$$\mathbf{H}_{an}(\mathbf{r},t) = \frac{2K_u}{\mu_0 M_s}\left\langle \mathbf{m}(\mathbf{r},t) \cdot \mathbf{u}(\mathbf{r})\right\rangle \mathbf{u}(\mathbf{r}), \tag{2.29}$$

$$\mathbf{H}_{ex}(\mathbf{r},t) = \frac{2A}{\mu_0}\Delta \mathbf{M}(\mathbf{r},t), \tag{2.30}$$

39

$$\mathbf{H}_Z(\mathbf{r},t) = \mathbf{H}_{app}(\mathbf{r},t), \tag{2.31}$$

while the demagnetizing field has being already defined by Formula (2.24).

The complexity of the problem can be substantially reduced in the case of homogeneous ferromagnetic objects with uniform uniaxial anisotropy $\mathbf{u}(\mathbf{r})=\mathbf{u}$ and regular shape. Let us consider that a uniform magnetic field is applied to such an object. A fundamental result from magnetostatic theory states that the corresponding demagnetizing field is also uniform (not necessary in the same direction as $\mathbf{H}$) if the surface of the object is of the second degree. The proof of this result was revealed by Poisson for the case of ellipsoidal bodies, and the discussion of the general case can be found in the classical book of Maxwell [78]. This result gives us the idea to consider a uniform magnetization vector field $\mathbf{M}_0(\mathbf{r})=\mathbf{M}_0$ as an initial condition and check the potentiality of the uniform modes as solutions for the integro-differential problem considered above. Thus, for a potentially uniform solution $\mathbf{M}(\mathbf{r},t)=\mathbf{M}(t)$, the demagnetizing field is simply given by $\mathbf{H}_{dem}(\mathbf{r},t) = \mathbf{H}_{dem}(t) = -\tilde{D}\mathbf{M}(t)$, where $\tilde{D}$ is known as demagnetizating tensor, the exchange field is zero, and for the anisotropy field we have $\mathbf{H}_{an}(\mathbf{r},t) = \mathbf{H}_{an}(t) = (2K_u/\mu_0 M_s)\langle \mathbf{m}(t)\cdot\mathbf{u}\rangle\mathbf{u}$. It is now apparent, that the solution of the following system of differential equations:

$$\frac{d\mathbf{M}}{dt} = -\gamma\mathbf{M}\times\mathbf{H}_{eff}(\mathbf{M},t) - \frac{\gamma\alpha}{M_s}\mathbf{M}\times\left(\mathbf{M}\times\mathbf{H}_{eff}(\mathbf{M},t)\right), \tag{2.32}$$

where

$$\mathbf{H}_{eff} = \mathbf{H} - \tilde{D}\mathbf{M}(t) + (2K_u/\mu_0 M_s)\langle \mathbf{m}(t)\cdot\mathbf{u}\rangle\mathbf{u}, \tag{2.33}$$

that satisfies the initial condition $\mathbf{M}(0)=\mathbf{M}_0$, leads to the spatially uniform solution $\mathbf{M}(\mathbf{r},t)=\mathbf{M}(t)$ of the integro-differential problem corresponding to the applied field $\mathbf{H}$

40

and the initial condition $\mathbf{M}(\mathbf{r},0)=\mathbf{M}_0$. The coordinate axes can be chosen such that the demagnetizing matrix has a diagonal form. In addition, let us assume that the magneto-crystalline anisotropy axis is along one of the principle demagnetizing axes, denoted by x. Consequently, the effective field formula can be rewritten as:

$$\mathbf{H}_{eff} = \mathbf{H} + D_x M_x \mathbf{e}_x - D_y M_y \mathbf{e}_y - D_z M_z \mathbf{e}_z,$$ (2.34)

where D_x accounts for demagnetizing and anisotropy field in x direction, while D_y and D_z account for demagnetizing field in y and z direction, respectively. It should be kept in mind the essential restriction on the surface geometry, which has to be of second order degree (for example ellipsoid). It is also important to be aware of the potential instability of the spatially uniform solution, which would make it less useful for the practical purposes.

However, the simplified Landau-Lifshitz equation (2.32)-(2.33) can also be used for ferromagnetic objects that do not satisfy the surface requirements, instead their dimensions are in nanometer range. This possibility is due to the strength of the exchange interaction, which imposes the alignment of the magnetic moments at such small dimensions. By using this simplifying assumption, we obtained spatially uniform magnetization fields that may not be exact solutions of the integro-differentiable problem, as in the previous discussion, but may offer a very good physical approximation of those spatially non-uniform solutions. The model obtained using this assumption is usually called *macrospin* model. It is clear that the macrospin model should be applied for "small enough" magnetic structures. There also exists an inferior limit to this assumption related to surface effects, which appear in small magnetic structures with dimensions on the order of a few nanometers.

There exists extensive evidence for the quantitative agreement between the experimental results on precessional magnetization reversals and Landau-Lifshitz equations for uniform cases (see [11-13, 41-48] and references therein). These comparisons are usually based on "snapshots" of the magnetization dynamics obtained by the numerical integration of Landau-Lifshitz equations (2.32)-(2.34). The aim of the next two chapters is to offer a systematic analytical study of precessional magnetization reversals based on these equations.

In conclusion, the framework of the continuum-magnetization dynamics was presented in this section. The complexity of the general nonlinear integro-differential problem requires numerical approaches to study the magnetization dynamics. In spite of the tremendous research efforts in this area, the current numerical algorithms offer good results for the short-time scale dynamics, but they generate considerable errors for longer time scales. Two cases that substantially reduce the complexity of the problem were discussed and they led to equations (2.32)-(2.34). The analytical study of this system is undertaken in the next two chapters in order to give a theoretical description of the precessional magnetization reversals in thin film media.

3. Precessional magnetization reversal in perpendicular media

> "Now, here, you see, it takes all the running you can do, to keep in the same place. If you want to get somewhere else, you must run at least twice as fast as that!" Lewis Carroll [78]

In this chapter, the analytical study of precessional switching in perpendicular thin film media is undertaken. This study is based on the Landau-Lifshitz equation to describe the magnetization dynamics in these media. The case of the perpendicular media subject to rectangular magnetic field pulses is first analyzed. The features of precessional magnetization switching and conventional mechanism of magnetization reversal are compared in the first section. By using integrals of motions and the "unit disk representation" of undamped magnetization dynamics, the expressions for critical field and pulse durations that guarantee precessional magnetization reversals are derived in the second section. This study is extended to non-rectangular magnetic field pulses in the third section, where the inverse problem approach is used to design magnetic field pulses that guarantee precessional switching.

The perpendicular oriented media have been introduced in HDDs in 2004 as an alternative solution to the longitudinal recording media for further improving areal density in the magnetic storage. They are expected to push areal densities beyond 1Tb/in^2 in the next few years. Although these media have been studied for more than thirty years [34-36], the costs of implementing them were not justified as long as the longitudinal media were developing at a very fast pace and a low cost. The current

fundamental limitations of the longitudinal recording technology shift the research and technology interests towards the perpendicular recording. A short discussion of perpendicular media is presented in Chapter 1. The experiments indicating the recording of magnetic patterns into perpendicular thin film media using ultrashort magnetic pulses, as well as the numerical simulations confirming the validity of Landau-Lifshitz equation approach to quantitatively describe these phenomena, can be found in References [8, 42-45]. In order to find the general features of precessional switching, as opposed to the selective snapshots offered by numerical simulations, the analytical treatment of the precessional switching in perpendicular media is considered in this chapter.

Traditionally, the magnetization reversal is produced by applying the magnetic field almost antiparallel with respect to the initial magnetization direction (see Figure 3.1 (a)). These reversals are initially relatively slow and are realized through numerous precessional oscillations (see Figure 3.2 (a)). They are driven by the relaxation (damping) processes and, for this reason they can be termed as "damping" switchings. When the field is applied in the perpendicular direction (see Figure 3.1 (b)), the reversal can be obtained employing the precessional magnetization dynamics, and that is why the corresponding reversal is called "precessional" switching (see Figure 3.2 (b)). This non-conventional switching is much faster than the traditional one, but it is much more sensitive to shapes and durations of magnetic field pulses. For example, the magnetic field should be switched off in some precise time windows when the magnetization component along the anisotropy axis (m_x) has negative values (see Figure 3.3 (b)). Otherwise, the magnetization will relax to the

initial position after the magnetic field is switched off (see Figure 3.4), and consequently, no switching of the magnetization orientation takes place. This is not the case in the conventional switching, where the magnetic field pulse has only a lower limit, as far as the timing of switching-off is concerned (see Figure 3.3 (a)). These discussions have their rigorous explanations presented in the next section.

It is clear from the above considerations that the price paid to obtain faster modes of magnetization reversals is the increased complexity of magnetic field design. In the second and third sections, this problem is addressed for rectangular and non-rectangular magnetic field pulses, respectively.

A remark should be made concerning the granular structure of the magnetic thin film media. First of all, the perpendicular media have a very high orientation ratio (see Chapter 1), *i.e.* the grains have approximately the same anisotropy axis that is oriented perpendicular to the thin film plane. This suggests that even if the exchange interactions between grains are completely neglected, the unison motion of the magnetization grains is expected to be a good approximation of the real magnetization dynamics in a memory cell. Second, the small dimensions of memory cells in the current recording media also suggest the use of simplified equations (2.35)-(2.37) in the macrospin interpretation due to the exchange interactions (see Chapter 2). These considerations, along with the agreement between experiments and numerical simulations, allow us to conclude that the results obtained for this simplified model represents not only a pure mathematical analysis, but also a reliable description of the physical precessional switchings.
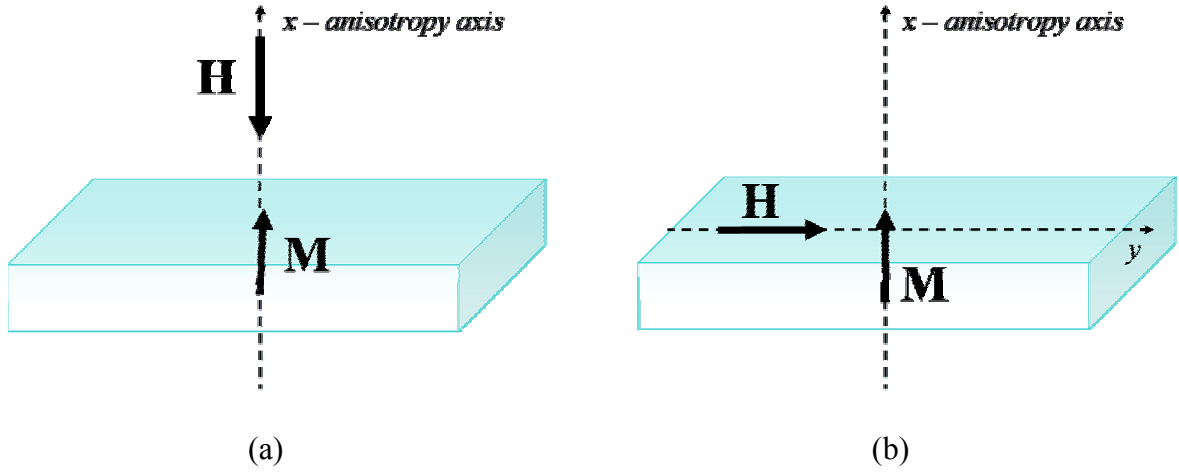
Figure 3.1: Configurations for magnetization reversals in perpendicular thin film media: (a) damping switching and (b) precessional switching.

(a)   (b)
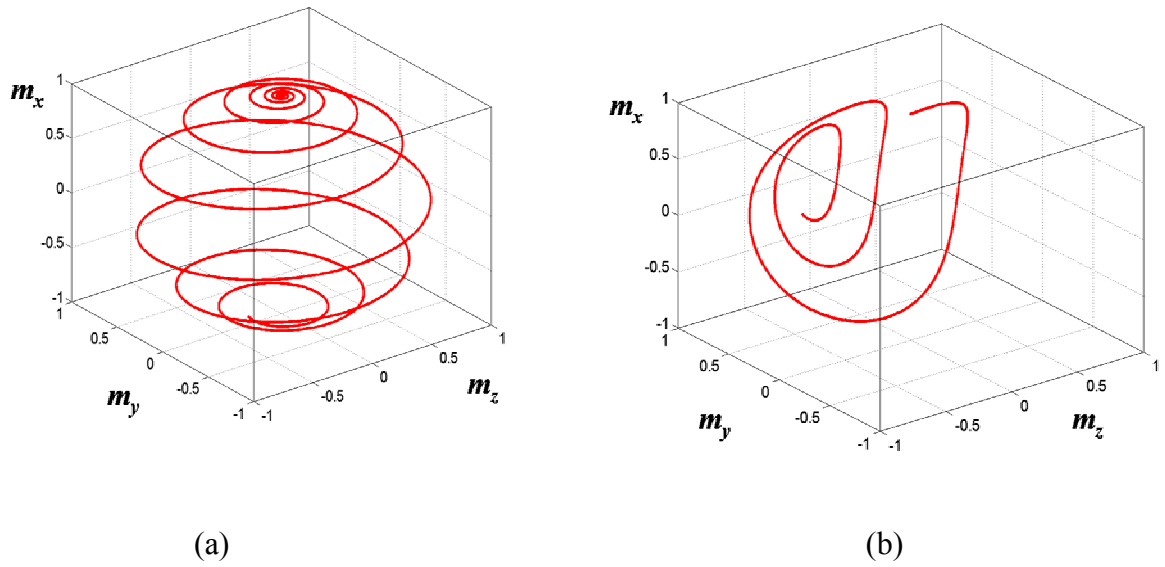
Figure 3.2: Magnetization trajectories for the configurations presented in Figure 3.1. Parts (a) and (b) are corresponding to part (a), respectively (b), of Figure 3.1.

(a)   (b)
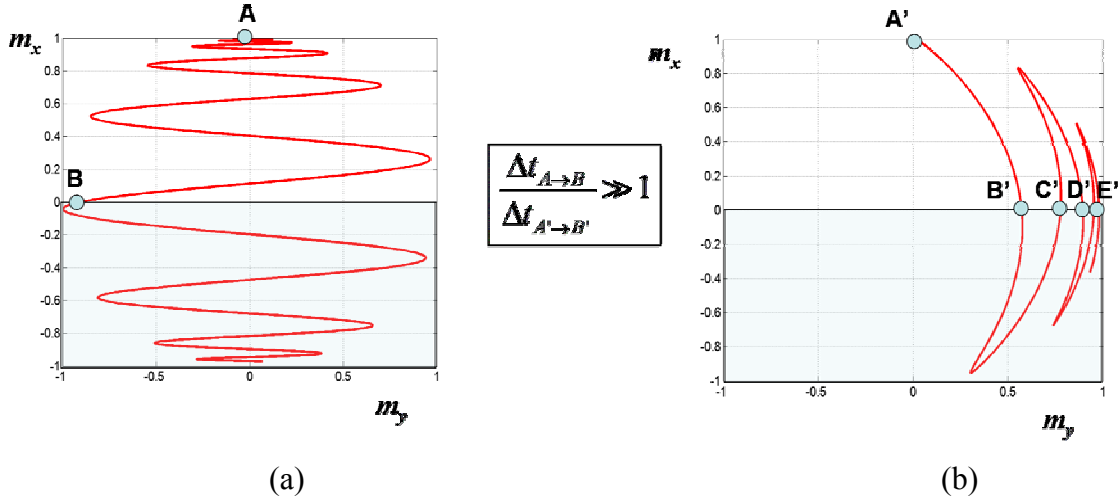
Figure 3.3: Projections on the (m_x, m_y) plane of the magnetization trajectories presented in Figure 3.2. The points of the trajectory intersections with the plane $m_x=0$ are marked.
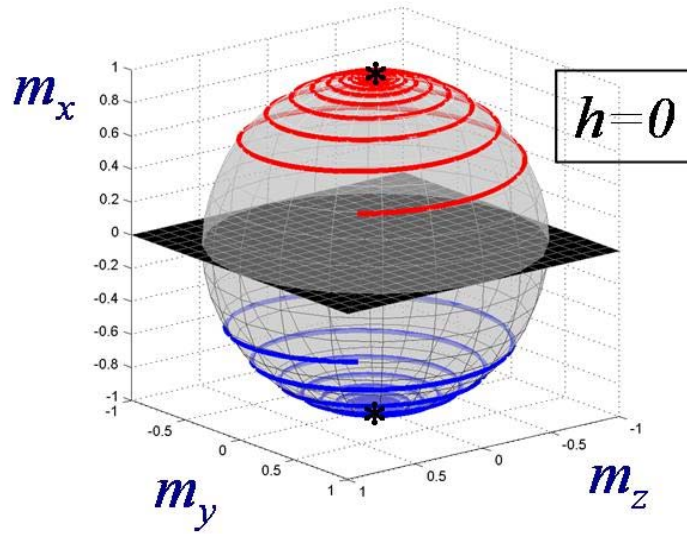
Figure 3.4: Magnetization relaxations in the absence on the applied field. When the initial magnetization is in the upper semispace, magnetization relaxes to the equilibrium point $m_x=1$ (upper curve). When the initial magnetization is in the lower semispace, it relaxes to the equilibrium $m_x=-1$ (lower curve).

3.1. Theoretical comparison of damping and precessional switchings

In this section, the analytical solutions to Landau-Lifshitz equations for "damping" and "precessional" switchings of magnetization in perpendicular media are found. These solutions lead to the expressions for switching times and critical fields. The comparison of these two distinct modes of switching is presented.

Consider "damping" switching in perpendicular media caused by a spatially uniform magnetic pulsed magnetic field applied along the anisotropy axis (see Figure 3.1 (a)). The Landau-Lifshitz equation can be written in the following dimensionless form:

$$\frac{d\mathbf{m}}{dt} = -\mathbf{m} \times \mathbf{h}_{eff} - \alpha\, \mathbf{m} \times \mathbf{m} \times \mathbf{h}_{eff}\,, \qquad (3.1)$$

where $\mathbf{m}=\mathbf{M}/M_s$, $\mathbf{h}_{eff}=\mathbf{H}_{eff}/M_s$, time is measured in units of $(\gamma M_s)^{-1}$. As it is defined in the previous chapter, M_s is the saturation magnetization, $\gamma = 2.21 \times 10^5\, mA^{-1}s^{-1}$ is the product of the vacuum permeability and the absolute value of gyromagnetic ratio, and α is the dimensionless damping constant. The effective magnetic field corresponding to the above considered damping switching is given by:

$$\mathbf{h}_{eff} = -D(m_z\mathbf{e}_z + m_y\mathbf{e}_y) + D_0 m_x\mathbf{e}_x - h\mathbf{e}_x\,. \qquad (3.2)$$

Here, the positive coefficients D and D_0 account for demagnetizing field and magnetocrystalline anisotropy, while h is the magnitude of applied field $\mathbf{h}$, which is assumed to be constant during the pulse duration (so-called rectangular field pulse).

Kikuchi [79] considered a similar problem for the case of an isotropic ferromagnetic sphere when the effective field is defined by $\mathbf{h}_{eff} = -D\mathbf{m} - h\mathbf{e}_x$. The difference in the mathematical forms of this effective field and the effective field

(3.2), results in profound differences in the physical phenomena of magnetization switching. In the case of effective field considered by Kikuchi, there exists an infinite set of equilibrium states for $h=0$ and no critical field is required to switch from one state to another. In our case of effective field (3.2), there are only two equilibrium states at $h=0$ with $m_x=1$ and $m_x=-1$, respectively, and the switching from one equilibrium state to another is only possible if applied field exceeds some critical field h_0.

Mallinson [80] studied the problem with the effective field given by formula (3.2). His analysis is based on the expression of Landau-Lifshitz-Gilbert equation in spherical coordinates. Our approach exploits the rotational symmetry of the problem.

It is apparent that the mathematical form of equations (3.1) and (3.2) is invariant with the respect to rotations of coordinates axes z and y around x axis. As a result of this rotational symmetry, it is expected that dm_x/dt depends only on the x component of $\mathbf{m}$. Indeed, by simple algebra, it is easy to find that:

$$(\mathbf{m} \times \mathbf{h}_{eff})_x = 0, \quad (\mathbf{m} \times \mathbf{m} \times \mathbf{h}_{eff})_x = (h - h_0 m_x)(1 - m_x^2), \quad (3.3)$$

where $h_0 = D_0 + D$. Thus, from equations (3.1) and (3.3), we derive:

$$\frac{dm_x}{dt} = \alpha(h_0 m_x - h)(1 - m_x^2). \quad (3.4)$$

It is clear from equation (3.4) that the magnetization switching from the state $m_x=1$ to the state $m_x=-1$ (or vice versa) is driven exclusively by damping. In this sense this switching can be regarded as damping switching. It seems from equation (3.4) that no switching is possible if magnetization is in equilibrium state $m_x=1$. However, due to thermal effects, magnetization $\mathbf{m}$ slightly fluctuates around the above equilibrium state. As a result, the value of m_x at the instant when the applied

49

field is turned on may be slightly different from 1, and consequently, the switching process is initiated. This argument justifies the solution of equation (3.4) with the initial condition (see Figure 3.1 (a)):

$$m_x \big|_{t=0} = m_{x_0}, \qquad (3.5)$$

where m_{x_0} is close to 1.

It is apparent from equation (3.4) that if $h > h_0$ then $dm_x/dt < 0$ and the switching to the equilibrium state $m_x = -1$ will proceed for any m_{x_0}. On the other hand, if $h < h_0$ then we find from equation (3.4) that $dm_x/dt > 0$ for m_{x_0} sufficiently close to 1, and consequently, no switching is possible. This reveals that h_0 has the meaning of critical field. The problem of critical field will be discussed in a more general case in Section 3.2. In the sequel, it is assumed that $h > h_0$.

By separating variables in equation (3.4) and performing the integration, we arrive at the following solution:

$$\frac{1}{2(h-h_0)} \ln \frac{1-m_x}{1-m_{x_0}} - \frac{1}{2(h_0+h)} \ln \frac{1+m_x}{1+m_{x_0}} + \frac{h_0}{h_0^2 - h^2} \ln \frac{h - h_0 m_x}{h - h_0 m_{x_0}} = \alpha t . \qquad (3.6)$$

From the last equation, the minimal pulse time needed for switching can be found. Indeed, if the duration of magnetic field pulse is such that a negative value of m_x is reached, then the magnetization will be in the basin of attraction of the equilibrium state $m_x = -1$, and the switching will be achieved. Thus, the minimal time can be found from equation (3.6) and the condition $m_x = 0$. By taking into account formula (3.6) and normalizations considered for equation (3.1) we derive the following expression for the minimal pulse time:

$$\tau = \frac{1}{\alpha\gamma}\left[\frac{\ln(1-\cos\theta_0)}{2(H_0-H)} + \frac{\ln(1+\cos\theta_0)}{2(H_0+H)} + \frac{H_0}{H_0^2-H^2}\ln\frac{H}{H-H_0\cos\theta_0}\right]. \qquad (3.7)$$

Here, $H_0=(D_0+D)M_s$ and $m_{x_0} = \cos\theta_0$, where θ_0 is the angle formed by the initial magnetization with x-axis. The graphical illustration of this formula is shown in Figure 3.5 (a) for $\theta_0=0.5^0$.

It is interesting to point out that for the typical case of small angles θ_0, the minimal pulse time τ is very close to the actual switching time at which m_x reaches a value almost equal to -1. This is because m_x decreases much faster for sufficiently small m_x (see equation (3.4)) than when m_x is close to its equilibrium values. This assertion is supported by our calculations, performed by using the analytical expression for m_x extracted from formula (3.6) and shown in Figure 3.6. It is apparent from this figure that the initial dynamics of m_x is very slow and takes most of the time, while the magnetization dynamics away from equilibrium is very fast. Thus, the switching time is close to the minimal pulse field time τ, calculated above.

It is apparent from formula (3.7) that for the typical case of very small initial angles θ_0, the first term in the right hand side of formula (3.7) is dominant. Thus, by neglecting two other terms and using simple trigonometry, we arrived at the following expression for the minimal pulse time (switching time):

$$\frac{1}{\tau} = \frac{\alpha\gamma}{\ln\dfrac{\sqrt{2}}{\theta_0}}(H-H_0). \qquad (3.8)$$
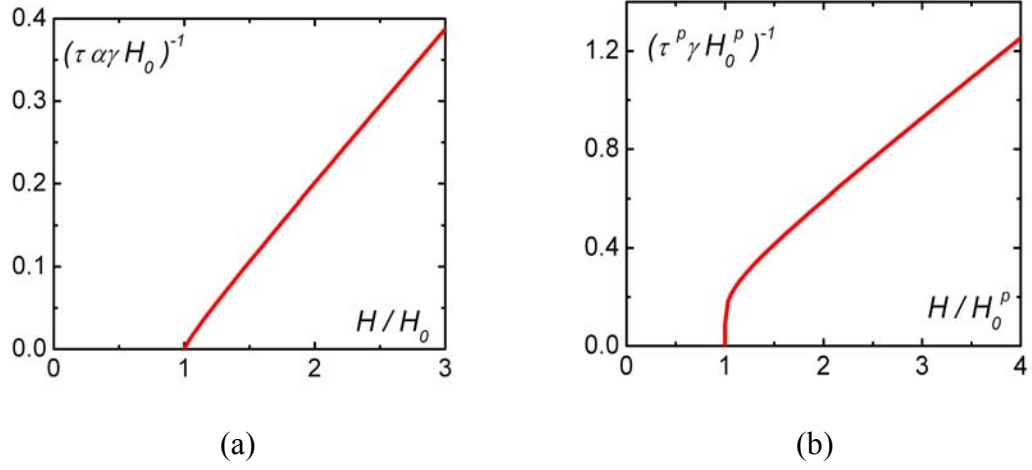
Figure 3.5: (a) Dependence of switching time on magnetic field for damping case, for $\theta_0 = 0.5^0$. (b) Dependence of switching time on magnetic field for precessional switching.
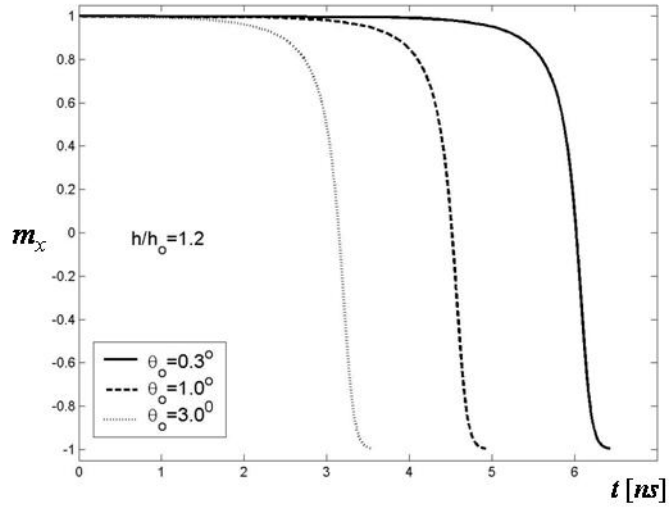
Figure 3.6: Evolution of m_x with time for different initial angles $\theta_0 = 0.3^0$, 1^0, and 3^0. Field ratio $H/H_0 = h/h_0 = 1.2$, product γH_0 is considered to be $4 \times 10^{11} s^{-1}$, and damping constant $\alpha = 0.01$.

For short pulse duration, the value of applied field needed for switching increases inversely proportional to pulse duration: $H \sim 1/\tau$ (which is consistent with Figure 3.5). In this sense, one may say that the dynamic (short-time) coercivity appreciably exceeds the static coercivity H_0. The last formula is also similar to the one that has been observed in numerous experiments [81]-[84]. It is usually written in the form:

$$\frac{1}{\tau} = \frac{1}{S}(H - H_0).$$
(3.9)

As it is visible from the above derivation, there is no need to resolve m_z or m_y dynamics in order to find the reversal time and the critical field corresponding to the damping switching. Nevertheless, the analysis of the precessional magnetization motion during the damping switching would be very instrumental for a deeper understanding of this magnetization reversal mechanism.

First, let us observe that effective field (3.2) can be written in the following form: $\mathbf{h}_{eff} = -D\mathbf{m} + \left[(D + D_0)m_x - h\right]\mathbf{e}_x$. Since the term proportional with the magnetization vector gives no contribution to equation (3.1) due to the vector product with the magnetization vector itself, this term can be dropped off from the expression of the effective field. As a consequence, the free energy corresponding to the reduced form of the effective field driving the magnetization dynamics is given by the following expression:

$$g = -\frac{D + D_0}{2}m_x^2 + hm_x.$$
(3.10)

53

Because the energy is independent of the azimuthal angle φ and polar radius ρ, Landau-Lifshitz dynamics (3.1)-(3.2) can be written using cylindrical coordinates in the subsequent form:

$$\begin{cases} \dot{m}_x = -\alpha\left(1-m_x^2\right)\dfrac{dg}{dm_x} \\ \dot{\varphi} = -\dfrac{dg}{dm_x} \\ \rho = \sqrt{1-m_x^2} \end{cases} \tag{3.11}$$

Since α is regarded as a small parameter, the above representation clearly illustrates the two-time scale of the magnetization dynamics in the case of damping switching: the fast time scale of precessional motion described by the azimuthal angle φ and the relatively slow time scale of relaxation dynamics described by the height component m_x. The relaxation rate is $\alpha\left(1-m_x^2\right)$ times slower than the precessional rate, this ratio being extremely low at the beginning and the final stages of the damping switching when the m_x is close to +1 and -1, respectively.

The precessional dynamics can be explicitly found as a function of the known m_x component. Indeed, expressing the precessional rate as:

$$\dot{\varphi} = \frac{\dot{m}_x}{\alpha\left(1-m_x^2\right)}, \tag{3.12}$$

the integration is straightforward and leads to the explicit formula:

$$\varphi(t) = \frac{1}{2\alpha}\ln\left(\frac{1+m_x(t)}{1-m_x(t)}\right)+2c, \tag{3.13}$$

where constant $c = (1/2)\varphi_0 + (1/4\alpha)\ln\left((1-m_{x_0})/(1+m_{x_0})\right)$. Since the magnetization motion takes place on the unit sphere, formulae (3.6) and (3.13)

54

completely describe in an analytical form the damping magnetization switching in perpendicular media. The time evolutions of magnetization components computed using analytical formulae (3.6) and (3.13) are presented in Figures 3.7 and 3.8.

An instructive quantity that can be immediately evaluated from formula (3.13) is the number of full precessional cycles elapsed during switching time τ:

$$N = \left[\frac{\varphi_0 - \varphi(\tau)}{2\pi} \right] = \left[\frac{1}{4\pi\alpha} \ln\left(\frac{1+m_{x_0}}{1-m_{x_0}} \right) \right]. \tag{3.14}$$

Here, parentheses [.] denote the integer part of a real number. In order to offer some idea about the magnitude of this number, we mention that it is on order of $[1/\alpha]$ for relatively large interval of initial conditions ($0.05^0 < \theta_0 < 5^0$). Since typical values for α are on the order of 10^{-3} up to 10^{-1}, it can be inferred that numerous (tens up to thousands) precessional cycles are traversed during the damping switching.

By inverting relation (3.13) and using simple algebra manipulations the trajectory equation for the damping switching can be written in the following form:

$$\begin{cases} m_x = \tanh(\alpha\varphi - c) \\ \rho = \mathrm{sech}(\alpha\varphi - c) \end{cases}. \tag{3.15}$$

Graphical illustrations of the formula (3.15) are given in the Figure 3.9 and 3.10. It is interesting to point out the absence of the magnetic field magnitude from this equation. Therefore, the magnetization trajectory is not dependent on the magnitude of applied field, which only establishes the orientation and the speed at which this trajectory is traversed. Moreover, when the field is turned off the magnetization follows the same trajectory as in the presence of the field, but at a slower pace.

55
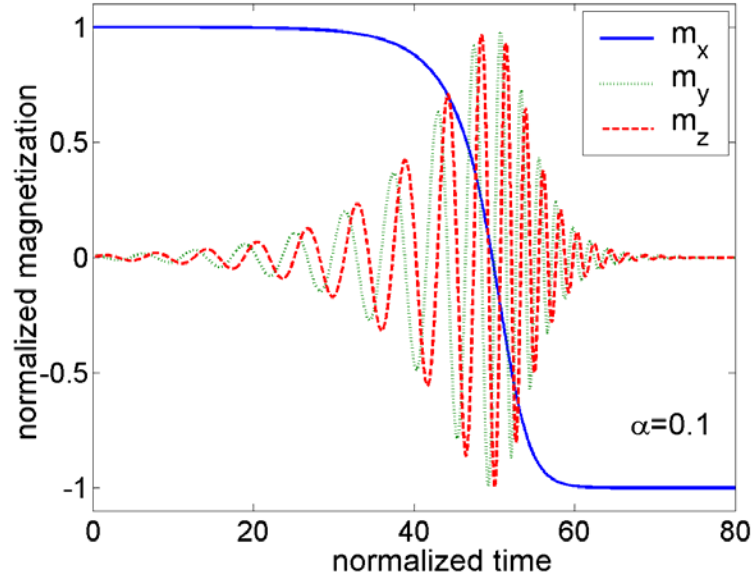
Figure 3.7: Analytical solutions for the damping switching. $\alpha = 0.1$, $\theta_0 = 0.5^0$, $\varphi_0 = 0^0$, $H / H_0 = 2$, and time is measured in units of $(\gamma H_0)^{-1}$.
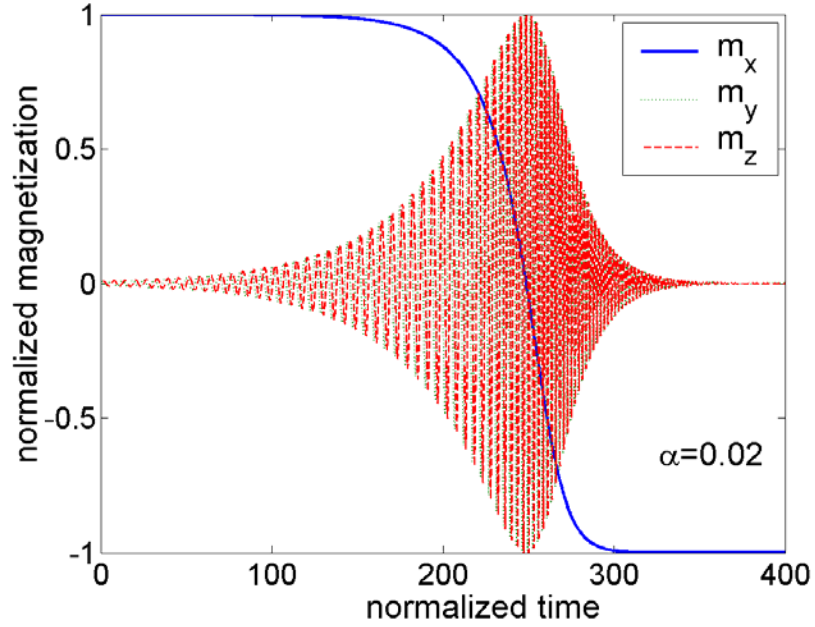
Figure 3.8: Analytical solutions for the damping switching. $\alpha = 0.02$, $\theta_0 = 0.5^0$, $\varphi_0 = 0^0$, $H / H_0 = 2$, and time is measured in units of $(\gamma H_0)^{-1}$.
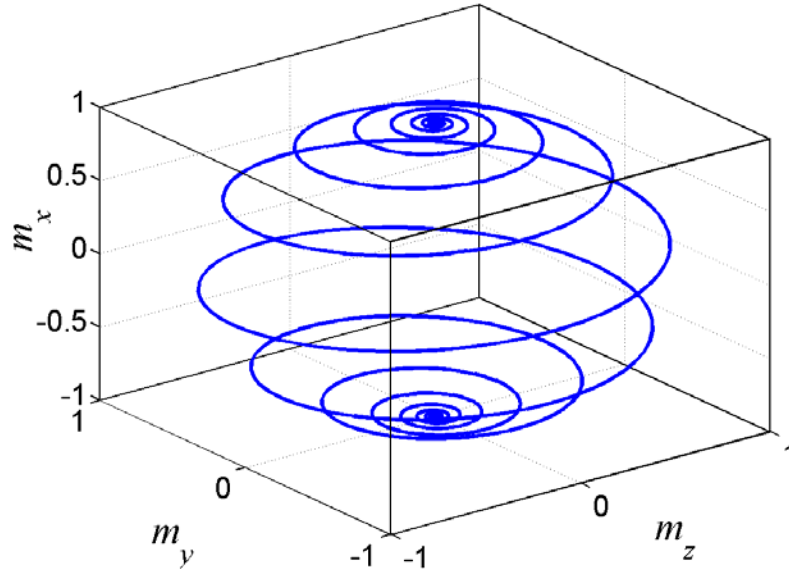
Figure 3.9: Magnetization trajectory for the damping switching computed using formula (3.15) and represented in cartesian coordinates; $\alpha = 0.1$, $\theta_0 = 0.5^0$, $\varphi_0 = 0^0$.
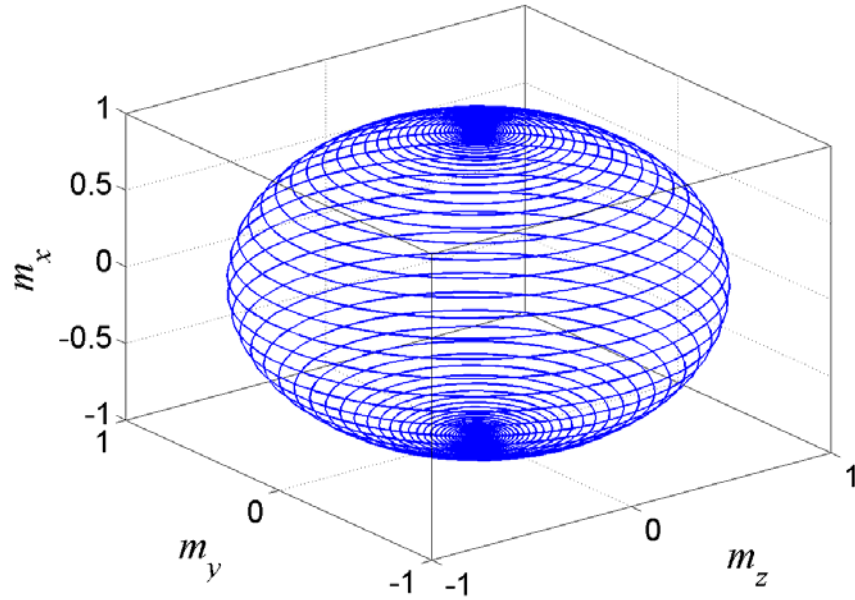
Figure 3.10: Magnetization trajectory for the damping switching computed using formula (3.15) and represented in cartesian coordinates; $\alpha = 0.02$, $\theta_0 = 0.5^0$, $\varphi_0 = 0^0$.

Next, we consider the "precessional" mode of switching when the field is applied along *y*-axis, i.e. perpendicular to the anisotropy axis (see Figure 3.1 (b)). As we learned from the description of the damping switching, the magnetization motion can be seen as a two time scales dynamics: the fast time scale of the precessional motion and the relatively slow time scale of magnetization relaxation. We have also observed that the damping switching is taking place on the slow time scale. It is then clear that a promising idea for decreasing the switching time of the magnetization reversal is to take advantage of the fast time scale of precessional motion.

We recall that in the case of zero applied field there are two stable equilibria $\mathbf{m} = \pm\mathbf{e}_x$ surrounded by two energy wells, which are separated by boundary plane $m_x=0$. Since the dissipation results in the decrease in magnetic free energy, it can be concluded that the time evolution of magnetization within each energy well inevitably leads to the stable equilibrium inside this well (see Figure 3.4). Thus, the essence of the precessional switching is to move the magnetization from one energy well to another using the precessional motion of magnetization. As soon as the magnetization reaches the second energy well, the applied field can be switched off and magnetization will relax to a new equilibrium as a result of damping.

The precessional switching is driven by the precessional torque (the first term in the right hand side of equation (3.1)), while the second term (damping) can be neglected during the time when the magnetic field is applied. This is justified on the grounds that the precessional switching occurs on very fast time scale on which dissipative effects are not appreciably pronounced. Thus, the analysis of precessional switching dynamics is reduced to the solution of the following equation:

58

$$\frac{d\mathbf{m}}{dt} = -\mathbf{m} \times \mathbf{h}_{eff} , \tag{3.16}$$

where the effective field is given by:

$$\mathbf{h}_{eff} = -D(m_z \mathbf{e}_z + m_y \mathbf{e}_y) + D_0 m_x \mathbf{e}_x + h\mathbf{e}_y . \tag{3.17}$$

The explicit analytical solution of equations (3.16)-(3.17) can be obtained by using two integrals of motion that express the conservation of magnetization magnitude:

$$m_x^2 + m_y^2 + m_z^2 = 1 , \tag{3.18}$$

and the conservation of magnetic free energy:

$$\frac{1}{2}D(m_z^2 + m_y^2) - \frac{1}{2}D_0 m_x^2 - hm_y = -\frac{1}{2}D_0 . \tag{3.19}$$

Due to constraint (3.18) the energy conservation law can be written in a simpler form:

$$\frac{1}{2}(D + D_0)m_x^2 + hm_y = \frac{1}{2}(D + D_0) \tag{3.20}$$

The above conservation laws implicitly define the trajectory of the precessional switching that can be geometrically represented as the intersection curve of the sphere (3.18) with the parabolic cylinder (3.20). The explicit equations for the trajectory of precessional switching can be written as:

$$m_z^2 = \frac{2h}{D + D_0}m_y - m_y^2, \qquad m_x^2 = 1 - \frac{2h}{D + D_0}m_y . \tag{3.21}$$

By using (3.16), (3.17), and (3.21), we arrive at the following differential equation with separable variables:

$$\frac{dm_y}{dt} = 2h_0^p m_x m_z = \pm 2h_0^p \sqrt{\left(\frac{h}{h_0^p}m_y - m_y^2\right)\left(1 - \frac{h}{h_0^p}m_y\right)} , \tag{3.22}$$

where $h_0^p = \dfrac{D_0 + D}{2} = \dfrac{h_0}{2}$. It is clear from the second equation in formula (3.21) that

m_y can only take positive values because m_x can not be larger than 1. According to the initial conditions $m_y(0)$ is equal to 0 and consequently, we can choose the positive sign in equation (3.22) for the first stage of the precessional motion. Since m_x has to reach negative values (basin of attraction of the equilibrium state $m_x = -1$), it can be proved that h_0^p has the meaning of the critical field for precessional switching (see Section 3.2). For $h > h_0^p$, the integration of equation (3.22) yields:

$$ht = \frac{1}{2} \int_0^{m_y} \frac{ds}{\sqrt{(1-ks)(k-s)s}}, \quad \text{for } 0 \le m_y \le k, \tag{3.23}$$

where $k = h_0^p / h$. The right hand side represents an elliptic type integral which can be inverted in terms of elliptic functions [85, 86]. Therefore, the solution of equation (3.22) can be written as follows:

$$m_y(t) = k \cdot sn^2(ht, k), \tag{3.24}$$

where $sn(u,k)$ is the "sine-type" Jacobi elliptic function. Although this formula was derived only for the first stage of the precessional motion, it can be proved that it is valid at any instant of time. By plugging this expression into formula (3.21) and making use of the fundamental relation for elliptic functions, the analytical solutions for m_x and m_z components are found to have the following expressions:

$$\begin{cases} m_x = cn(ht, k) \\ m_z = sn(ht,k)dn(ht,k) \end{cases}, \tag{3.25}$$

where $cn(u,k)$ and $dn(u,k)$ denotes "cosine-type" and "delta-type" Jacobi elliptic functions. A graphical illustration of these analytical solutions is shown in Figure

3.11 for the same parameters used in the representation of damping switching in Figure 3.6. Since the precessional switching is not sensible to small variations of angle θ, the initial condition for the precessional switching is taken $\theta_0=0^\circ$. By using the numerical method presented by Serpico, Mayergoyz and Bertotti, in [75], we have solved equation (3.1) and found the precessional switching trajectories corresponding to various values of the damping constant. Selected numerical results are presented in Figure 3.12. It is apparent from this figure that the "undamped" trajectory offers indeed a good approximation of the precessional switchings corresponding to damping parameters of physical interest ($\alpha \in (10^{-3}, 10^{-1})$). An analytical approach to compute the damping corrections can be found in Section 3.2. We stress that Figures 3.6 and 3.12 have their time scales offered in nanoseconds and picoseconds, respectively. It is apparent from these figures that the precessional switchings are substantially faster than the damping ones. This aspect is next analyzed in a systematic way.

It is clear from the first formula in (3.25) that m_x will reach the value of -1 at the time τ^p equal to half period of $cn(ht, k)$. Thus, the switching time for the precessional mode of magnetization reversal is given by the formula:

$$\tau^p = \frac{2K(k)}{\gamma H} = \frac{2K(H_0^p / H)}{\gamma H}, \tag{3.26}$$

where $K(k)$ is the first kind complete elliptical integral, and $H_0^p = H_0/2$. The dependence of $1/\tau^p$ on H, as follows from formula (3.26), is presented in Figure 3.5 (b). It is apparent that $1/\tau^p$ can be considered linearly dependent on H for sufficiently large H.

It is important to stress that in the case of the precessional switching the timing of switching-off the applied magnetic field is crucial, in the sense that there is a certain time-window during which switching-off must occur. It is easy to see that this time-window is defined by the formula:

$$\frac{K(k)}{\gamma H} < \tau^p < \frac{3K(k)}{\gamma H}, \tag{3.27}$$

that guarantees that after switching-off the magnetization will be in the basin of the attractor m_x=-1. We recall that the damping switching is sensitive to the minimum pulse time and "insensitive" to the maximum pulse time. Despite this disadvantage, the precessional switching has clear advantages over the damping switching. Namely, the critical field H_0^p is half of the critical field H_0 for the "damping" case and the switching is much faster than in the "damping" case. The ratio between the two switching times computed by using formulae (3.7) and (3.26) gives:

$$\frac{\tau^p}{\tau} = \alpha f_1(b), \tag{3.28}$$

where $f_1(b) = \dfrac{2K(1/2b)}{b\left[\dfrac{\ln(1-\cos\theta_0)}{2(1-b)} + \dfrac{\ln(1+\cos\theta_0)}{2(1+b)} - \dfrac{1}{1-b^2}\ln\dfrac{b-\cos\theta_0}{b}\right]}$ and $b = H/H_0$.

The graph of $f_2(b)$ for selected values of θ_0 is shown in Figure 3.13. It is clear from this Figure and formula (3.28) that the precessional switching is on the order of $1/\alpha$ times faster than the damping switching. For applied fields close to respective damping critical fields (β close to 1), this advantage is even more pronounced.

It is instructive to compare switching times for precessional and damping switchings for the same ratio of applied fields to respective critical fields: $\beta = h/h_0 = h^p/h_0^p$. By using formulas (3.7) and (3.26), we find:

$$\frac{\tilde{\tau}^p}{\tilde{\tau}} = \alpha f_2(\beta),$$ (3.29)

where $f_2(\beta) = \dfrac{4K(1/\beta)}{\beta\left[\dfrac{\ln(1-\cos\theta_0)}{2(1-\beta)} + \dfrac{\ln(1+\cos\theta_0)}{2(1+\beta)} - \dfrac{1}{1-\beta^2}\ln\dfrac{\beta-\cos\theta_0}{\beta}\right]}$.

The graph of $f_2(\beta)$ for selected values of θ_0 is shown in Figure 3.14.

Even though the switching is guaranteed if the applied magnetic field is switched-off during the time-window given in formula (3.27), some additional time is needed for magnetization to relax to the new equilibrium state. This aspect is known as "ringing" phenomena associated to precessional switching. The additional time can be computed using formula (3.6) in which $h=0$, m_{x_0} will be the value of x-component of magnetization at the switching-off moment, and m_x is the desired final value sufficiently close to the equilibrium state $m_x=-1$.
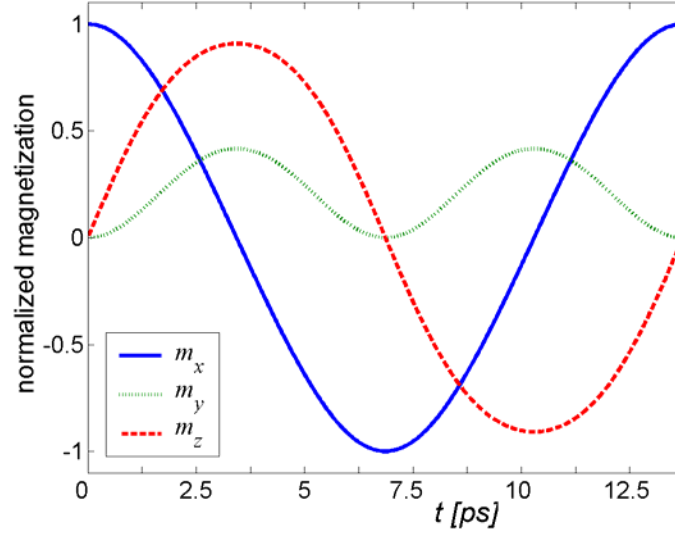
Figure 3.11: Evolution of magnetization components with time for precessional switching corresponding to field ratio $H/H_0 = h/h_0 = 1.2$. The initial condition is $m_x = 1$, product γH_0 is considered to be $4 \times 10^{11} s^{-1}$, and the damping is neglected.
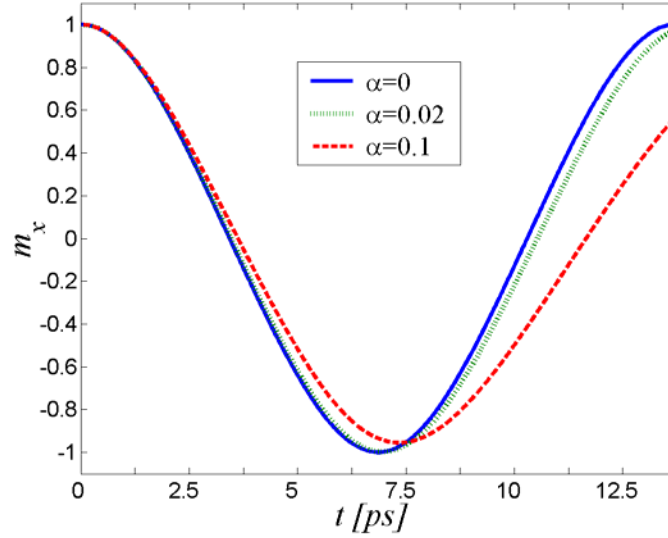
Figure 3.12: Numerical solutions for m_x dynamics of precessional switching for field ratio $H/H_0 = h/h_0 = 1.2$ and selected values of α. The initial condition is $m_x = 1$, and product γH_0 is considered to be $4 \times 10^{11} s^{-1}$.
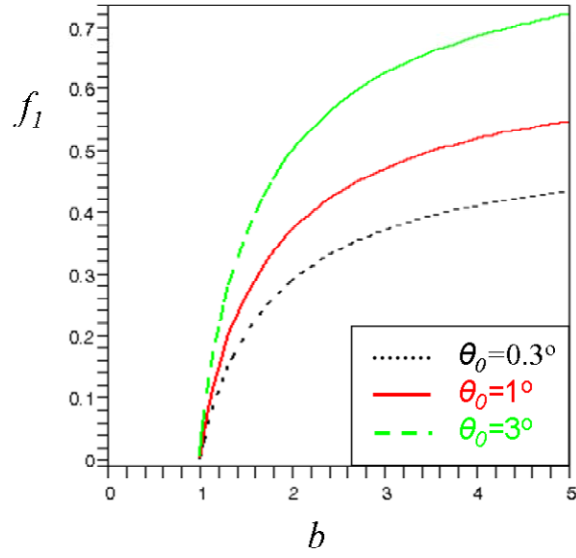
Figure 3.13: Dependence of function f_1 on ratio $b=h/h_0$ for selected values of initial angle θ_0.
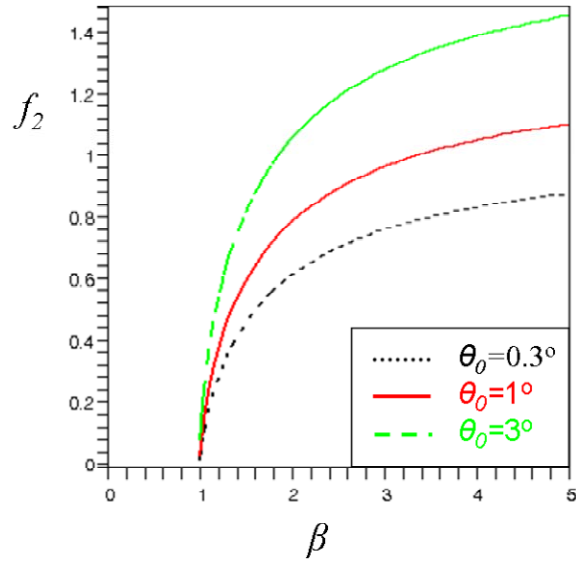
Figure 3.14: Dependence of function f_2 on ratio $\beta = h/h_0 = h^p/h_0^p$ for selected values of initial angle θ_0.

3.2. Dynamical critical field curve for precessional switchings

In this section, explicit expressions for critical fields and field pulse durations, which guarantee the magnetization switching for arbitrary orientations of the applied field, are derived. In the end, the effect of damping on the critical field is discussed.

The efficiency of magnetization switching process in uniformly magnetized thin films and nanoparticles subject to a rectangular pulsed magnetic field can be mainly characterized by the critical field pulse duration of the magnetic field that guarantee the switching. In the previous section we have derived the expressions for these quantities in the case of perpendicular media having the pulsed magnetic fields applied along and perpendicular to the easy axis. Here, we extend these results to arbitrary orientations of the applied field.

Consider a uniformly magnetized perpendicular thin film subject to a rectangular pulse of spatially uniform magnetic field applied at some obtuse angle with respect to x-axis (See Figure 3.15). As discussed in the previous section, the essence of the precessional switching is to move the magnetization from the equilibrium point $\mathbf{m} = \mathbf{e}_x$ to the basin of attraction corresponding to the other equilibrium point $\mathbf{m} = -\mathbf{e}_x$ using the precessional component of the magnetization dynamics. This process is driven by a short pulsed magnetic field that should be switched off during the time when the magnetization motion occurs in the basin of attraction of $-\mathbf{e}_x$. If this condition is satisfied the magnetization will relax, as a result of damping, to the new equilibrium position.
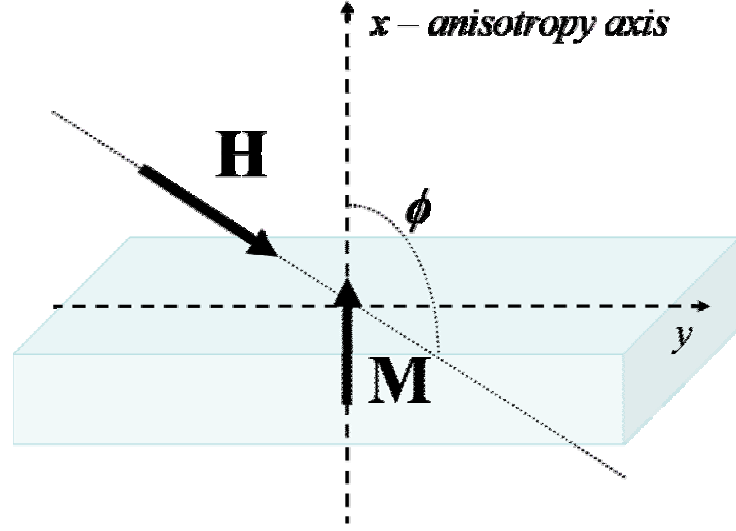
Figure 3.15: Configuration for precessional switching in perpendicular media.

As discussed in the previous section, the precession of magnetization is very fast, and consequently, the dissipative effects can be neglected during the time when the external magnetic field is applied. This means that the dynamics of magnetization under the applied magnetic field can be studied using the "reduced" equation:

$$\frac{d\mathbf{m}}{dt} = -\mathbf{m} \times \mathbf{h}_{eff}(\mathbf{m}).\qquad(3.30)$$

where $\mathbf{h}_{eff} = -D(m_z\mathbf{e}_z + m_y\mathbf{e}_y) + D_0 m_x\mathbf{e}_x - h_x\mathbf{e}_x + h_y\mathbf{e}_y = -D\mathbf{m} + D_x m_x\mathbf{e}_x - h_x\mathbf{e}_x + h_y\mathbf{e}_y$

with $D_x = D + D_0$. Since the term proportional with $\mathbf{m}$ has no influence on the magnetization dynamics, an equivalent equation is obtained by dropping off this term from the expression of effective field. Thus, the effective field can be written as:

$$\mathbf{h}_{eff} = D_x m_x\mathbf{e}_x - h_x\mathbf{e}_x + h_y\mathbf{e}_y.\qquad(3.31)$$

Because the magnetic field is applied at some obtuse angle with respect to x-axis, the possible values taken by h_x are all positive. The free energy associated to this effective field reads:

$$g = -\left(D_x/2\right)m_x^2 + h_x m_x - h_y m_y \qquad (3.32)$$

In the case of rectangular pulses, this equation admits two integrals of motion that express the conservation of magnetization magnitude:

$$m_x^2 + m_y^2 + m_z^2 = 1, \qquad (3.33)$$

and the conservation of magnetic free energy:

$$-\left(D_x/2\right)m_x^2 + h_x m_x - h_y m_y = -\left(D_x/2\right) + h_x. \qquad (3.34)$$

These two conservation laws define the trajectory of the magnetization that can be geometrically represented as the intersection curve between the sphere (3.33) and the parabolic cylinder (3.34). The projection of precessional magnetization motion on the (m_x,m_y)-plane occurs along the parabola (3.34) that is confined within the unit disk $m_x^2 + m_y^2 \leq 1$. Depending on the values of h_x and h_y, there are two distinct classes of parabolic trajectories. Trajectories of the first class consist of a single piece of parabola (for instance, O-B in Figure 3.16) while trajectories of the second class consist of two disjoint pieces of the parabola (for instance, O-E and F-G in Figure 3.16). It is apparent that every piece of the parabola inside the unit circle corresponds to recurrent (periodic) motion on the unit sphere. This back-and-forth motion occurs along the curves located on positive (m_z>0) and negative (m_z<0) hemispheres, and these curves are symmetric with respect to the (m_x,m_y)-plane. As a consequence of this symmetry these back-and-forth pieces of actual magnetization trajectories are orthogonally projected into the same pieces of parabolic trajectories on the (m_x,m_y)-plane.
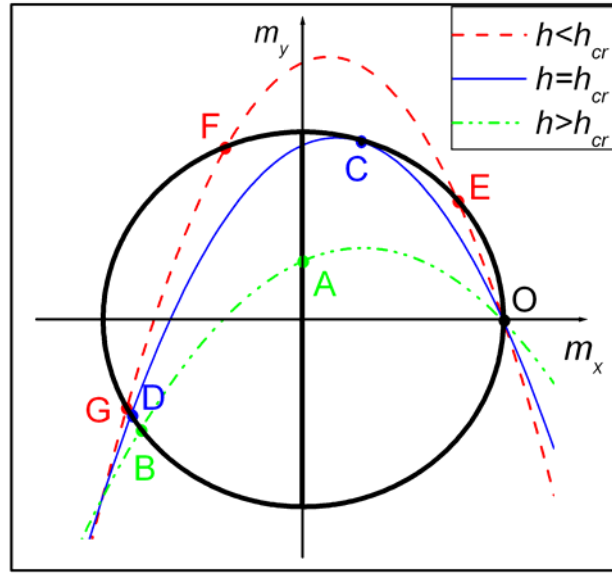
Figure 3.16: Orthogonal projections of magnetization trajectories on (m_x, m_y)-plane.
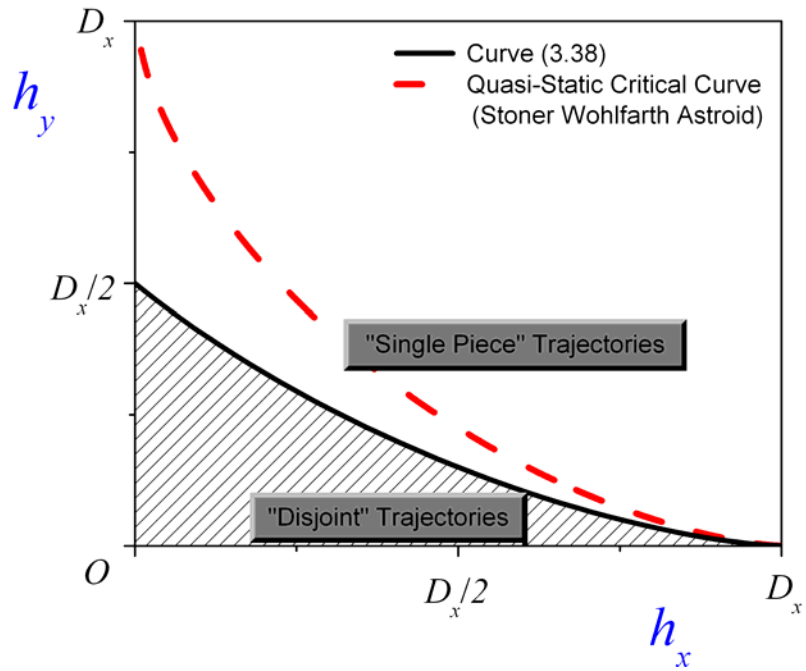
Figure 3.17: "Separating" curve (3.38) and regions in (h_x, h_y)-plane corresponding to the first and second classes of parabolic trajectories.

It is clear from the above discussion that the precessional switching may only take place along the "single-piece" trajectories that intersect the unit circle:

$$m_x^2 + m_y^2 = 1,$$
(3.35)

at negative values of m_x. The "disjoint" parabolic trajectories are separated from single-piece parabolic trajectories by the parabola O-C-D that is tangent to the unit circle. By using the implicit differentiation, one can find from (3.34) and (3.35) that the condition of tangency of parabolic trajectory to the unit circle leads to the following relation:

$$D_x m_x m_y - h_x m_y - h_y m_x = 0.$$
(3.36)

At point C (Figure 3.16), three equations (3.34), (3.35), and (3.36) are satisfied. These three equations define the curve h_y versus h_x that separates the values of h_x and h_y which correspond to the first and second classes of parabolic trajectories, respectively. This h_y versus h_x curve can be easily found in parametric form by introducing the polar angle θ such that:

$$m_x = \cos\theta, \qquad m_y = \sin\theta.$$
(3.37)

By substituting (3.37) into (3.34) and (3.36), and solving these equations with respect to h_x and h_y, we arrive at the following parametric equation for the "separating" curve:

$$h_x = D_x \cos\theta \cos^2(\theta/2), \qquad h_y = D_x \sin\theta \sin^2(\theta/2),$$
(3.38)

which is represented in Figure 3.17.

The separating curve (3.38) is valid only for positive values of h_x. For negative values of h_x, all the parabolic trajectories emanating from point O (see Figure 3.16) intersect the unit circle only once. Formulas similar to (3.38) were derived using a

70

different reasoning in [87]. Curves similar to the ones obtained using formula (3.38) were also numerically found by using a "trial and error" method to determine the critical fields for precessional switching [42].

Next, we shall find the conditions on h_x and h_y that guarantee that single-piece parabolic trajectories intersect the unit circle (3.35) at negative values of m_x. By using (3.34) and (3.35), we find that m_x corresponding to the above intersection satisfies the following cubic equation:

$$D_x^2 m_x^3 + D_x\left(D_x - 4h_x\right)m_x^2 - \left(D_x^2 - 4h_x^2 - 4h_y^2\right)m_x + 4h_y^2 - \left(2h_x - D_x\right)^2 = 0 . \quad (3.39)$$

For a single-piece parabolic trajectory intersecting the unit circle (3.35) at a negative value of m_x, the last equation must have two complex conjugate roots and one negative root. This implies that:

$$4h_y^2 < \left(2h_x - D_x\right)^2 . \quad (3.40)$$

This region is bounded by the intersecting lines given by the following formula:

$$h_y = \pm\left[h_x - (D_x / 2)\right]. \quad (3.41)$$

By combining this region with the single-piece trajectory region bounded by "separating" curve (3.38), we conclude that the values of h_x and h_y that guarantee the precessional switching correspond to the (h_x, h_y)-points outside the shaded area shown in Figure 3.18. The boundary of this region corresponds to the critical fields for precessional switching of perpendicular media ("dynamical critical curve"). The minimum field amplitude for switching is $0.385 D_x$, and it corresponds to the field orientation $h_y / h_x = \sqrt{2}$.

71
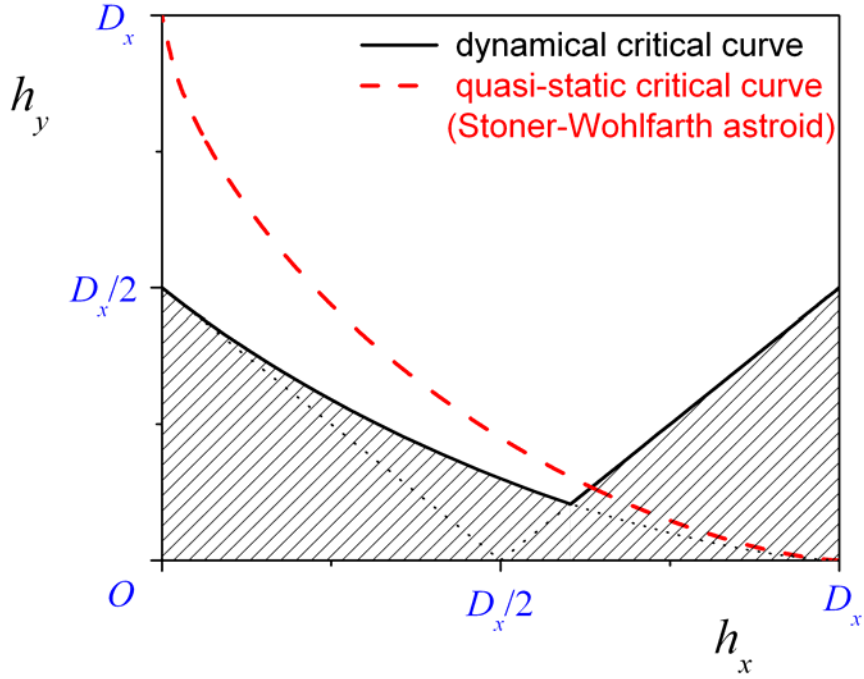
Figure 3.18: Critical field curve for precessional switching and quasi-static critical curve for the conventional magnetization reversal.

In Figure 3.18, the dynamical critical curve computed above is plotted against the quasi-static critical field curve which represents the limit of the present approach to magnetization reversal in magnetic recording. The analytical expressions for the quasi-static case can be derived by analyzing the stability conditions for the free energy minima. This analysis was first published in the seminal article of Stoner and Wohlfarth [27] along with the computation of hysteresis cycles for various orientation of the applied field. It is proved that the quasi-static critical field curve is an astroid, known as Stoner-Wohlfarth astroid in magnetic recording. This curve has its implicit

expression given by $\left(h_x\right)^{2/3}+\left(h_y\right)^{2/3}=\left(D_x\right)^{2/3}$, which can be explicitly described in the following form:

$$\begin{cases} h_x = D_x \cos^3 \varphi \\ h_y = D_x \sin^3 \varphi \end{cases}, \tag{3.42}$$

where φ is the curve parameter, which takes values from 0 to $\pi/2$ in order to completely describe the curve plotted in Figures 3.17 and 3.18

For magnetic fields corresponding to the points located below the astroid (see Figure 3.18), the energy expression has two minima, while for the points located above the astroid, the corresponding energy has only one minimum. In the case of the quasi-static magnetization reversal, the external magnetic field applied at some obtuse angle with respect to x-axis is "slowly" increased from zero to some given value. The magnetization, initially oriented along $+\mathbf{e}_x$, is simply following the metastable state continuously related to its initial equilibrium state. When the field is reaching its critical value the corresponding magnetization state becomes unstable and the magnetization "jumps" to the stable state. During this jump, the magnetization is reversing its orientation with respect to x-axis. Once the transition to the new equilibrium state is completed, the applied field can be slowly decreased to the zero value, and the magnetization will be finally oriented along $-\mathbf{e}_x$.

Since the whole process may take place on a microsecond time scale, the use of the word "slow" for the previous description of the external field evolution may be found somehow confusing. That is why we mention that this term is used with respect to energy relaxation time scale (nanosecond scale).

In the case of precessional switching, the timing of switching off the magnetic field is crucial, in the sense there exists a periodic sequence of time windows during which the switching-off must occur. These time-windows correspond to the time intervals when the magnetization moves back-and-forth between the points A and B on the generic trajectory O-A-B shown in Figure 3.16. To find these time windows, we shall recall equation (3.30), whose x-component can be written as follows:

$$\frac{dm_x}{dt} = h_y m_z .$$ (3.43)

By using equations (3.33) and (3.34), one can easily find:

$$h_y m_z (m_x) = \pm \sqrt{h_y^2 \left(1 - m_x^2\right) - \left(-(D_x/2)m_x^2 + h_x m_x + (D_x/2) - h_x\right)^2} .$$ (3.44)

From equations (3.43) and (3.44), the time-windows for switching the field off can be expressed as:

$$n\left(t_i + t_f\right) + t_i < t < n\left(t_i + t_f\right) + t_f, \quad (n=0,1,2 \ldots),$$ (3.45)

where:

$$t_i = \int_0^1 \frac{dm_x}{\left|h_y m_z (m_x)\right|},$$ (3.46)

$$t_f = t_i + 2 \int_{\tilde{m}_x}^0 \frac{dm_x}{\left|h_y m_z (m_x)\right|},$$ (3.47)

and $m_x=1$, $m_x=0$ and $m_x=\tilde{m}_x$ correspond to points O, A and B, respectively. The value of $\tilde{m}_x$ can be found by solving simultaneous equations (3.34) and (3.35). It can be also remarked that integrals (3.46) and (3.47) can be reduced to elliptic integrals. We stress that the accuracy of the equation (3.45) decreases with the number of precessional cycles n as a result of damping, which was neglected in this derivation.

74

Examples of constant t_i field lines calculated from equations (3.45) and (3.46), are shown in Figure 3.19. These lines give the field threshold that must be exceeded if one wants to force switching in time shorter than the indicated values of t_i. The normalized constant $(D_x \gamma M_s)$ is on order of 10^{11} s^{-1}, and usually, it takes values between 2 and 6 on this scale. As an example, let us consider $D_x \gamma M_s = 4 \times 10^{11} s^{-1}$ and consequently, the normalized time presented in this Figure should be multiplied by 2.5 *ps,* in order to obtain the real initial time. As the "dynamical critical curve" is approached, the corresponding switching time tends to infinity.
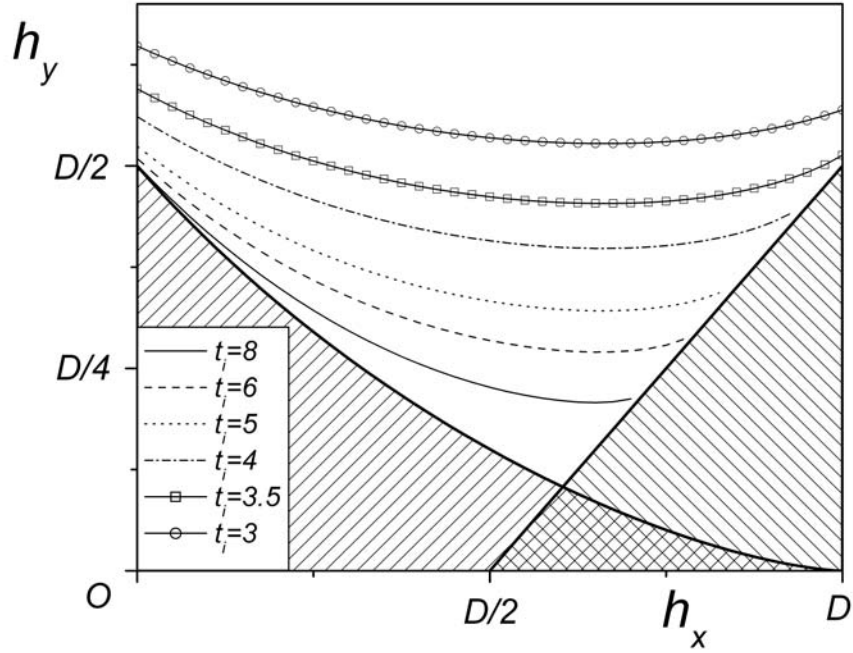
Figure 3.19: Lines of constant minimum switching times t_i calculated from equations (3.44) and (3.46). The corresponding values of t_i are expressed in units of $(D_x \gamma M_s)^{-1}$.

Next, we shall discuss the effect of damping on critical fields for the precessional switching in perpendicular media. Using the numerical method previously mentioned and presented in [86] we have solved equation (3.1), coupled to the effective field (3.31), and found the critical field for precessional switching as a function of damping parameter α. This has been done for various orientations of the applied field. We have observed that the critical field is linearly increasing with α as it is illustrated by the Figure 3.20.

In order to explain this linear behavior and to derive an analytical formula for these "damping corrections", we first extract from equations (3.1), (3.31), and (3.32), the following equation for the rate of the energy dissipation:

$$\frac{dg}{dt}(t) = -\alpha \left\| \mathbf{m}(t) \times \mathbf{h}_{eff}(\mathbf{m}(t)) \right\|^2 . \qquad (3.48)$$

For the sake of presentation, let us consider the case when the field is applied along y direction. Thus, at the beginning of the motion the energy is equal to $-D_x/2$ and the condition of switching requires that m_x should reach zero, and consequently, the energy should be equal with $-h_y m_y$ at that instant of time. The minimum applied field required to switch the magnetization corresponds to the magnetization trajectory that passes through the points $(m_x = 1, m_y = 0)$ and $(m_x = 0, m_y = 1)$. By using equation (3.48), the following relation is found for the critical field associated to this "critical" trajectory:

$$h_{cr}^\alpha - D_x / 2 = \alpha \int_0^{T_1} \left\| \mathbf{m}(t) \times \mathbf{h}_{eff}^\alpha (\mathbf{m}(t)) \right\|^2 dt , \qquad (3.49)$$

where T_1 represents the instant of time when m_x reaches zero. Although the analytical expressions for the solutions of equation (3.1), coupled to (3.31), are not readily

76

available, the above critical trajectory can be well approximated by the trajectory of the undamped motion (equations (3.30)-(3.31)) passing through the same limit points. The analytical expressions for these undamped solutions have been presented in the previous section. Thus,

$$\frac{h_{cr}^{\alpha}}{D_x} - \frac{1}{2} \approx \alpha \frac{1}{4} \int_0^{K(1)} \left[1 - sn^4 \left(\frac{t}{2}, 1 \right) \right] dt \approx \alpha \cdot 0.667, \tag{3.50}$$

where K and sn denote the first kind complete elliptic integral and "sine-type" Jacobi elliptic function, respectively. The linear dependence of critical field h_{cr}^{α} on α is now apparent.
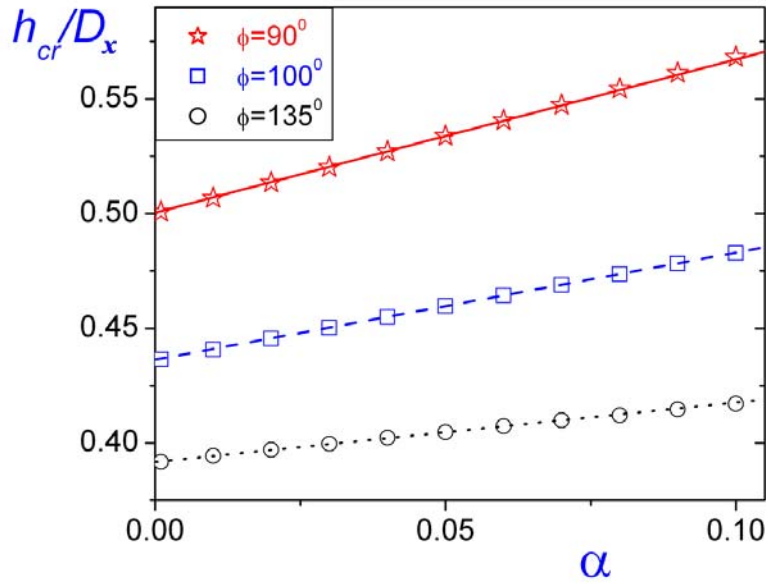
Figure 3.20: Damping corrections for critical fields; numerical results are represented by symbols and the analytical result given by formula *(3.50)* is plotted by solid line. The angle between the direction of applied field and x-axis is denoted by ϕ.

77

3.3. Inverse problem approach to the design of magnetic field pulses for precessional switching

In this section the inverse problem approach to the analysis of precessional switching in perpendicular thin films subject to time varying magnetic field is presented. This approach leads to direct calculations of expressions for magnetic field pulses that guarantee the precessional switching. The effectiveness of the developed technique is illustrated by examples.

A central problem of the research studies on precessional magnetization reversals is the design of magnetic field pulses that guarantee the precessional switching. This problem has been addressed experimentally and numerically by using a "trial and error" method. Next, the "inverse problem" approach is developed. This approach is purely algebraic in nature and leads to the direct calculations of expressions for the magnetic field pulses that guarantee precessional switching.
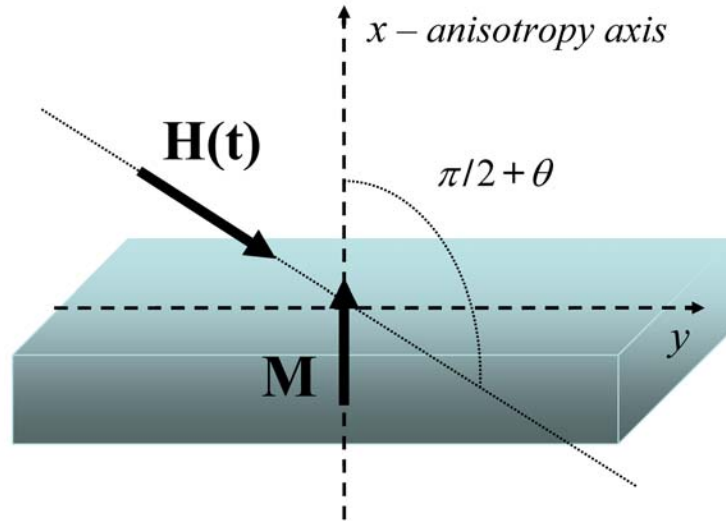
Figure 3.21: Configuration for precessional switching in perpendicular media.

To start the discussion, consider a thin film that is uniformly magnetized along anisotropy x-axis and subject to a spatially uniform pulsed magnetic field applied at some angle $\pi/2+\theta$ with respect to anisotropy axis (see Figure 3.21). The precessional switching is usually so fast that damping effects can be neglected during the time when the magnetic field pulse is applied. Therefore, this switching can be studied by using the "reduced" form of Landau-Lifshitz equation, which has the following dimensionless expression:

$$\frac{d\mathbf{m}}{dt} = -\mathbf{m} \times \mathbf{h}_{\textit{eff}}(\mathbf{m},t), \qquad (3.51)$$

where the effective field is given by:

$$\mathbf{h}_{\textit{eff}}(\mathbf{m},t) = \left(D_x m_x - h(t)\sin\theta\right)\mathbf{e}_x + h(t)\cos\theta\,\mathbf{e}_y. \qquad (3.52)$$

Positive constant D_x accounts for perpendicular x-anisotropy and demagnetizing field.

Vector dynamic equation (3.51) is equivalent to three coupled scalar dynamic equations for cartesian components of $\mathbf{m}$. Since vector dynamic equation (3.51) has the integral of motion

$$\left|\mathbf{m}(t)\right| = 1, \qquad (3.53)$$

this equation can be used instead of the scalar equation for dm_z/dt. This leads to the following coupled equations:

$$\frac{dm_x}{dt} = m_z h(t)\cos\theta, \qquad (3.54)$$

$$\frac{dm_y}{dt} = -\left(D_x m_x - h(t)\sin\theta\right)m_z, \qquad (3.55)$$

$$m_x^2 + m_y^2 + m_z^2 = 1. \qquad (3.56)$$

An inverse problem approach to this problem consists of choosing the desired dynamics for one component of the magnetization and finding the other components and the magnetic field pulse from equations (3.54)-(3.56). Since our goal is to find magnetic field pulses that guarantee precessional switchings of magnetization, the most appealing choice is the dynamics of m_x component. From equations (3.54)-(3.56) the following relation can be derived:

$$\frac{dm_y}{dt} = D_x m_x \sqrt{1 - m_x^2 - m_y^2} + \frac{dm_x}{dt} \tan \theta, \tag{3.57}$$

where the negative sign of the square root is chosen in the expression of m_z and, without essentially limiting the generality of the solution, this sign is maintained constant during the precessional switching. Since $m_x(t)$ is given, formula (3.57) can be treated as a differential equation with respect to $m_y(t)$. By solving this equation and using equation (3.54), we can recover the pulsed magnetic field:

$$h(t) = \frac{-1/\cos\theta}{\sqrt{1 - m_x^2 - m_y^2}} \frac{dm_x}{dt}, \tag{3.58}$$

which will guarantee the desired precessional switching.

Although the "desired" inverse problem approach is straightforward, it has two drawbacks. First, the dynamics of m_x should be chosen such that the existence and uniqueness of the solution for equation (3.57) is guaranteed. Second, this approach requires numerical integration of differential equation (3.57) and does not lead to analytical expressions for $h(t)$. However, the mathematical structures of equations (3.54)-(3.56) are such that an alternative approach to the solution of inverse problem of finding $h(t)$, which leads the magnetization switching, can be developed.

The alternative inverse approach, which is purely algebraic in nature, is facilitated by the elimination of magnetic field $h(t)$ from equation (3.55). This is achieved by introducing the component $\tilde{m}_y(t)$ of magnetization along the field direction:

$$\tilde{m}_y = -m_x \sin\theta + m_y \cos\theta, \tag{3.59}$$

and writing coupled equation (3.54)-(3.56) in terms of $m_x(t)$, $\tilde{m}_y(t)$ and $m_z(t)$:

$$m_x m_z = -\frac{1}{D_x \cos\theta} \frac{d\tilde{m}_y}{dt}, \tag{3.60}$$

$$\left(m_x + \tilde{m}_y \sin\theta\right)^2 + m_z^2 \cos^2\theta = \left(1 - \tilde{m}_y^2\right)\cos^2\theta. \tag{3.61}$$

In this inverse problem approach, the dynamics of $\tilde{m}_y(t)$ that leads to the precessional switching must be first chosen. Then, equations (3.60) and (3.61) can be treated as coupled algebraic equations with respect to m_x and m_z. Solving this system, $m_x(t)$ and $m_z(t)$ are found as functions of $\tilde{m}_y(t)$ and its derivative. In addition, by differentiating equations (3.60) and (3.61) with respect to time we arrived at coupled linear equations for dm_x/dt and dm_z/dt. The solution of these equations yields the formula for dm_x/dt as an algebraic function of $\tilde{m}_y(t)$ and its first two derivatives. Then, the pulsed magnetic field $h(t)$ is found from equation (3.54) as an algebraic expression of $\tilde{m}_y(t)$ and its first two derivatives. The main difficulty in this approach is the choice of appropriate $\tilde{m}_y(t)$ that guarantees the precessional switching. Next, it is discussed how this difficulty can be dealt with.

First, it can be observed that the solution of coupled algebraic equations (3.60) and (3.61) can be illustrated geometrically as the points of intersections of a hyperbola represented by equation (3.60) and an ellipse represented by equation (3.61) (see Figure 3.22). These hyperbola and ellipse are changed as $\tilde{m}_y(t)$ evolves with time. The main stages in a scenario for precessional switching are qualitatively illustrated by "bold dots" on Figure 3.22. At the initial instant of time, $d\tilde{m}_y/dt = 0$ and the hyperbola "coincides" with axes $m_x = 0$ and $m_z = 0$. Point $(1,0)$ of intersection of the ellipse with these axes corresponds to the initial state of the magnetization (see Figure 3.22(a)).
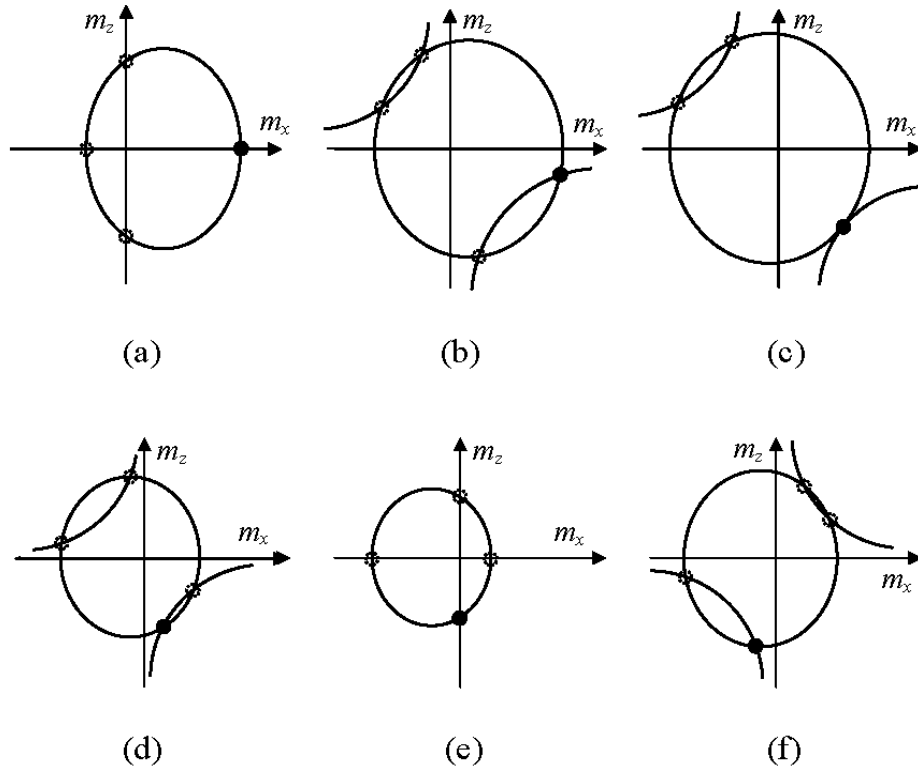
Figure 3.22 (a)-(f): Geometrical scenario for the solutions of the system (3.60)-(3.61) at selected instants of time.

As $\tilde{m}_y(t)$ is monotonically increased, the initial magnetization evolution corresponds to the solution of equations (3.60)-(3.61) with the largest positive value of m_x (see Figure 3.22(b)). At some point of time t_0, the two solutions of equations (3.60)-(3.61) with positive values of m_x coincide (Figure 3.22(c)). As $\tilde{m}_y(t)$ is further increased, the magnetization evolution follows the solution of equations (3.60)-(3.61) with the smallest positive value of m_x (Figure 3.22(d)). When the maximum value of $\tilde{m}_y(t)$ is reached ($d\tilde{m}_y/dt = 0$), m_x is equal to zero (Figure 3.22(e)). As $\tilde{m}_y(t)$ is monotonically decreased, m_x takes negative values (Figure 3.22(f)). It is clear from the discussions presented in the previous sections that if m_x has a negative value when the magnetic field pulse is stopped, magnetization will relax to the equilibrium state $m_x = -1$.

It can be inferred from the above discussion that the precessional switching of magnetization will occur if during the monotonic increase of $\tilde{m}_y(t)$ there are two solutions of equations (3.60)-(3.61) with positive values of m_x and at some intermediate instant of time t_0 these two solutions coincide. Next, this assertion is rigorously proved and the above conditions are framed in purely algebraic terms. To this end, we reduce the coupled algebraic equations (3.60)-(3.61) to the following quartic equation:

$$F(m_x,t) = m_x^2 \left[m_x + a(t) \right]^2 - b(t)m_x^2 + c^2(t) = 0, \qquad (3.62)$$

$$a(t) = \tilde{m}_y(t)\sin\theta, \quad b(t) = \left[1 - \tilde{m}_y^2(t) \right]\cos^2\theta, \quad c(t) = (1/D_x)d\tilde{m}_y/dt. \quad (3.63)$$

During the monotonic increase of $\tilde{m}_y(t)$, positive solutions of quartic equation (3.62) are of interest. It can be inferred from equation (3.61) that positive m_x-solutions are only possible if $\tilde{m}_y(t) < \cos\theta$. Thus, we restrict our attention to $\tilde{m}_y(t)$ trajectories that satisfy this condition.

From (3.62)-(3.63), we derive:

$$\frac{dF}{dm_x} = 2m_x\left[2m_x^2 + 3a(t)m_x + a^2(t) - b(t)\right], \tag{3.64}$$

$$a^2(t) - b(t) = \tilde{m}_y^2(t) - \cos^2\theta. \tag{3.65}$$

Since the discriminant of the second order polynomial found inside the square brackets $\Delta(t) = a^2(t) + 8b(t) \geq 0$, the function $\frac{dF}{dm_x}$ has three real zeros: 0, $m_x^{(s)}$, and $m_x^{(l)}$, where the superscripts $^{(s)}$ and $^{(l)}$ imply that $m_x^{(s)} \leq m_x^{(l)}$. According to the Viète's relations for the roots of polynomial (3.64), $m_x^{(s)}$ and $m_x^{(l)}$ satisfy:

$$\begin{cases} m_x^{(s)} + m_x^{(l)} = -\dfrac{3}{2}\tilde{m}_y(t)\sin\theta \\ m_x^{(s)} \cdot m_x^{(l)} = \dfrac{1}{2}\left(\tilde{m}_y^2(t) - \cos^2\theta\right) \end{cases}, \tag{3.66}$$

It is clear form these formulae that $m_x^{(s)}$ is negative and $m_x^{(l)}$ is positive for $-\cos\theta \leq \tilde{m}_y \leq \cos\theta$, while for $-1 \leq \tilde{m}_y \leq -\cos\theta$, both roots are positive. The Rolle sequences associated to equation (3.62) for these two cases are given in Tables 1 and 2. Results $\lim\limits_{m_x \to \pm\infty} F(m_x) = +\infty$ and $F(0) = c^2(t) \geq 0$ are apparent from formula (3.62).

Moreover, when $-1 \leq \tilde{m}_y \leq -\cos\theta$, and consequently $m_x^{(s)}$ is positive, $F\left(m_x^{(s)}\right)$ can be written:

$$F\left(m_x^{(s)}\right) = \left(m_x^{(s)}\right)^3 \left(m_x^{(s)} + a(t)\right) + c^2(t)$$

$$= \left(m_x^{(s)}\right)^3 \left[\frac{\sqrt{a^2(t) + 8b(t)} - a(t)}{4}\right] + c^2(t). \tag{3.67}$$

Since $b(t)$ is positive the expression found inside square brackets is positive, and consequently, $F\left(m_x^{(s)}\right)$ is positive. These remarks justify the signs presented in Tables 1 and 2.

x	$-\infty$	$m_x^{(s)}$	0	$m_x^{(l)}$	$+\infty$
$F(x)$	$+$	$F(m_x^{(s)})$	$+$	$F(m_x^{(l)})$	$+$

Table 1: The Rolle sequence associated to equation (3.62) for $-\cos\theta \le \tilde{m}_y \le \cos\theta$.

x	$-\infty$	0	$m_x^{(s)}$	$m_x^{(l)}$	$+\infty$
$F(x)$	$+$	$+$	$+$	$F(m_x^{(l)})$	$+$

Table 2: The Rolle sequence associated to equation (3.62) for $-1 \le \tilde{m}_y \le -\cos\theta$.

According the Rolle theorem from the basic calculus, the results presented in these tables imply that quartic equation (3.62) has two positive solutions if and only if:

$$F\left(m_x^{(l)}(t), t\right) \le 0. \tag{3.68}$$

These two solutions are distinct and separated by $m_x^{(l)}$ in the case of strict inequality in formula (3.68). On the other hand, these two positive solutions coincide with one another and with $m_x^{(l)}$ when the equality is achieved in formula (3.68).

Moreover, since we are interested in positive solutions which are smaller than one, let us notice that $F(1,t) = \left[\tilde{m}_y(t) + \sin\theta\right]^2 + c^2(t) > 0$ and the relation $m_x^{(l)} \leq 1$ is finally equivalent to $\left(\tilde{m}_y + \sin\theta\right)^2 + \left(1 - \tilde{m}_y^2\right) \geq 0$ which is obviously true. Therefore the condition (3.68) is tantamount to the fact that function $F(m_x,t)$ has two positive solutions on the interval [0, 1].

Since $m_x^{(l)}(t)$ is a function of $\tilde{m}_y(t)$, inequality (3.68) can be phrased as the algebraic condition on $\tilde{m}_y(t)$ that guarantees the switching of magnetization from the state when $m_x = 1$ to the state when $m_x = 0$. Namely, the above switching will occur for any monotonically increasing function $\tilde{m}_y(t)$ on the interval [0, T_1], such that formula (3.68) is valid and the equality in this formula is achieved at some instant of time belonging to $[0, T_1]$, denoted by t_0. Indeed, during the time interval [0, t_0] the evolution of m_x coincides with the evolution of the largest positive solution of quartic equation. This is because $m_x(0) = 1$. During the time interval [t_0, T_1] the evolution of m_x coincides with the evolution of the smallest positive solution of quartic equation (3.62), and in this way, m_x reaches zero. It can be proved that this "switch" at time t_0 between the largest and the smallest positive solutions of equation (3.62) is imposed by the differentiability of m_x at $t = t_0$, as it is required by the Landau-Lifshitz

86

equation. This proof is quite involved and for the sake of presentation is not given here. For the particular case of symmetric switching ($\theta=0^o$), the proof is similar to the one presented in the next chapter for precessional switching in longitudinal media.

By substituting $m_x^{(l)}(t)$ in terms of $\tilde{m}_y(t)$, the function $F\left(m_x^{(l)}(t),t\right)$ can be represented in the following form:

$$F\left(m_x^{(l)}(t),t\right)=\Phi\left(\tilde{m}_y(t)\right)+c^2(t). \tag{3.69}$$

As a conclusion, the conditions imposed on $\tilde{m}_y(t)$ in order to guarantee the switching can be written in the following concise form:

$$\max_{t\in[0,T_1]}\left\{\Phi\left(\tilde{m}_y(t)\right)+\left[\frac{1}{D_x}\frac{d\tilde{m}_y}{dt}\right]^2\right\}=0. \tag{3.70}$$

Next, we discuss a technique of how to choose functions $\tilde{m}_y(t)$ that guarantee the switching of magnetization from $m_x=1$ to $m_x=0$. To this end, consider a class of functions

$$\tilde{m}_y(t)=-\sin\theta+\lambda f(t), \tag{3.71}$$

where:

$$0\leq\lambda\leq\sin\theta+\cos\theta, \tag{3.72}$$

while monotonically increasing function $f(t)$ is subject to the conditions

$$f(0)=0,\quad f'(0)=0,\quad f(T_1)=1,\quad f'(T_1)=0. \tag{3.73}$$

Next, we demonstrate that λ can be chosen in such a way that condition (3.70) is satisfied. By using the above representation of $\tilde{m}_y(t)$, relation (3.70) can be reduced to the following equation with respect to λ:

$$\Psi(\lambda) = \max_{t \in [0,T_1]} \left\{ \Phi\left[-\sin\theta + \lambda f(t)\right] + \left[(\lambda/D_x)f'(t)\right]^2 \right\} = 0. \qquad (3.74)$$

It is easy to see that $\Psi(\lambda)$ is a continuous function of λ. It can be also shown that:

$$\Psi(0) < 0, \qquad \Psi(\sin\theta + \cos\theta) \geq 0. \qquad (3.75)$$

This implies the existence of a solution of equation (3.74) on the interval $[0, \sin\theta + \cos\theta]$. Thus, appropriate values of λ can be found by solving one-dimensional nonlinear algebraic equation (3.74).

The effectiveness of the inverse problem technique for the design of magnetic field pulses that lead to precessional switching in perpendicular media is illustrated by Figures 3.23 and 3.24. In these figures, magnetization components are normalized by M_s, $h = H / D_x M_s$, and time is measured in units of $(\gamma M_s D_x)^{-1}$. Figure 3.23 presents the case when the direction of the applied magnetic field is perpendicular to the anisotropy axis ($\theta = 0^o$). The chosen dynamics for $\tilde{m}_y(t)$ is plotted by continuous line while the corresponding $m_x(t)$ and the shape of the pulsed field $h(t)$ found by using inverse problem approach are plotted by dash and dot lines, respectively. As a test for our method, we have numerically solved the direct problem (3.51) corresponding to the magnetic field found by inverse problem approach and we have compared the results. The numerical solutions of the direct problem (3.51), $\tilde{m}_y^{(n)}(t)$ and $m_x^{(n)}(t)$, are plotted by symbols in Figure 3.23. The case of $\theta = 20^o$ is illustrated in Figure 3.24.
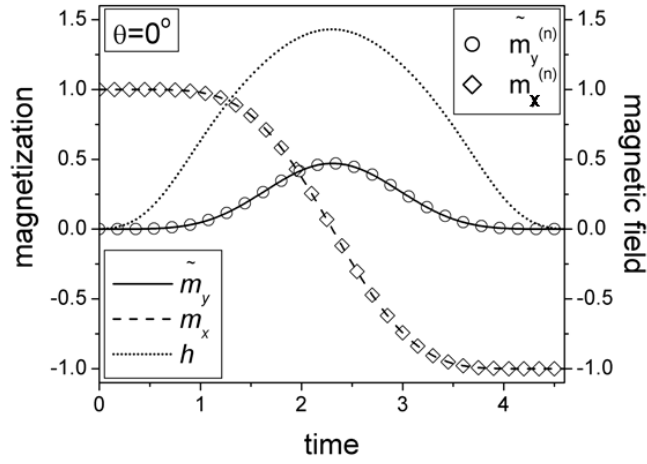
Figure 3.23: Chosen dynamics for $\tilde{m}_y(t)$ (plotted by continuous line), and corresponding $m_x(t)$ and normalized magnetic field $h(t)$ found by using inverse problem approach (plotted as dash and dot lines, respectively); numerical solutions (plotted as symbols) for the direct problem when magnetic field h is given; ($\theta=0^o$).
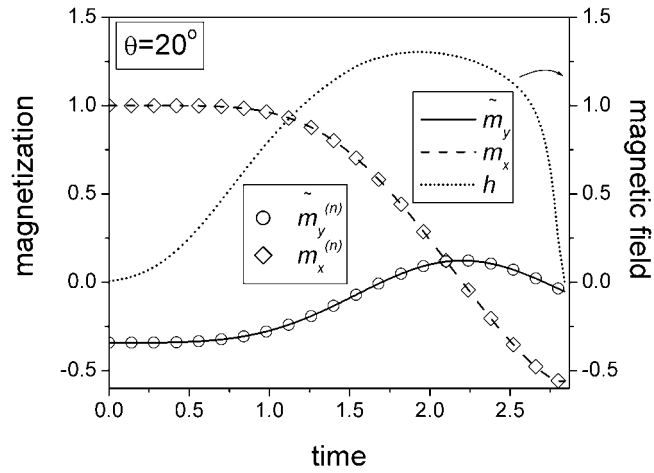
Figure 3.24: Chosen dynamics for $\tilde{m}_y(t)$ (plotted by continuous line), and corresponding $m_x(t)$ and normalized magnetic field $h(t)$ found by using inverse problem approach (plotted as dash and dot lines, respectively); numerical solutions (plotted as symbols) for the direct problem when magnetic field h is given; ($\theta=20^o$).

89

The assumption that damping effects play a negligible role in the design of magnetic field pulses that generate precessional switching has been tested by introducing the classical Landau-Lifshitz damping term in equation (3.51) and by solving numerically this equation for the magnetic fields found by inverse problem approach. The resulting $m_x^{damp}(t)$ dynamics and the non-damp dynamics $m_x(t)$ were sufficiently close even for high values of damping coefficient α, such as $\alpha=0.1$. Figure 3.25 presents the results of this comparison for the magnetic field pulses found by inverse problem approach and presented in Figures 3.23 and 3.24. This comparison suggests that dissipative effects can be neglected for the design of the magnetic field pulses.
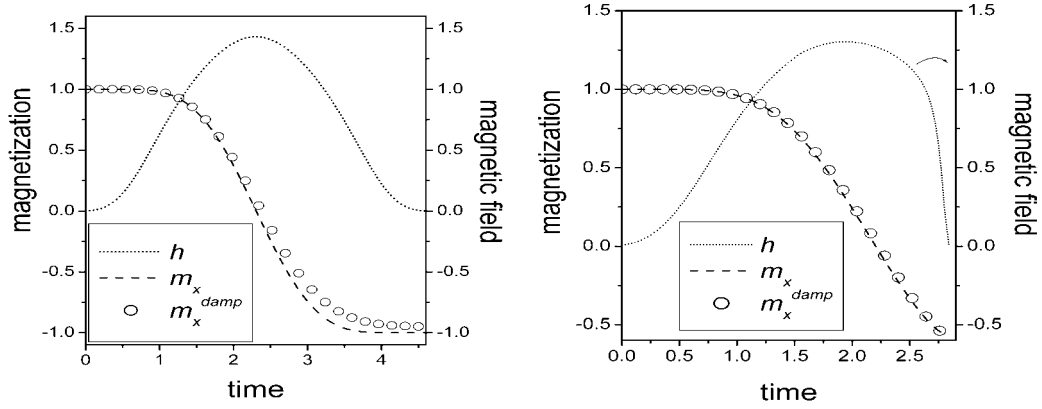
Figure 3.25: Evolution of m_x in the case of precessional switching for $\alpha=0$ (denoted by m_x) and $\alpha=0.1$ (denoted by m_x^{damp}), and the corresponding magnetic field pulses. Magnetization component is normalized by M_s, $h=H/D_xM_s$, and time is measured in units of $(\gamma D_x M_s)^{-1}$.

4. Inverse problem approach to the analysis of precessional magnetization reversals in longitudinal media

> "A thing appears random only through the incompleteness of our knowledge."
>
> Benedict de Spinoza [88]

In this chapter, the precessional magnetization switching in longitudinal thin film media is discussed. After a short summary of the research studies existent on this topic, the inverse problem approach to the analysis of precessional switching in these media is presented. This approach leads to explicit expressions for the magnetic field pulses that guarantee the precessional switching. The effectiveness of the developed technique is illustrated by examples.

The precessional switching in longitudinal thin film media has been the focus of considerable research in recent years. This research can be divided into two main directions oriented to the hard and soft magnetic materials, respectively. In the case of hard magnetic materials, the coercive field is very large (on the order of 10^5-10^6 A/m), which makes it very difficult to produce short magnetic pulses with such high amplitude. The experiments done in this direction [11, 44-45, 89] are similar to the ones for perpendicular media mentioned in the previous chapter and are of direct relevance to the increase in speed data processing in hard disk drives. However, the current experimental techniques used for these studies are based on a special current source, namely Stanford Linear Accelerator, which rather limits the technological

applicability of this method. Impelled by the recent developments in magnetic random access memories, the second direction of research is being flourishing for the last five years. The soft thin film media have much smaller coercive fields (on the order of 10-10^2 A/m) and consequently, they are susceptible to switch their magnetization at much smaller applied magnetic fields, as compared to the hard magnetic materials case. As a result, it is much easier to design technologically realizable field pulses with reasonable high amplitude and short time duration. Various experimental set-ups for this case can be found in References [12-13, 46-49]. Numerous comparisons of experimental techniques and numerical simulations have confirmed the validity of Landau-Lifshitz equation approach to quantitatively describe precessional switching phenomena both in hard and soft magnetic materials [11-13, 42-49].

Over the last three years, the analytical analysis of the precessional switching in longitudinal thin film media has been successfully developed by Bertotti, Mayergoyz, and Serpico, and their results are presented in References [90-94]. Interesting analytical results on this topic have also been published by Devolder and Chappert in References [95-97]. Here, the inverse problem approach to the analysis of precessional switching in these media is presented.

The magnetization dynamics in longitudinal thin film media is governed by the competition between the applied field, the in-plane anisotropy field and the demagnetizing field perpendicular to the plane. While in hard magnetic materials the strength of the anisotropy field is comparable to the one of the demagnetizing field, in soft magnetic materials the latter is much stronger. In the absence of the applied

field, there are two stable equilibrium directions, and the magnetization lies along one of them. The precessional switching between these two minima can be produced by a short magnetic field pulse applied in the thin film plane at some angle with the anisotropy axis. In longitudinal soft magnetic materials, this reversal mode can be essentially described as a two-phase process: first, the applied magnetic field tilts the magnetization out of the thin film plane and, as a result, it creates a strong demagnetizing field, oriented perpendicular to the plane; in the second phase, magnetization starts to precess about the demagnetizing field and moves from the basin of attraction of one energy minima to the one of the other energy minima. If the magnetic field pulse is properly designed, the magnetization would be in the basin of attraction of the latter energy minima by the time when the magnetic field is switched off. Therefore, a central problem of this direction of research is the design of magnetic field pulses that will guarantee the precessional switching. This problem has been addressed experimentally and numerically by using a "trial-and-error" method. In this section, the "inverse problem" approach is developed that leads to the explicit expressions for magnetic field pulses that guarantee the precessional switching of magnetization in thin magnetic films.

An important remark should be made before starting this analysis. In contrast to the perpendicular media case, presented in the previous chapter, the experiments on soft longitudinal media reveal a "stochastic" behavior of magnetization precessional switchings [48]. A possible explanation of this seemingly stochastic nature of the precessional switching is given in [91] and is based on the approximately "riddled" basins of attraction property [98-99] exhibited by Landau-Lifshitz equation. Thus,

the phase portraits of Landau-Lifshitz equation in the absence of the applied field present three distinct regions. Two clearly separated regions surround the two energy minima, and the time evolution of the magnetization inside each one of them inevitable leads to the corresponding energy minimum. In the third region, magnetization trajectories leading to different energy minima are closely entangled resulting in approximately "riddled" basins of attractions. If the magnetic field is switched off when the magnetization is in latter region, the result of subsequent damping driven relaxation is practically uncertain, as a consequence of the very close entanglement of magnetization trajectories leading to different equilibria. In conclusion, the applied magnetic field pulse applied should not only change the orientations of the magnetization from positive m_x to negative m_x (see perpendicular media case), but also move the magnetization into a specific region surrounding $-\mathbf{e}_x$, which finally ensures the relaxation to this equilibrium position.
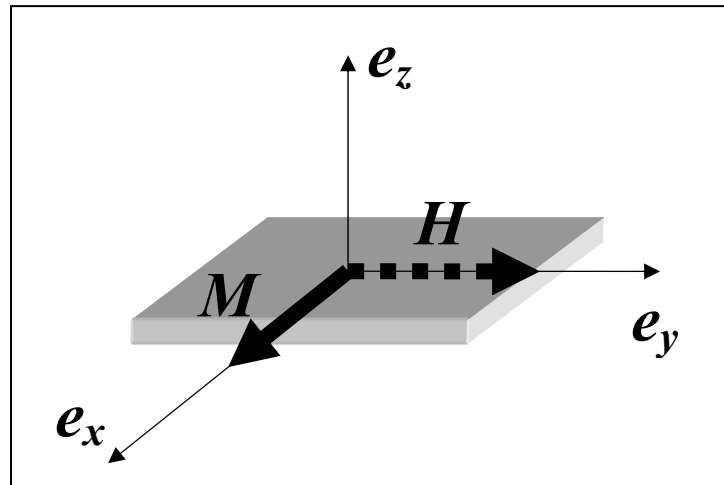
Figure 4.1: Configuration for precessional switching in longitudinal thin films.

To start the discussion, consider a uniformly magnetized longitudinal thin film subject to spatially uniform pulsed magnetic fields applied along y-axis (see Figure 4.1). The magnetization dynamics is described by the Landau-Lifshitz (LL) equation. This equation will be used in the following dimensionless form:

$$\frac{d\mathbf{m}}{dt} = -\mathbf{m} \times \mathbf{h}_{eff} - \alpha \mathbf{m} \times \mathbf{m} \times \mathbf{h}_{eff} . \qquad (4.1)$$

Here, $\mathbf{m} = \mathbf{M}/M_s$, $\mathbf{h}_{eff} = \mathbf{H}_{eff}/M_s$ (normalized effective field), and time t is measured in units of $(\gamma M_s)^{-1}$. As considered in the previous chapters, M_s is the saturation magnetization, γ and α are the precessional and damping constants.

Since the film is assumed to be very thin, the demagnetizing factors in the film plane and perpendicular to the film plane are practically equal to zero and 1, respectively. This leads to the following expression for the effective field:

$$\mathbf{h}_{eff} = Dm_x \mathbf{e}_x + h_y \mathbf{e}_y - m_z \mathbf{e}_z , \qquad (4.2)$$

where D accounts for the in-plane x-axis anisotropy.

The precessional switching is so fast that dissipative effects can be neglected and the switching can be studied by using the equation:

$$\frac{d\mathbf{m}}{dt} = -\mathbf{m} \times \mathbf{h}_{eff} . \qquad (4.3)$$

In the absence of the applied field, there are two stable equilibrium points with $\mathbf{m} = \pm \mathbf{e}_x$, respectively. Suppose that the magnetization is initially at the equilibrium point $\mathbf{m} = \mathbf{e}_x$, and we want to find such a pulse magnetic field $h_y(t)$ that will result in the precessional switching of magnetization to the equilibrium state $\mathbf{m} = -\mathbf{e}_x$.

In the "inverse problem" approach, the desired monotonic dynamics of $m_x(t)$ between equilibrium points $m_x=1$ and $m_x=-1$ is chosen and then equations (4.2) and

95

(4.3) are used to find the appropriate $h_y(t)$. Since the vector dynamic equation (4.3) has the integral of motion $|\mathbf{m}(t)| = 1$, this equation can be used instead of the scalar equation for $\dfrac{dm_z}{dt}$. This leads to the following coupled equations:

$$\frac{dm_x}{dt} = \left(m_y + h_y\right)m_z \,, \tag{4.4}$$

$$\frac{dm_y}{dt} = -(1+D)m_x m_z \,, \tag{4.5}$$

$$m_x^2 + m_y^2 + m_z^2 = 1 \,. \tag{4.6}$$

From equations (4.5) and (4.6), we easily derive

$$\frac{dm_y}{dt} = (1+D)m_x(t)\sqrt{1-m_x^2(t)-m_y^2} \,, \tag{4.7}$$

where the negative sign of the square root is chosen and this sign is maintained constant during the precessional switching process.

Since the desired dynamics of $m_x(t)$ that leads to the precessional switching of magnetization is chosen, formula (4.7) can be treated as a differential equation with respect to $m_y(t)$. By solving this equation with zero initial condition, $m_y(t)$ can be found. Then, from equation (4.4) we can recover the pulsed magnetic field

$$h_y(t) = \frac{-1}{\sqrt{1-m_x^2(t)-m_y^2(t)}} \frac{dm_x}{dt}(t) - m_y(t), \tag{4.8}$$

that will guarantee the desired precessional switching.

The described approach is straightforward because it is always easy to choose such a function $m_x(t)$ that guarantee the precessional switching. However, this approach requires numerical integration of differential equation (4.7) and does not

lead to the explicit analytical expressions for $h_y(t)$. It turns out that there exists an alternative approach that can be more preferable as far as explicit expressions for $h_y(t)$ are concerned. In this approach, the dynamics of $m_y(t)$ that leads to the precessional switching must be first chosen. Then, by using equation (4.5) and (4.6), $m_x(t)$ and $m_z(t)$ are computed. Afterwards, the pulsed magnetic field $h_y(t)$ is found from equation (4.4). The main difficulty in this approach is the choice of the appropriate $m_y(t)$ that guarantees the precessional switching. Next, it is discussed how this difficulty can be dealt with.

By assuming that $m_y(t)$ is known, equations (4.5) and (4.6) can be treated as algebraic equations with respect to $m_x(t)$ and $m_z(t)$. By eliminating $m_z(t)$ from (4.5) and (4.6), we arrive at the following equation for $m_x(t)$:

$$m_x^4 - \left(1 - m_y^2\right)m_x^2 + \frac{1}{(1+D)^2}\left(\frac{dm_y}{dt}\right)^2 = 0. \tag{4.9}$$

It is easy to see that equations (4.5) and (4.6) are symmetric with respect to $m_x(t)$ and $m_z(t)$. This implies that equation (4.9) is valid for $m_z(t)$ as well. Therefore, we find:

$$m_{x,z}^2 = \frac{1}{2}\left(1 - m_y^2 \pm \sqrt{\left(1 - m_y^2\right)^2 - \frac{4}{(1+D)^2}\left(\frac{dm_y}{dt}\right)^2}\right). \tag{4.10}$$

Thus, there are "positive" and "negative" solutions (branches) of equation (4.9) that correspond to "+" and "- " signs in formula (4.10), respectively. It is apparent that different branches in (4.10) should be identified with $m_x(t)$ and $m_z(t)$. At the beginning of precessional switching, this identification is performed on the basis of the initial conditions. Thus, at the beginning of the precessional switching $m_x(t)$ must be identified with the positive branch of (4.10), while the negative branch

corresponds to $m_z(t)$. However, these branches may be switched between $m_x(t)$ and $m_z(t)$ during the precessional process.

Now, we shall discuss the conditions on $m_y(t)$ that guarantee the precessional switching. To this end, we consider the discriminant

$$\Delta(t) = \left[1 - m_y^2(t)\right]^2 - \frac{4}{(1+D)^2}\left(\frac{dm_y}{dt}(t)\right)^2. \qquad (4.11)$$

It is obvious from (4.10) and (4.11) that those $m_y(t)$ for which $\Delta(t) < 0$ at some instant of time are not physically realizable. It is also apparent that those $m_y(t)$ for which $\Delta(t)$ is strictly positive do not correspond to the precessional switching. Indeed, if $\Delta(t) > 0$ then the positive and negative branches in (4.10) are separated (see Figure 4.2). Since $m_x(t)$ is a continuous function of t and it is identified with the positive branch of (4.10) at the beginning of magnetization dynamics, it must be identified with this branch at all instants of time. Then, according to formula (4.10), $m_x(t)$ is strictly positive and cannot reach zero and, consequently, no precessional switching may occur.

Next, we demonstrate that, when $m_y(t)$ is such that $\Delta(t) \geq 0$ and $\Delta(t) = 0$ has an odd number of solutions before the negative branch from (4.10) reaches zero, the precessional switching will occur. We shall provide the demonstration for the simplest case of "symmetric" precessional switching when $h_y(t)$ and $m_y(t)$ are even functions of time in [-T/2, T/2], and $\Delta(t) = 0$ has one solution t_0 in [-T/2, 0] (see Figure 4.2). It is apparent from (4.10) and (4.11) that at the time t_0 positive and negative branches are not continuously differentiable. Indeed, from (4.10) and (4.11) we find:

$$m_{x,z}(t)\frac{dm_{x,z}}{dt}(t) = g'(t) \pm \frac{1}{8}\frac{\Delta'(t)}{\sqrt{\Delta(t)}}, \tag{4.12}$$

where the notation $g(t) = \left(1 - m_y^2(t)\right)/4$ is used.

Using Taylor expansions for $\Delta(t)$ and $\Delta'(t)$ around t_0, we derive:

$$m_{x,z}(t_0)\frac{dm_{x,z}}{dt}(t_{0-}) = g'(t_0) \pm \left(-\frac{1}{4}\sqrt{\frac{\Delta''(t_0)}{2}}\right), \tag{4.13}$$

$$m_{x,z}(t_0)\frac{dm_{x,z}}{dt}(t_{0+}) = g'(t_0) \pm \left(\frac{1}{4}\sqrt{\frac{\Delta''(t_0)}{2}}\right), \tag{4.14}$$

where $\dfrac{dm_{x,z}}{dt}(t_{0-})$ and $\dfrac{dm_{x,z}}{dt}(t_{0+})$ denote the limits from "below" and "above" t_0.

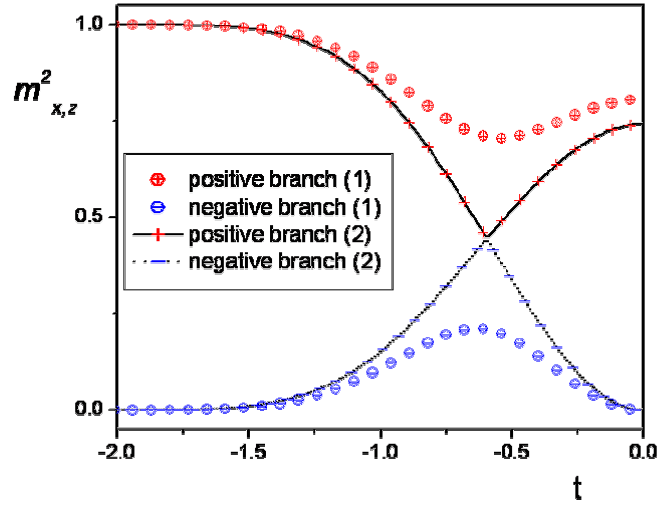Figure 4.2: Positive and negatives branches of equation (4.10) for: (1) when $\Delta(t)>0$ and (2) when $\Delta(t) \geq 0$ and zero is attained.

It is clear from formulas (4.13) and (4.14) that positive and negative branches of the solution (4.10) are not continuously differentiable at $t=t_0$, and consequently, these branches cannot be identified with $m_x(t)$ and $m_z(t)$ on the entire time interval [-T/2, 0].

It is also clear from formulas (4.13) and (4.14) that the negative branch for $t > t_0$ is a continuously differentiable extension of the positive branch for $t < t_0$ and vice versa. Thus, $m_x(t)$ can be identified with the positive branch for $-\dfrac{T}{2} \leq t \leq t_0$ and with the negative branch for $t_0 \leq t \leq 0$. Since $m_y(t)$ is continuously differentiable even function, $\dfrac{dm_y}{dt}(0) = 0$ and, according to (4.10), the negative branch and $m_x(t)$ reach zero at $t=0$. For the time interval $[0, T/2]$, $m_x(t)$ is the odd extension of $m_x(t)$ in the time interval $[-T/2, 0]$, and this is tantamount to the precessional switching. In the previous reasoning, it was tacitly assumed that $\Delta''(t) \neq 0$. However, the reasoning can be easily modified for the case $\Delta''(t) = 0$, because the first non-zero derivative of $\Delta(t)$ at $t=t_0$ is of even order. The latter is the consequence of the fact $\Delta(t)$ is non-negative and assumes its minimum zero value at $t=t_0$.

Thus, we have found the conditions on $m_y(t)$ in terms of $\Delta(t)$ that result in the precessional switching. From equations (4.4) and (4.10), the applied magnetic field corresponding to this switching is given by:

$$h_y(t) = \frac{D-1}{2} m_y + \frac{D+1}{2} \frac{\left(1-m_y^2\right)m_y + \dfrac{2}{\left(D+1\right)^2}\dfrac{d^2 m_y}{dt^2}}{\sqrt{\left(1-m_y^2\right)^2 - \dfrac{4}{\left(1+D\right)^2}\left(\dfrac{dm_y}{dt}\right)^2}} . \tag{4.15}$$

Now, we present a technique that helps to choose $m_y(t)$ in such a way that the conditions for precessional switching will be satisfied. To this end, consider a set of functions

$$m_y(t) = bf(t), \tag{4.16}$$

100

depending on parameter $b \in (0,1]$. It is assumed that $f(t)$ is even on [-T/2, T/2], and $f(0)=1$. From initial conditions follows that $f(-T/2)=0$. It turns out that there exists only one value of b such that $\Delta(t) \geq 0$ on (-T/2, 0) and zero is attained in this interval. The proof proceeds as follows. It is apparent form formulas (4.11) and (4.16) that the previous assertion is equivalent to the existence of a unique solution for the following equation:

$$F(b) = \max_{t \in \left(-\frac{T}{2}, 0\right)} \left[b^2 f^2(t) + \frac{2b}{1+D} |f'(t)| - 1 \right] = 0 \tag{4.17}$$

It is easy to see that $F(b)$ is a continuous and monotonically increasing function of b and:

$$\lim_{b \to 0} F(b) = -1, \qquad \lim_{b \to 1} F(b) \geq 0. \tag{4.18}$$

Thus, there is only one solution for equation (4.17), and consequently, there is only one b that satisfies our assertion. This b can be found by solving one-dimensional non-linear equation (4.17).

The "inverse problem" technique for the design of magnetic field pulses for precessional switching is illustrated by Figures 4.3 and 4.4. A thin magnetic film with M_s=1.1T and D=0.008 has been considered and the following classes of functions $m_y(t) = \beta(1+\cos(2\pi t/T))^\delta$ and $m_y(t) = \tilde{\beta}(1-(2t/T)^2)^{\tilde{\delta}}$ have been chosen. In Figure 4.3 we present the results for the first type of m_y-dynamics, where T=300ps, δ=3 and amplitude β has been chosen such that the condition for switching is satisfied. The accuracy of this technique has been tested through numerical solution of the direct problem (4.3) corresponding to the magnetic field found by the

inverse problem approach. Figure 4.4 presents the results of a similar analysis for

the second type of m_y-dynamics mentioned above, with T=300ps and $\tilde{\delta}$=10.

In Figure 4.5 the damping (with α=0.01) is taken into account and it is

confirmed that dissipative effects can be neglected for the design of the magnetic

field pulses leading to precessional switching.

Figure 4.3: The chosen dynamic for m_y and the corresponding m_x, m_z, and magnetic

field H_y. Numerical solutions $\underline{m}_x$, $\underline{m}_y$ and $\underline{m}_z$ for the direct problem given H_y.
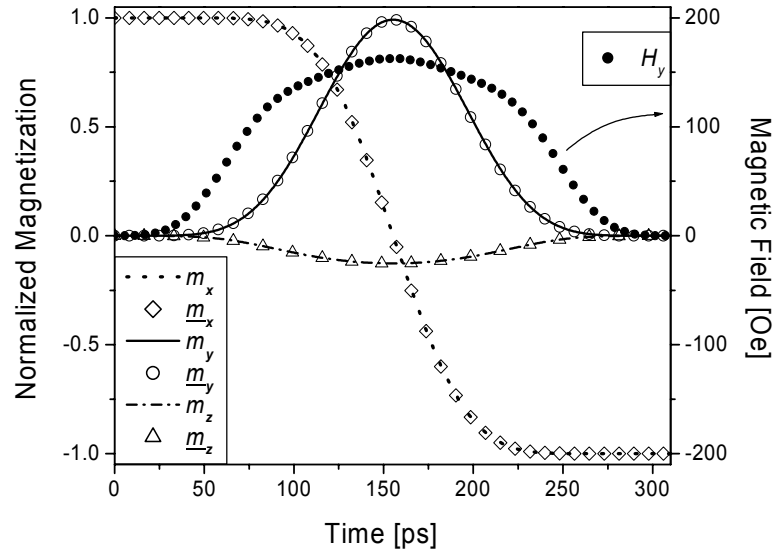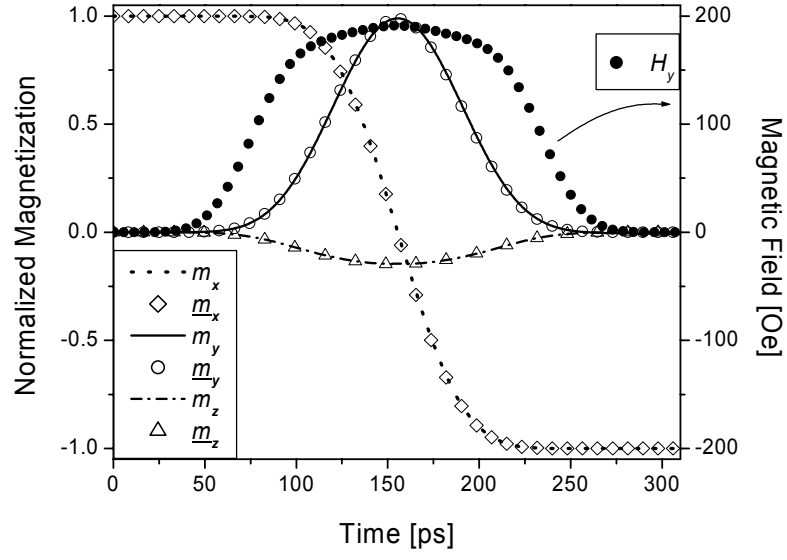
Figure 4.4: The chosen dynamic for m_y and the corresponding m_x, m_z, and magnetic field H_y. Numerical solutions $\underline{m}_x$, $\underline{m}_y$ and $\underline{m}_z$ for the direct problem given the magnetic field H_y.

(a)

(b)
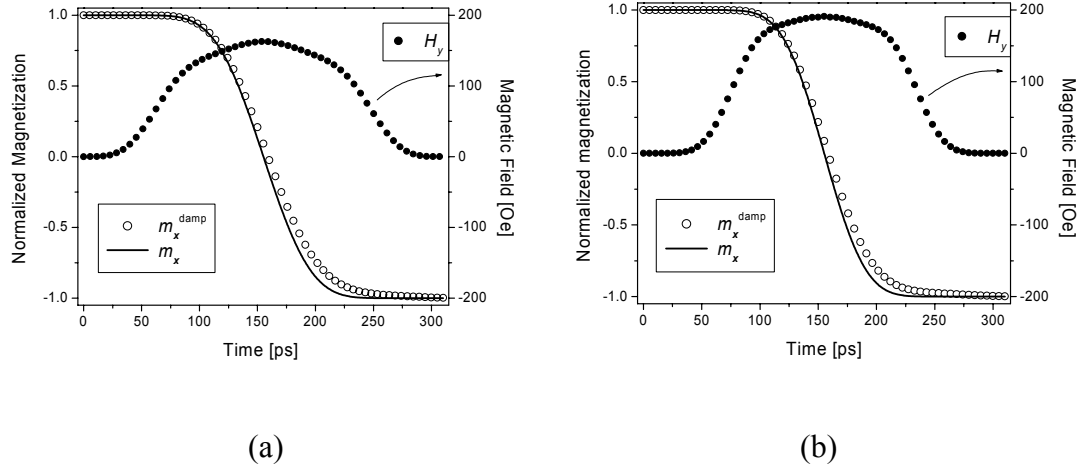
Figure 4.5: Evolution of m_x in the case of precessional switching when α=0, denoted by m_x, and when α=0.01, denoted by m_x^{damp}.

5. Surface effects on magnetization reversals in nanoparticles

"Very often such, a simplified model throws more light on the real workings of nature than any number of ab initio calculations of individual situations, which even where correct often contain so much detail as to conceal rather than reveal reality." Philip W. Anderson [100]

In this chapter, the study of surface anisotropy effects on magnetization reversals in nanoparticles is presented. The multi-spin dynamics in magnetic nanoparticles is found by using Landau-Lifshitz equation with the effective field derived from Heisenberg-type Hamiltonian. The expressions for critical magnetic fields that guarantee the quasi-static and precessional reversals are derived analytically for the case of very strong exchange and weak surface anisotropy. These analytical results are also used to test the numerical approach, which is applied to the general case of the problem. The distinct features of the quasi-static and precessional reversals in nanoparticles are examined.

Magnetic nanoparticles have attracted the attention of many researchers since the pioneering work of Neel in the late 1940's, due to their novel behavior and remarkable potential for technological applications. However, it took almost half a century to find reliable techniques for manufacturing nanoparticles with desired structure, dimension, and other technological characteristics. Recently, numerous experimental and theoretical studies on magnetic properties of isolated nanoparticles

have been published (see [101-111] and references therein). However, many aspects of the experimental results are still waiting for satisfactory theoretical explanations. Moreover, these studies have been focused on the quasi-static magnetic characteristics of nanoparticles. No comparable effort has been made to study the dynamic behavior of magnetization in nanoparticles, which is becoming increasingly important in various applications. For instance, the study of surface effects on the precessional switching of nanoparticles has not been attempted. In this chapter we present surface anisotropy effects on the hysteretic (quasi-static) and dynamical properties of magnetization in ferromagnetic nanoparticles.

Surface effects strongly influence the properties of magnetic nanoparticles, and entail large deviations from the bulk behavior. This influence is increasingly pronounced as the dimensions of the particle decrease. It is useful to understand surface effects in magnetic materials in order to control the properties which are relevant for technological applications. Surface effects are due to the breaking of crystal-field symmetry, and this is a local effect. In order describe this contribution one has to resort to microscopic theories, which are capable of distinguishing between different atomic environments. Our approach is to consider a semiclassical multi-spin description of a nanoparticle by using the Landau-Lifshitz equation for each spin with the effective field derived from a Heisenberg-type Hamiltonian. The analysis presented here deals with the effect of surface anisotropy on the behavior of spherical nanoparticles with uniaxial anisotropy in the core and radial single-site anisotropy for spins on the boundary.

5.1. Hamiltonian model and computational method

In this section, the Hamitonian model and physical parameters are defined, and the method used to compute hysteretic and dynamic properties of magnetic nanoparticles is presented.

Within the classical approximation it is convenient to represent the atomic spin as the three-component spin vector $\mathbf{s}_i$ of unit length on the lattice site i. We will consider the following Heisenberg-type Hamiltonian that includes the exchange interaction, Zeeman energy, and magnetocrystalline anisotropy energy:

$$H = -\frac{1}{2}\sum_{<i,j>} J_{ij} S^2 \mathbf{s}_i \cdot \mathbf{s}_j - (g\mu_B \mu_0 S)\mathbf{H} \cdot \sum_{i=1}^{n} \mathbf{s}_i - \sum_{i=1}^{n} K_i \left(\mathbf{s}_i \cdot \mathbf{e}_i\right)^2 . \qquad (5.1)$$

Here, J_{ij} is the strength of the nearest-neighbor exchange interaction, which is taken in these calculations the same everywhere ($J_{ij}S^2$ will be denoted by J); <i,j> denotes the fact that the sum is made only over the nearest neighbors. The constant g is the Lande factor, μ_B is the Bohr magneton, μ_0 is the vacuum permitivity, and S is the value of the atomic spin. The constant n is the total number of spins, while $\mathbf{H}$ is the uniform magnetic field applied in the direction ψ with respect to the reference z axis. The in-site magnetocrystalline uniaxial anisotropy is described by easy axis $\mathbf{e}_i$ and anisotropy constants K_i. This anisotropy contains two contributions stemming from the core and surface, and depends on the system under consideration. In the case of spherical particle considered below, all core spins "feel" uniaxial anisotropy along the z easy axis with the same constant K_c, whereas each surface spins is assume to have its anisotropy axis along radial direction with the constants K_s. As an illustration of this structure see Figure 5.1 where the spins are almost align to their anisotropy axis.

A remark should be made concerning the dipole-dipole interactions. It has been shown [112] that these contributions are negligible in very small spherical particles as compared with the contribution of exchange interactions. Moreover, continuum micromagnetic simulations for cubo-octahedral particles [113] also suggest that the influence of dipole-dipole interactions on the magnetic properties is not important even in relatively large nanoparticles with dimensions up to 60 nm. For these reasons, we think that dipole-dipole interactions do not play a significant role in the behavior of spherical nanoparticles with diameters of a few nanometers, and consequently, they are not taken into account in Hamiltonian (5.1).
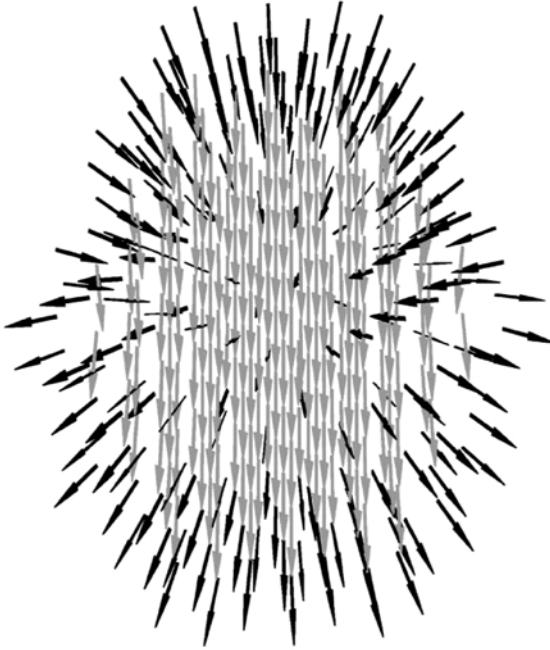

Figure 5.1: Magnetic structure of a spherical nanoparticle in an equilibrium state. This nanoparticle has 360 spins, K_c=1, K_s=1, weak exchange J=0.1, and no external magnetic field is applied (**H**=0).

The computational method of quasi-static characteristics presented in this section tries to follow physical dynamic processes that lead to the quasi-static characteristics, as opposed to energy minimization techniques usually applied for quasi-static studies. Due to this property the method used here is naturally suitable for both quasi-static and dynamic studies of ferromagnetic nanoparticles. Various models of a nanoparticle are considered. In each case, we simulate the lattice with simple cubic (sc) crystal structure and then assign to each site a length-fixed three-component spin vector. For the calculation of a hysteresis loop we start with a magnetic configuration where all spins are pointing in the same direction –z, which corresponds to the saturation state. The hysteresis loop is due to the existence of metastable states in the system. Starting from the initial configuration and applied field, the integration of Landau-Lifshitz equation (see below) tends towards a new configuration that is an energy minimum.

We choose K_c as the energy scale and normalize the other physical constants accordingly, i.e.,

$$t \to \frac{2K_c}{\hbar} t, \quad \mathbf{h} = \frac{g\mu_B \mu_0 S}{2K_c} \mathbf{H} .$$

(5.2)

Then, the Landau-Lifshitz equation for a spin $\mathbf{s}_i$ at site i, reads

$$\frac{d\mathbf{s}_i}{dt} = -\mathbf{s}_i \times \mathbf{h}_i^{eff} - \alpha \, \mathbf{s}_i \times \mathbf{s}_i \times \mathbf{h}_i^{eff} ,$$

(5.3)

where $\mathbf{h}_i^{eff}$ is the effective field acting on the spin $\mathbf{s}_i$ and is given by

$$\mathbf{h}_i^{eff} = \mathbf{h} + \frac{j}{2} \sum_{j=1}^{z_i} \mathbf{s}_j - k_i (\mathbf{s}_i \cdot \mathbf{e}_i) \mathbf{e}_i .$$

(5.4)

Here, z_i is the number of nearest neighbors considered, and there are used the reduced parameters $j=J/K_c$ and $k_i=K_i/K_c$ ($k_i=1$ if the spin belong to the core of the nanoparticle). Therefore for each site i we arrive at three coupled equations (for spin components), and because of the second term in equation (5.4) we actually obtain a system of $3n$ (local) coupled nonlinear equations.

After having constructed the magnetic structure (lattice and spin vectors in it), we apply a magnetic field **H** at some angle ψ with respect to the reference z axis, with values chosen in a regular mesh. Then we calculate the local effective field (5.4) , for all spins and thereby the right-hand sides of the Landau-Lifshitz equations (5.3) and proceed with the time integration. Time integration is made by using a Runge-Kutta method and the technique presented in [75]. As this is done, the total energy in equation (5.1) smoothly decreases, and some criterion must be used for stopping the integration for the given value of the applied field and moving to the next value. In our calculations we proceed to the next field value when

$$\frac{1}{n}\sum_{i=1}^{n}\left|\frac{d\mathbf{s}_i}{dt}\right|<\varepsilon\,,\tag{5.5}$$

which implies that the system is close to a stationary state, ε being a small parameter of order of 10^{-5}-10^{-7}.

Next, the stationary state thus obtained is used as the initial state for the next value of the field. Iteration of this process over a sequence of applied fields, of given magnitude and direction ψ, renders the hysteresis loop. For each value of this angle we determine the critical field. The whole procedure finally renders the critical field as a function of the angle (critical curve, or limit-of-metastability curve).

5.2. Critical magnetic field curves for magnetization reversals in nanoparticles with weak surface anisotropy

In this section, the expressions for quasi-static and dynamic critical magnetic fields that guarantee the magnetization reversals in spherical nanoparticles are analytically derived for the case of strong exchange and weak surface anisotropy.

The analysis of the surface anisotropy effects can be appreciably simplified in the case of a very strong exchange ($j \gg \max\{1, k_s\}$). In this case the spins motion can be considered uniform and their dynamics can be described by one spin motion which obeys the Landau-Lifshitz equation with the effective field derived from the reduced Hamiltonian:

$$H_r = -n(\mathbf{h} \cdot \mathbf{s}) - \frac{1}{2} n_c (\mathbf{s} \cdot \mathbf{e}_z)^2 - \frac{1}{2} k_s \sum_{i=1}^{n_s} (\mathbf{s} \cdot \mathbf{e}_i)^2 , \qquad (5.6)$$

where, n_c and n_s are total number of core spins and surface spins, respectively. Moreover, taking into account the spherical symmetry of the problem, it will be proved in the next paragraph that the last term in (5.6) is independent on spin orientation, and consequently, it leads to an irrelevant constant in the Hamiltonian expression. In conclusion, in the case of strong exchange and weak surface anisotropy the quasi-static and dynamic problems are reduced to the scaled versions of the uniaxial ferromagnetic object problems employed in Chapter 3 for the study of perpendicular oriented thin film media.

The last sum in formula (5.6) can be written in the following form:

$$\sum_{i=1}^{n_s}\left(\mathbf{s}\cdot\mathbf{e}_i\right)^2 = s_x^2\sum_{i=1}^{n_s}\left(e_x^i\right)^2 + s_y^2\sum_{i=1}^{n_s}\left(e_y^i\right)^2 + s_z^2\sum_{i=1}^{n_s}\left(e_z^i\right)^2$$
$$+ 2s_xs_y\sum_{i,j=1}^{n_s}\left(e_x^ie_y^j\right) + 2s_xs_z\sum_{i,j=1}^{n_s}\left(e_x^ie_z^j\right) + 2s_zs_y\sum_{i,j=1}^{n_s}\left(e_z^ie_y^j\right) \qquad (5.7)$$

where, e_x^i, e_y^i, and e_z^i are the cartesian coordinates of radial unit vector $\mathbf{e}_i$. Since the crystal and surface anisotropy structures are invariant under the $\pi/2$ rotations around the each axis of coordinates, we have the following identities:

$$\sum_{i=1}^{n_s}\left(e_x^i\right)^2 = \sum_{i=1}^{n_s}\left(e_y^i\right)^2 = \sum_{i=1}^{n_s}\left(e_z^i\right)^2. \qquad (5.8)$$

$$\sum_{i,j=1}^{n_s}\left(e_x^ie_y^j\right) = -\sum_{i,j=1}^{n_s}\left(e_x^je_y^i\right), \quad \sum_{i,j=1}^{n_s}\left(e_x^ie_z^j\right) = -\sum_{i,j=1}^{n_s}\left(e_x^je_z^i\right), \quad \sum_{i,j=1}^{n_s}\left(e_z^ie_y^j\right) = -\sum_{i,j=1}^{n_s}\left(e_z^je_y^i\right). \qquad (5.9)$$

It is obvious that all sums in (5.9) are actually equal to zero. Therefore, the formula (5.7) can be written:

$$\sum_{i=1}^{n_s}\left(\mathbf{s}\cdot\mathbf{e}_i\right)^2 = \left(s_x^2 + s_y^2 + s_z^2\right)\sum_{i=1}^{n_s}\left(e_z^i\right)^2 = \sum_{i=1}^{n_s}\left(e_z^i\right)^2, \qquad (5.10)$$

and consequently, this sum is independent on the spin orientation. In conclusion, this term can be removed from Hamiltonian expression (5.6) and now the reduced Hamiltonian reads:

$$H_r = -n\left(\mathbf{h}\cdot\mathbf{s}\right) - \frac{1}{2}n_c\left(\mathbf{s}\cdot\mathbf{e}_z\right)^2. \qquad (5.11)$$

Without restricting the generality of the foregoing, the magnetic field is assumed to be applied in z-y plane at some angle Ψ with the z-axis (anisotropy axis) and the energy is simply rewritten:

$$H_r = -n\left(h_zs_z + h_ys_y\right) - \frac{1}{2}n_cs_z^2. \qquad (5.12)$$

111

Energy (5.12) is only a scaled version, up to axes notation, of the energy used for the study on perpendicular media. Therefore, the results presented in Chapter 3 can be rephrased for this special case of spherical nanoparticles with very strong exchange and weak surface anisotropy. Thus, by taking into account formula (3.42) from Chapter 3, the analytical expression for critical field curve for quasi-static reversal process is given by:

$$\begin{cases} h_z = (n_c/n)\cos^3\varphi \\ h_y = (n_c/n)\sin^3\varphi \end{cases}, \quad \varphi \in [-\pi, \pi], \tag{5.13}$$

which is nothing else than the scaled version of Stoner-Wohlfarth astroid, the scale factor being the ratio between the number of core spins and the total number of spins. It is apparent that considering a radial distribution for surface anisotropy, leads, even in the case of very strong exchange, to important quantitative deviations from the classical Stoner-Wohlfarth results. In particular, the corresponding astroid falls inside that of SW, and the larger the surface contribution the more the astroid shrinks.

To check our numerical code we computed critical fields corresponding to various orientations of the applied field and particle diameters, and compared with the values given by formula (5.13). Selected results of this comparison are plotted in Figure 5.2. This evaluation also provides us with a range of validity for the assumption used at the beginning of this section for our analytical analysis. Thus, for $j/k_s \geq 100$ the spins motion can be considered as unison.

Next, we turn our attention towards the dynamical case. Considering formulae (3.38) and (3.41) from Chapter 3, the critical field curve for precessional switching can be described (in the first quadrant) by using the following formulae:

$$\begin{cases} h_z = (n_c/n)\cos\theta\cos^2(\theta/2) \\ h_y = (n_c/n)\sin\theta\sin^2(\theta/2) \end{cases}, \ \theta \in [0,\pi/2], \quad (5.14)$$

$$h_y = \pm\left[h_z - (n_c/2n)\right]. \quad (5.15)$$

In Figure 5.2 the analytically derived dynamical critical curves (plotted as lines) and the computed critical fields (plotted as symbols) are presented for various values of the particle diameter. These numerical simulations confirm that the assumption of uniformity is valid for the ratio $j/k_s \geq 100$. For smaller values of this ration, the multi-spin dynamics deviates from coherent motion and these deviations become more and more pronounced as this ratio decreases. These non-uniform modes and their influences on critical fields are analyzed in the next sections.
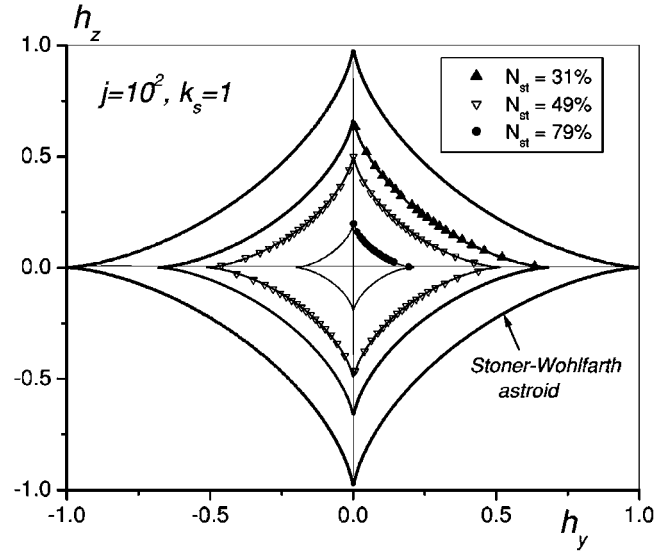
Figure 5.2: Astroid for different values of surface-to-volume ratio $N_{st}=n_s/n$. The analytical results are plotted as continuous lines, while the numerical results for $k_s=1$, $j=100$ are plotted as symbols.

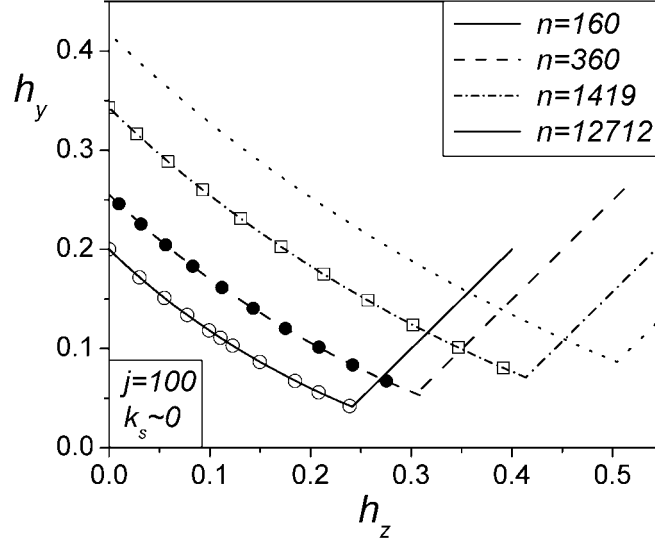Figure 5.3: Dynamic critical curves for selected values of the total number of spins n. The analytical results are plotted as continuous lines, while the numerical results for $k_s=0.1, j=100$ are plotted as symbols.
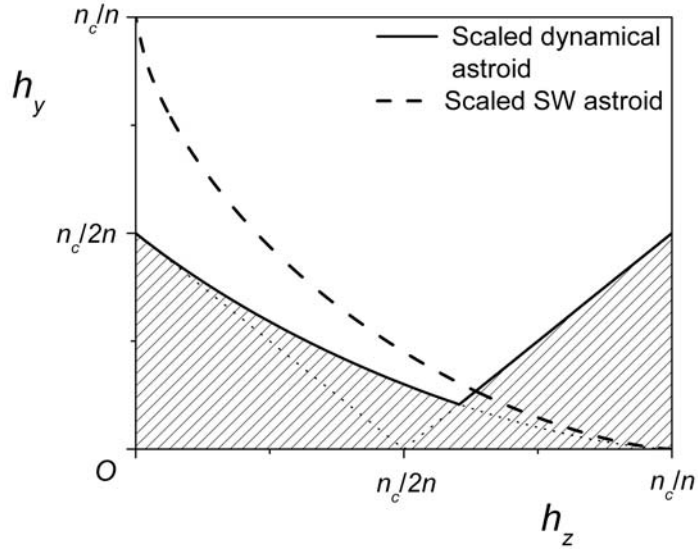

Figure 5.4: Scaled "dynamical astroid" and scaled Stoner-Wohlfarth (SW) astroid of a spherical nanoparticle with weak surface anisotropy.

114

5.3. Surface anisotropy effects on hysteretic properties of nanoparticles

In this section we consider a spherical nanoparticle of simple cubic structure with uniaxial anisotropy in the core having reduced anisotropy constant $k_c=1$, and radial anisotropy on the surface with reduced constant k_s. Our main goal here is to investigate the influence of surface anisotropy, both in direction and strength, on the hysteresis loop and quasi-static critical curve. However, we will also study the effect of exchange coupling and particle's size.

For later reference, we plot in Figure 5.5 the critical field h_c and the height of the magnetization jump (i.e. m_u-m_d) as function of the angle ψ between the direction of the field and core easy axis for a macrospin (or equivalently, one classical spin) problem. The dependence $h_c(\psi)$ in Figure 5.5 (left) is nothing else than the Stoner-Wohlfarth astroid but plotted in different coordinates . In the right figure we note a surprising and much less known property of magnetization jumps employed in this classical SW model: the height of magnetization jump has an almost linear dependence on ψ, except for the final portion $76°< \psi <90°$. This final portion corresponds to hysteresis cycles with crossing branches [27]. Again for later reference, we plot in Figure 5.6 the distribution of surface anisotropy axes of the spherical particle containing $N=360$ spins (176 surface spins and 184 core spins) as a function of the azymuthal angle ψ_s between a surface spin easy axis and applied field. This Figure will be also useful to our attempts at giving intuitive explanations to the computational results.
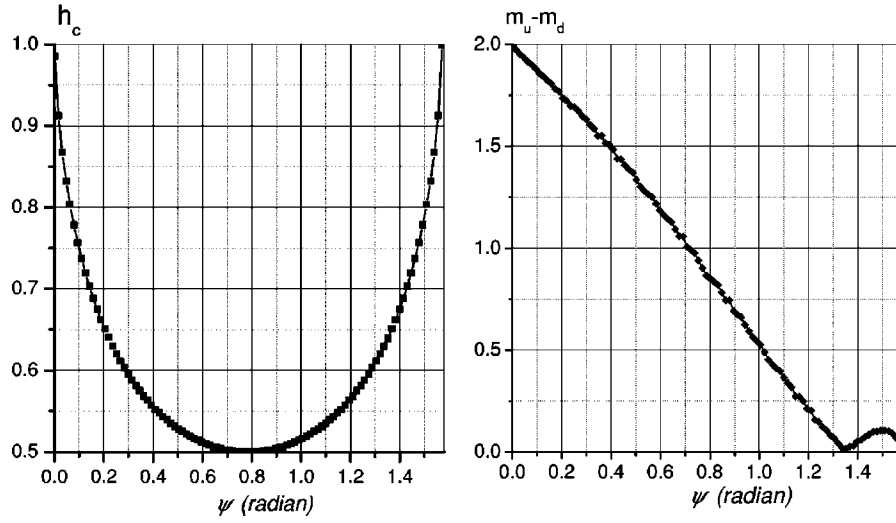
Figure 5.5: One-spin problem. Left: critical field as function of ψ. Right: height of magnetization jumps as function of ψ.
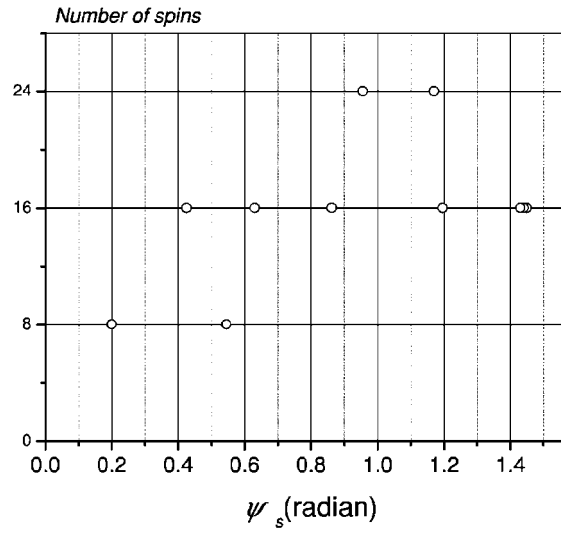

Figure 5.6: Distribution of surface anisotropy axes versus the azymuthal angle ψ_s for a spherical particle with diameter $D=10$ ($n=360$: 176 surface spins and 184 core spins).

Effects of the exchange coupling

In this subsection we focus on the effects of exchange coupling on the hysteretic loops of the nanoparticle described above. We first consider the case in which the anisotropy constants in the core and on the surface are equal, i.e., k_s=1.0, and the magnetic field applied along the easy axis of the core spins, so as to investigate the influence of radial direction of surface anisotropy. For $j \ll 1$, i.e., j=0, 0.01, we can see along portion 1–2 in Figure 5.7 a progressive increase in the magnetization, which is due to the alignment of surface spins, since as the field direction is along the core easy axis, the core spins have a rectangular cycle and the jump is at h=1.0. Next, along portion 2–3 we can see two jumps. Indeed, according to the distribution of surface easy axes in Figure 5.6, and the critical field as a function of ψ in Figure 5.5 (left), those surface spins with ψ_s between 0.6 and 1.0 are responsible for the first jump, and those with ψ_s between 0.4 and 0.6 or 1.0 and 1.2 are responsible for the second jump. Next, along portion 3–4 we have successive small jumps and thereby a slight increase in the magnetization. The origin of these small jumps resides in two contributions. One contribution comes from those surface spins whose easy axis makes an angle around 0.2 with the field. Even though the corresponding height of jump is large (see Figure 5.5 (right)), their number is rather small (see Figure 5.6) thus rendering a small contribution to the magnetization. The other contribution is due to surface spins with an angle ψ_s~1.4, which yield a small contribution owing to the fact that the height of the corresponding jump is very small (see Figure 5.5, ψ_s>1.2), even though their number is relatively large. On the last portion of the lower branch of the hysteresis in Figure 5.7, we see another big jump, which is due to the

switching of core spins at the field h_c=1.0. At last, there is a slow increase of magnetization due to a final adjustment of surface spins along the field direction. In the present case, the surface fully switches before the core (see Figure 5.8).

For j=0.1, we see that the surface behavior remains almost the same as in the previous cases, whereas the core spins now switch clusterwise as can be seen in the fourth picture of Figure 5.8. Indeed, regarding the exchange field as a small perturbation of the applied magnetic field, it is clear that the core spins located near the surface are subject to an effective field whose direction is slightly deviated from their easy axis, i.e., the corresponding angle ψ is slightly different from zero. Now, in Figure 5.5(left) we can see that this little deviation in ψ produces an important change in the switching field. On the contrary, we find that this effect is almost absent in what concerns the jumping field of surface spins, as can be seen along portion 2–3 in Figure 5.7 upon comparing the loops for j=0, j=0.01, and j=0.1. Indeed, the surface spins responsible for these jumps have their easy axes at an angle $0.6< \psi_s <1.0$, and hence the change in the corresponding critical field is very small (see Figure 5.5 (left)). In Figure 5.7 we can also see that for j=0.1, i.e., when the exchange energy becomes comparable with anisotropy and Zeeman energy, there are more jumps that can be attributed to the switching of different spherical shells of core spins starting from surface down to the center. This situation is sketched in Figure 5.8. For example, for h=0 one can see that the exchange has a little influence on surface spins, as they are directed almost along their easy axes; for h=0.64 the surface spins show the same behavior as in the absence of exchange, but part of core spins, located near the surface, are deviated from their easy axes. At the field h=0.8 all these core spins

have already switched and the similar processes happened for other shells of core

spins as the field is slowly increased (see the plot corresponding to h=0.88). Finally,

for large enough applied fields the magnetization saturates, so all spins switched and

are approximately oriented along the same direction.

For j=1~k_s , although there is only one jump, the hysteresis loop is not

rectangular owing to the fact that the spins rotate in a noncoherent way, as can be

seen in Figure 5.9. This is due to a compromise between anisotropy and exchange

energies, see, for example, the picture for h=0. Moreover, even a small number of

neighbors lying in the core produce a large effect via exchange on the behavior of a

surface spin.
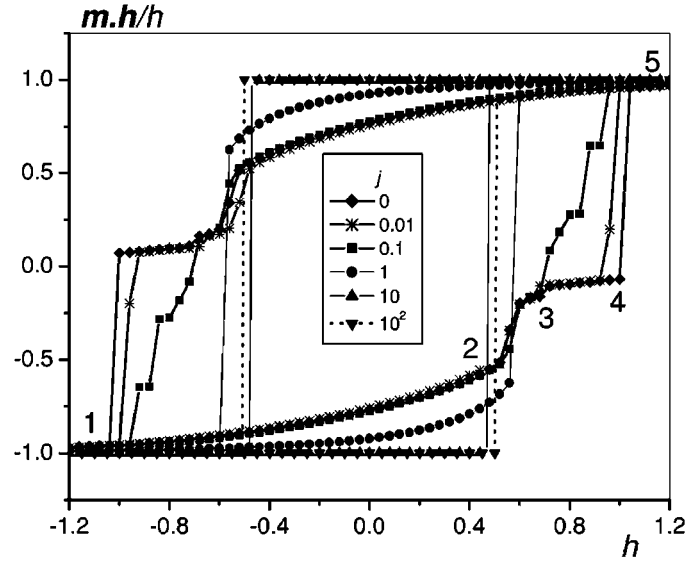
Figure 5.7: Hysteresis loop, i.e., plot of the magnetization projection on the field

direction as a function of the (reduced) field h, for ψ=0, k_s=1 and different values of j.

n=360.
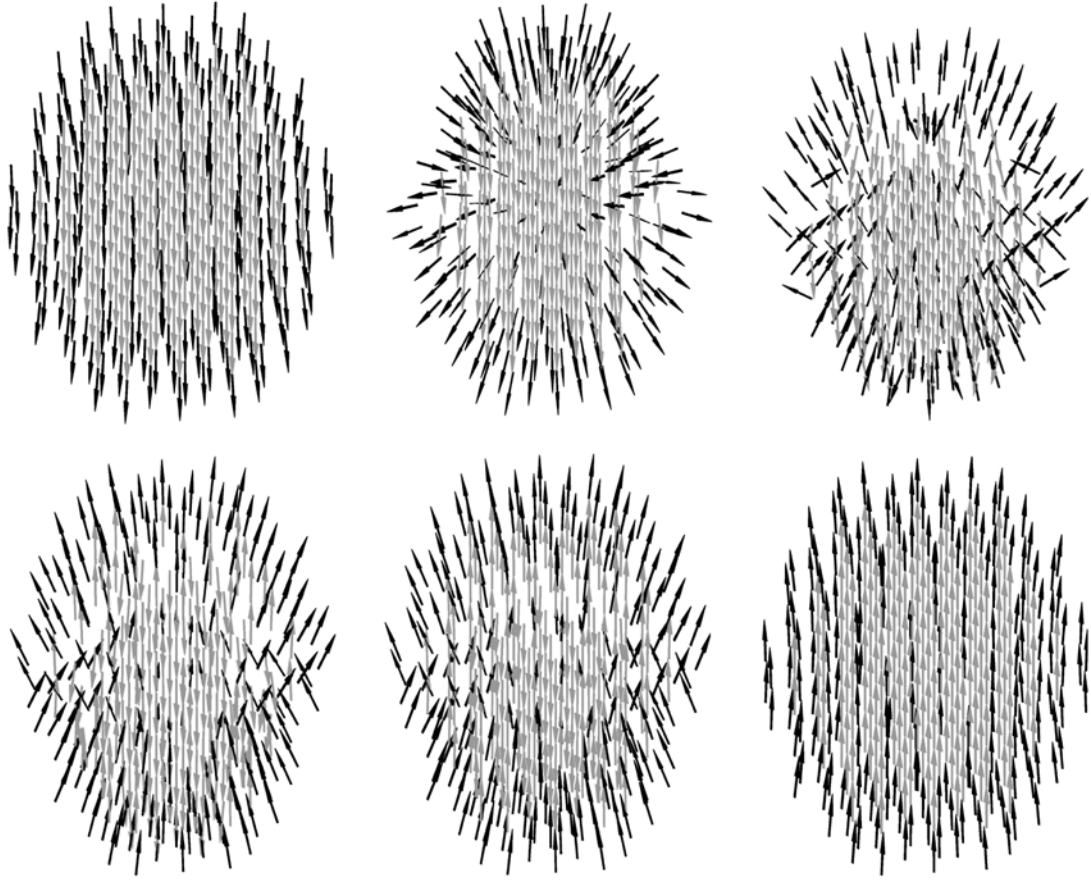
Figure 5.8: Magnetic structure for j=0.1, k_s=1 for the field values h=-4.0, 0, 0.64, 0.8, 0.88, 4 which correspond to the saturation states and different switching fields shown in Figure 5.7. These field values correspond to the pictures when starting from the upper array and moving right, down left, and then right. Gray arrows represent core spins and black arrows represent surface spins.
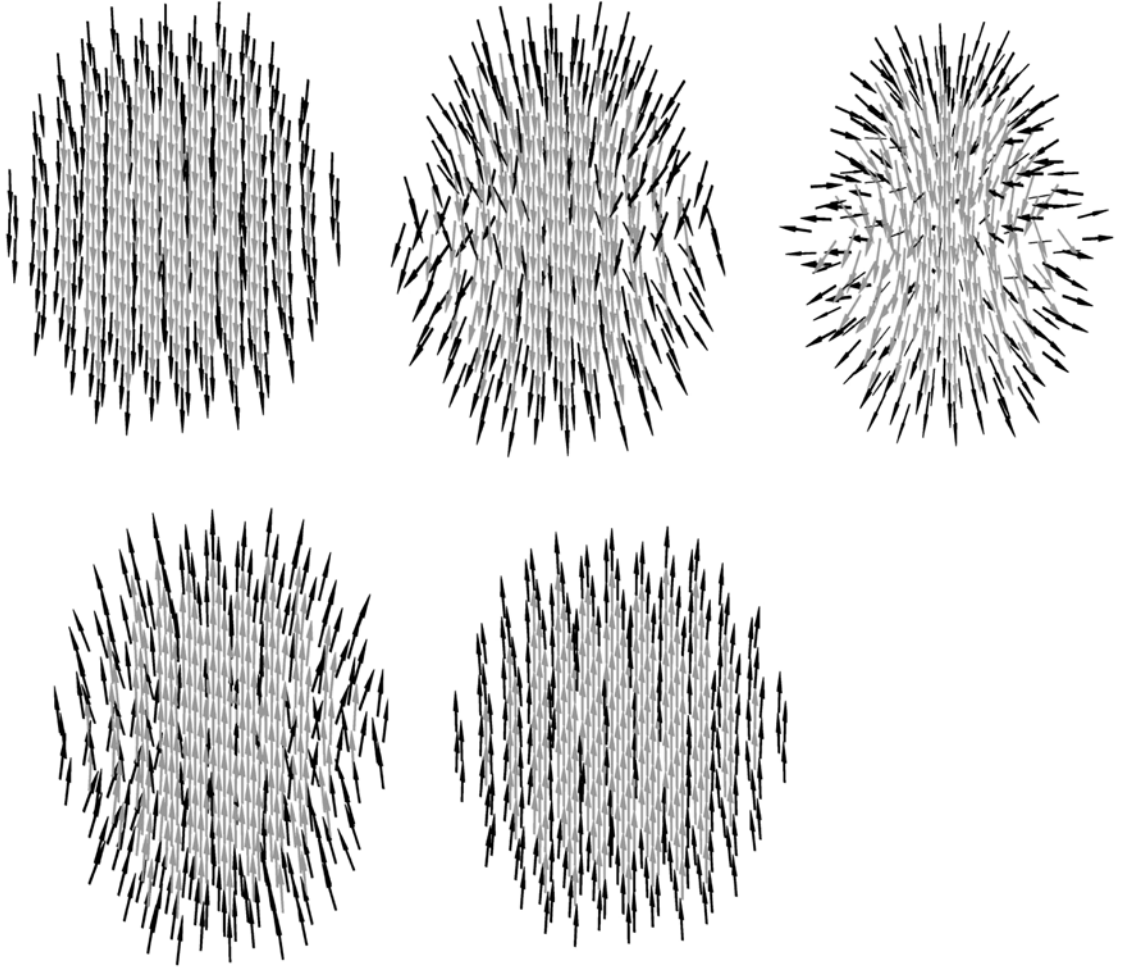
Figure 5.9: Magnetic structure for j=1, k_s=1 for the field values h=-4.0, 0, 0.56, 0.6, 4 which correspond to the saturation states and different switching fields shown in Figure 5.7. Gray arrows represent core spins and black arrows represent surface spins.

For much larger values of j the spins are tightly coupled and move together, and the corresponding (numerically obtained) critical field h_c coincides with the analytical expression obtained in the limit $j \rightarrow \infty$, i.e., $h_c = n_c/n$, where n_c is the number of core spins (see the previous section for an extensive discussion).

Next we consider the case of larger values of k_s, e.g., $k_s = 10$, so as to investigate the influence of surface anisotropy both in direction and strength. The results are presented in Figure 5.10 (left). Here, a notable difference with respect to the previous case, $k_s = 1$, is the fact that the core now switches before the surface and at higher fields. Moreover, there appear more jumps which may be attributed to the switching of various clusters of surface spins. Both cases show that as the ratio j/k_s decreases, the magnetization requires higher fields to saturate. This is further illustrated by Figure 5.10 (right) where $k_s = j = 100$ for a smaller particle.
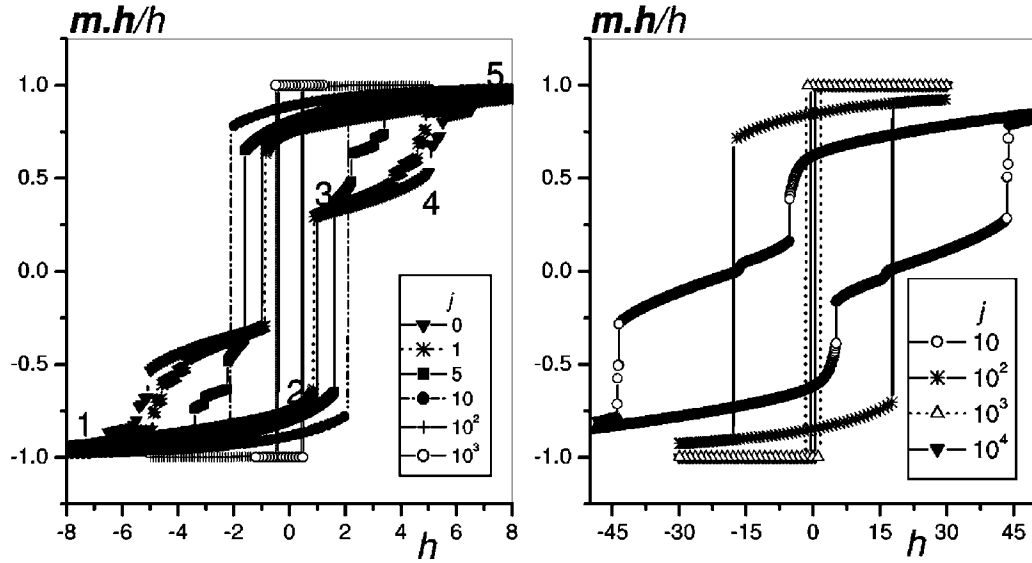

Figure 5.10: Left: Hysteresis loops for $\psi = 0$, $k_s = 10$, and selected values of j. $D = 10$ ($n = 360$). Right: Hysteresis loops for $\psi = 0$, $k_s = 100$, and selected values of j. $D = 7$ ($n = 123$).

Let us now summarize the ongoing discussion. We recall that considering a radial distribution for surface anisotropy, leads, even in the case of strong exchange and weak surface anisotropy, to important quantitative deviations from the classical Stoner-Wohlfarth model. In particular, the critical field in our model is given by:

$$h_c^r = \frac{n_c}{n} h_c^u ,$$ (5.16)

where h_c^r is the critical field for a spherical particle with radial anisotropy on the surface and uniaxial anisotropy in the core (i.e. the above discussed case) and h_c^u is the critical field for a spherical particle with uniaxial anisotropy for all spins (Stoner-Wohlfarth case). Then, when j and k_s become comparable, the compromise between exchange coupling, favoring a full alignment of the spins along each other, and surface anisotropy, which favors the alignment of surface spins along their radial easy axes, produce large deviations from uniform spin motion, and obviously from Stoner-Wohlfarth results. More precisely, the shape of hysteresis loop for the case of the magnetic field applied along anisotropy axis is no longer rectangular, and moreover, there appear multiple jumps.

Effect of the particle's size

Here, we study the effect of varying the particle's size while keeping j and k_s fixed. So we use the same value of anisotropy constant for all spins and strong exchange (for the first discussed case $k_s=1$, $j=100$) and vary the particle's diameter from 6 ($n=56$) to 30 ($n=12712$). In Figure 5.11 (left) there are presented hysteresis cycles of a particle with different diameters when the field is along the core easy axis, and on the right the variation with the particle's diameter of the critical field (in

123

diamonds) obtained from the numerical solution of the Landau-Lifshitz equation, and (in circles) the analytical results [see Equation (5.16) and Section 5.2]. The figure on the left shows that for such a value of k_s the hysteresis loop is rectangular for all sizes, and that the critical field decreases with the particle's size. The latter fact is clearly illustrated by the figure on the right.

Next, in Figure 5.12 (left) we present the hysteresis loop in the case where the surface anisotropy constant k_s equals the exchange coupling and the field is applied along the core easy axis, and in Figure 5.12 (right) the switching field, which marks the magnetization reversal, as a function of the particle's diameter D. As opposed to previous cases, this field no more coincides with the critical field, which marks the limit of metastability. This is obviously related to the appearance of the multiple jumps in hysteresis cycles. Moreover the values of the switching field are much higher, and more important its behavior is opposite to that of the previous case. Indeed, here we see that the switching field increases when the particle's size is lowered. For such high values of k_s ($K_s \gg K_c$) surface spins are almost aligned along their radial easy axis, and because of the strong exchange coupling they also drive core spins in their switching process. Thus the smaller the particle the larger the surface contribution and the larger the field required for complete reversal of the particle's magnetization. This could explain the nonsaturation of magnetization that has been observed in, e.g., cobalt particles [111].
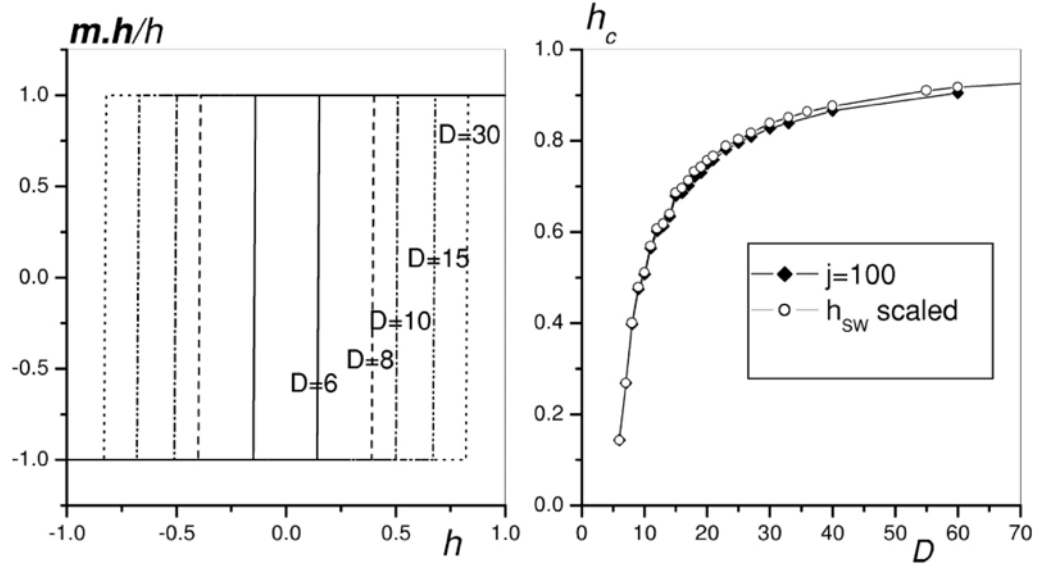
Figure 5.11: Left: Hysteresis loops for $\psi=0$, $k_s=1$, $j=100$ for different values of the particle diameter D. Right: Switching field for the same parameters as function of D.
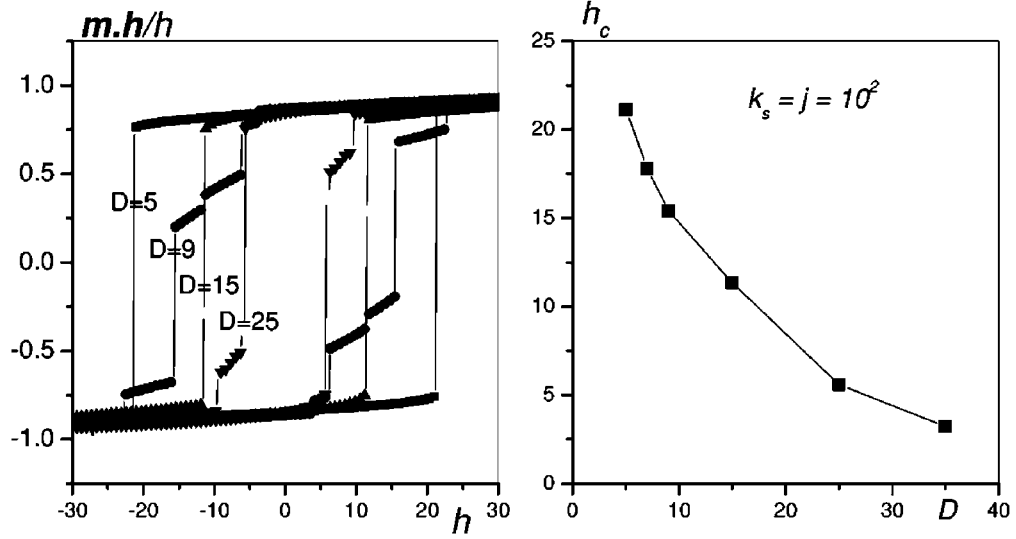
Figure 5.12: Left: Hysteresis cycles for $\psi=0$, $k_s=100$, $j=100$, and different values of the particle diameter D. Right: Switching field as a function of D for the same parameters.

Effect of the surface anisotropy constant k_s

Now, we fix the exchange coupling constant j, the particle's total number of spins N, and vary the surface anisotropy constant k_s. Because K_c is in general two to three orders of magnitude smaller than J, we have investigated the effect of surface anisotropy constant in the case of $j=J/K_c=100$.

In contrast with the case $k_s \leq 1$ and $j=10^2–10^3$ where the hysteresis loop and the limit-of-metastability curve scale with the Stoner-Wohlfarth ones with the same scaling constant for all angles between the applied field and core easy axis, we find that for $1<k_s<20$ the scaling constant depends on the angle ψ, as can be seen in Figure 5.13. This fact explains the deformation of the Stoner-Wohlfarth astroid, which is a depression in the core easy direction and an enhancement in the perpendicular direction.
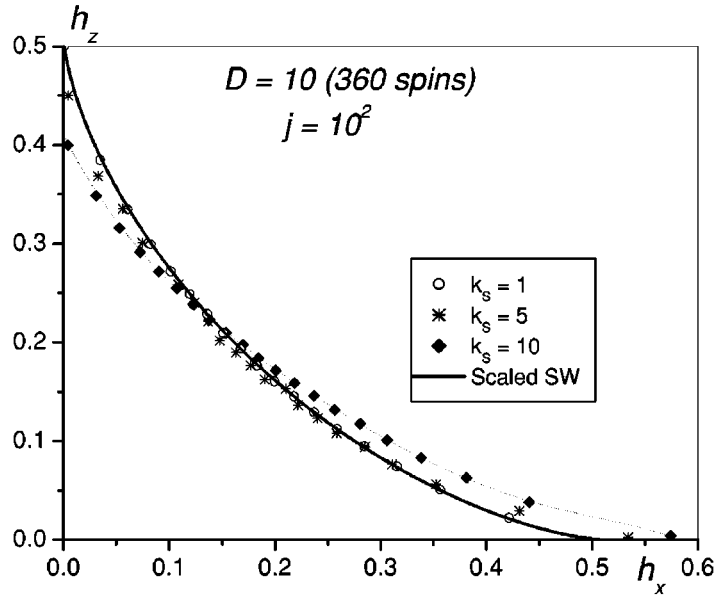
Figure 5.13: Astroid for $j=10^2$, $n=360$ and different values of surface anisotropy constant k_s. The full line is the Stoner-Wohlfarth astroid scaled with n_c/n.

For larger values of k_s the computed hysteresis loops for $\psi=0$, $n=360$, $j=100$ are given in Figure 5.14. Here, we first note that the shape of the hysteresis loop is rather different from that rendered by the Stoner-Wohlfarth model, since for $k_s=30$, for instance, the hysteresis loop is no longer rectangular, even that $\psi=0$. As explained earlier, this effect is due to the now more pronounced nonuniform rotation of surface spins and core spins located near the surface, and thereby that of the particle's magnetization.
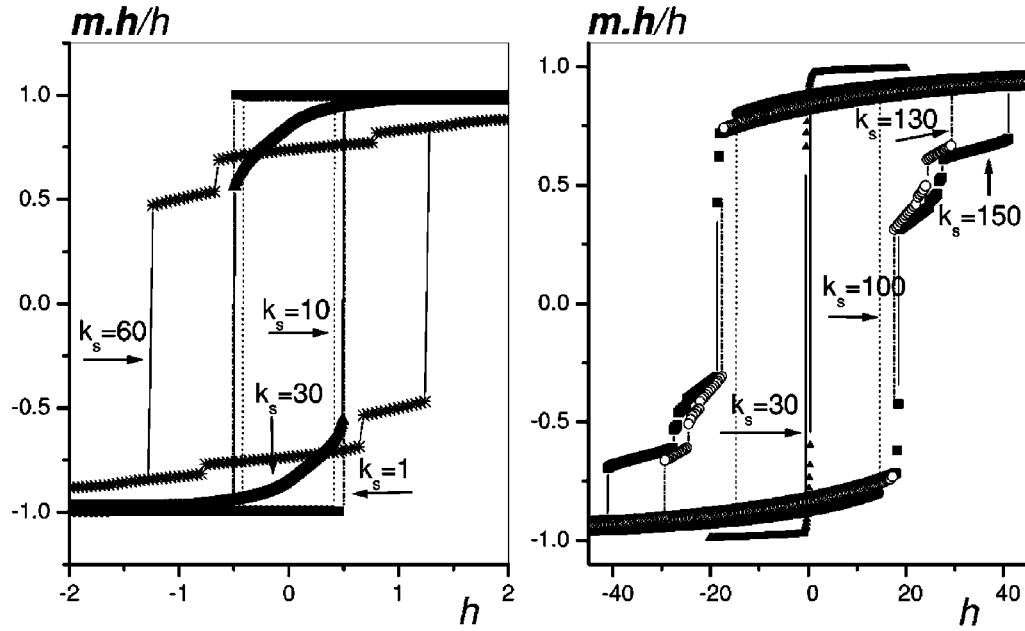
Figure 5.14: Hysteresis loops for $\psi=0$, $j=100$, $D=10$ and various values of surface anisotropy constant k_s. These two sets of data are presented as two plots because of scaling mismatch.

Our model of a spherical particle with uniaxial anisotropy in the core and radial anisotropy on the surface leads to three pertinent regions as far as the competition between surface anisotropy energy and exchange energy is concerned:

For small values of this parameter, e.g., $k_s/j<0.01$, our model renders hysteresis loops and limit-of-metastability curves that scale with the Stoner-Wohlfarh results for all values of the angle ψ between the core easy axis and the applied field, the scaling constant being n_c/n. The critical field increases with the particle's size and tends to the Stoner-Wohlfarth critical field in relatively large systems.

For larger values of k_s/j, but $k_s/j<0.2$, we still have some kind of scaling but the corresponding constant depends on ψ. This is reflected by a deformation of the limit-of metastability curve. More precisely, the latter is depressed in the core easy direction and enhanced in the perpendicular direction. However, there is still only one jump in the hysteresis loop implying that the magnetization reversal can be considered as close to the uniform mode. The small deviations to the uniform motion are observed and they are confined to a small boundary region.

For larger values of k_s/j, there appear multiple steps in the hysteresis loop which may be associated with the switching of spin clusters. The appearance of these steps makes the computed hysteresis loops qualitatively different from those of the above cases, as strongly pronounced nonuniformities exist in the magnetization reversal. In addition, in the present case, there are two more new features: the values of the switching field are much higher, and more importantly, its behavior as a function of the particle's size is opposite to that of the previous cases. More precisely, here we find that this field increases when the particle's size is lowered.

5.4. Influence of surface anisotropy on precessional magnetization switchings in nanoparticles

In this section, the study of surface anisotropy effects on the precessional magnetization switchings in nanoparticles is presented.

In the previous section it is shown that in the absence of the applied field there are two well-defined states with the global magnetization oriented along $\mathbf{e}_z$ and $-\mathbf{e}_z$, respectively, as long as the surface anisotropy constant k_s is small in comparison with the exchange j ($k_s / j \leq 0.2$). This situation is consistent with experimental results, as has been observed in Reference [101]. These two stable minima are surrounded by two energy wells, separated by the boundary corresponding to the global magnetization component $m_z=0$. Thus, the precessional switching can be defined with respect to the global magnetization in a similar mode to the one given in Chapter 3 for precessional magnetization switching in perpendicular media.

The behavior of this dynamical system is determined by an interplay between four parameters: the dimension of the particle (diameter), reduced exchange constant j ($\gg 1$), reduced surface anisotropy constant k_s and the damping parameter α ($\ll 1$). Our analysis leads to the following conclusions regarding the precessional switching of magnetic nanoparticles. First, the dimension of the particle can be considered as a scaling parameter. This effect is apparent from Eqs. (10) and (12) and has been illustrated in Figure 5.3. Second, the damping parameter α leads only to first order corrections to the critical field curves of precessional switching found by using undamped magnetization dynamics during the time period when the magnetic field is applied. These corrections are typically less than 5%. Finally, three distinct regions

can be observed as far as the competition between surface anisotropy and exchange is concerned. In the first region, corresponding to $k_s/j<0.01$, the spins motion can be considered uniform (macrospin region). In this region, the critical curve is a scaled version of the critical curve for bulk material (when all spins are considered to have the same anisotropy direction and constant). In a second region, corresponding to $0.01<k_s/j<0.2$, small deviations from the uniform motion are observed and they are confined to a small boundary region (boundary layer phenomena). These deviations lead to the decrease in the critical switching magnetic field for large obtuse angles (see Figure 5.15). The third region ($0.2<k_s/j$) corresponds to strongly pronounced nonuniformities in the magnetization dynamics as has also been observed in the quasi-static studies. In this region, the notion of precessional switching can not be well defined as far as the final spatial configuration of magnetization is concerned.
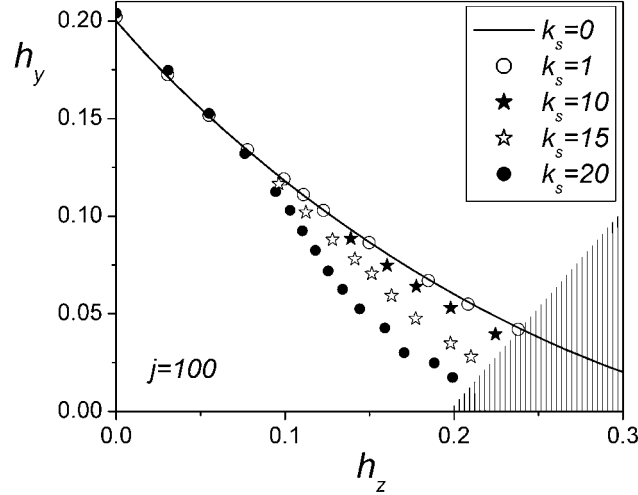

Figure 5.15: Critical curves for selected values of surface anisotropy constant k_s. Exchange constant $j=100$, diameter $D=7$ ($n=123$), and damping parameter $\alpha=0.01$.

6. Conclusions

The evolution of data storage technology has been impressive over the last fifty years. However, the paradigm of magnetic data storage is approaching its fundamental limits for areal storage density, as well as for speed in data processing. As a result, there is an urgent need for finding reliable alternatives to current magnetic recording media, which are based on longitudinal thin film, and to the conventional mechanism of magnetization reversal, based on damping switching.

In this dissertation, faster modes of magnetization reversals, using precessional magnetization motion, were analyzed in traditional longitudinal media and in its promising alternatives: perpendicular and patterned media. This analysis used multi-spin description of magnetic nanoparticles and continuum micromagnetics for thin film media. The spins dynamics in both discrete and continuum versions was modeled by Landau Lifshitz type equations.

The case of the perpendicular media subject to rectangular magnetic field pulses was first analyzed. The features of precessional magnetization switching and conventional magnetization reversal were compared, based on analytical solutions found for these problems. By using integrals of motion and "unit disk representation" of undamped magnetization dynamics, the expressions for critical fields and pulse durations that guarantee precessional reversals were analytically derived. This study was then extended to non-rectangular magnetic field pulses by using the inverse problem approach to design magnetic field pulses that guarantee precessional switching.

The analysis of precessional magnetization switching in longitudinal thin film media was then undertaken. After a short summary of the research studies on this topic, the inverse problem approach to the analysis of precessional switching in these media was presented. This approach led to explicit expressions for the magnetic field pulses that guarantee the precessional switching.

In the end, the study of surface anisotropy effects on magnetization reversals in nanoparticles was presented. Magnetic nanoparticles are the building blocks in patterned magnetic media, which represent a very promising direction for further improvement of magnetic data storage technology. The expressions for critical magnetic fields that guarantee the quasi-static and precessional reversals were derived analytically for the case of very strong exchange and weak surface anisotropy. These analytical results have also been used to test the numerical approach applied to the general case of the problem. The distinct features of the quasi-static and precessional reversals in nanoparticles were examined and their dependence on various parameters of the problem was discussed.

In conclusion, this thesis provides a theoretical analysis of magnetization dynamics in nanometer scale structures over picosecond time scales. The results presented here are of direct technological relevance for increasing the speed of data processing in HDD and MRAM. They offer valuable information for the design of magnetic field pulse that guarantee precessional switching and are also filling many gaps existent in understanding ultrafast magnetization reversals in nanostructures.

REFERENCES

1. J.G. Zhu, "New heights for hard disk drives", *Materials Today*, vol. 6, no.7-8, 2003, pp.22-31.

2. A. Moser, K. Takano, D.T. Margulies, M. Albrecht, Y. Sonobe, Y. Ikeda, S. Sun, and E.E. Fullerton, "Magnetic Recording: advancing into the future", *J. Phys. D: Appl. Phys.*, vol. 35, 2002, pp. R157-R167.

3. S.X. Wang and A.M. Taratorin, "Magnetic Information Storage Technology", *Academic Press*, San Diego 1999.

4. D.E. Speliotis, "Magnetic recording beyond the first 100 years", *J. Magn. Magn. Mater.*, vol. 193, 1999, pp. 29-35.

5. J. DeBrosse, D. Gogl, A. Bette, H. Hoenigschmid, R. Robertazzi, C. Arndt, D. Braun, D. Casarotto, R. Havreluk, S. Lammers, W. Obermaier, W.R. Reohr, H. Viehmann, W.J. Gallagher, and G. Müller, "A high-speed 128-kb MRAM core for future universal memory applications", *IEEE J. Solid-State Circuits*, vol. 39, no. 4, 2004, pp. 678-683.

6. R.P. Cowburn, "The future of universal memory", *Materials Today*, vol. 6, no. 7-8, 2003, 32-38.

7. B.N. Engel, J. Akerman, B. Butcher, R. W. Dave, M. DeHerrera, M. Durlam, G. Grynkewich, J. Janesky, S. V. Pietambaram, N. D. Rizzo, J. M. Slaughter, K. Smith, J. J. Sun, and S. Tehrani, "A 4-MB toggle MRAM based on a novel bit and switching method", *IEEE Trans. Magn.*, vol. 41, no.1, 2005, pp. 132-136.

8. S. Tehrani, J.M. Slaughter, E. Chen, M. Durlam, J. Shi, and M. DeHerrera "Progress and outlook for MRAM technology", IEEE Trans. on Magn., vol. 35, no. 5, 1999, pp. 2814-2819.

9. Z. Gai, J.Y. Howe, J. Guo, D.A. Blom, E.W. Plummer, J. Shen, "Self-assembled FePt nanodot arrays with mono-dispersion and –orientation", *Appl. Phys. Let.*, vol. 86, 2005, art. no. 023107.

10. S. Sun, C.B. Murray, D. Weller, L. Folks, A. Moser, "Monodisperse FePt nanoparticles and ferromagnetic FePt nanocrystal superlattices", *Science*, vol. 287, 2000, pp. 1989-1991.

11. H.C. Siegmann, E.L. Garwin, C.Y. Prescott, J. Heidmann, D. Mauri, D. Weller, R. Allenspach, W. Weber, "Magnetism with picosecond field pulses", *J. Magn. Magn. Mater.*, vol. 151, 1995, pp. L8-L12.

12. B. Hillebrands and K. Ounadjela (eds.), "Spin dynamics in confined magnetic structure I", *Springer*, Berlin, 2001.

13. B. Hillebrands and K. Ounadjela (eds.), "Spin dynamics in confined magnetic structure II", *Springer*, Berlin, 2003.

14. J. C. Mallinson, "Magneto-resistive and spin valve heads: fundamentals and applications", *Academic Press*, San Diego, 2001.

15. D.A. Thompson and J.S. Best, "The future of magnetic data storage technology", *IBM J. Res. Develop.*, vol. 44, no. 3, 2000, pp 311-322.

16. C.A. Ross, "Patterned magnetic recording media", *Annu. Rev. Mater. Res.*, vol 31, 2001, pp. 203-235.

17. K. Stoev, F. Liu, Y. Chen, X. Dang, P. Luo, J. Chen, J. Wang, K. Kung, M. Lederman, M. Re, G. Choe, J.N. Zhou, M. Yu, "Demonstration and characterization of 130 Gb/in(2) magnetic recording systems", *J. Appl. Phys.*, vol. 93, no. 10, 2003, pp 6552-6554.

18. Zhang Z, et al, "Magnetic recording demonstration over 100Gb/in^2", *IEEE Trans. Magn.*, vol. 38, no. 5, 2002, pp. 1861-1866.

19. G. Choe, J.N. Zhou, B. Demczyk, M. Yu, M. Zheng, R. Weng, A. Chekanov, K.E. Johnson, F. Liu, K. Stoev, "Highly in-plane oriented CoCrPtB longitudinal media for 130-Gb/in(2) recording", *IEEE Trans. Magn.*, vol. 39, no. 2, 2003, pp. 633-638.

20. Aharoni A., "Introduction to the theory of ferromagnetism", *Clarendon Press*, Oxford, 1998.

21. W.F. Brown, "The fundamental theorem of fine-ferromagnetic–particle theory", *J. Appl. Phys.*, vol. 39, no. 2, 1968, pp. 993-994.

22. W.F. Brown, "Micromagnetics", *Interscience Publisher*, New York, 1963.

23. A. Hubert and R. Schafer, "Magnetic domains: the analysis of magnetic microstructures", Springer, Berlin, 1998.

24. H. Kronmuller and M. Fahnle, "Micromagnetism and the microstructure of ferromagnetic solids", *Cambridge University Press*, Cambridge, 2003.

25. W. Wernsdorfer, "Classical and quantum magnetization reversal studied in nanometer-sized particles and clusters", *Adv. Chem. Phys.*, vol. 118, 2001, pp. 99-190.

26. A. Aharoni, "Perfect and imperfect particles", *IEEE Trans. Magn.*, vol. 22, 1986, pp. 478-483.

27. E.C. Stoner and E.P. Wohlfarth, "A mechanism of magnetic hysteresis in heterogeneous alloys", *Phil. Trans. Roy. Soc.*, vol. 240, 1948, pp. 599-642. Reprinted in *IEEE Trans. Magn.*, vol. 27, no. 4, 1991, pp. 3475-3518.

28. L. Neel, "Théorie du trainage magnétique des ferromagnétique en grains fins avec applications aux terres cuites", *Ann. Geophys.*, vol. 5, 1949, pp. 99-135.

29. D. Weller and A. Moller, "Thermal effect limits in ultrahigh-density magnetic recording", *IEEE Trans. Magn.*, vol. 35, no. 6, 1999, pp. 4423-4439.

30. R.H. Victora, "Predicted time dependence of the switching field for magnetic materials", *Phys. Rev. Lett.*, vol. 63, no. 4, 1989, pp. 457-460.

31. O.A. Chubykalo, B. Lengsfield, B. Jones, J. Kaufman, J.M. Gonzalez, R.W. Chantrell, R. Smirnov-Rueda, "Micromagnetic modelling of thermal decay in interacting systems", *J. Magn. Magn. Mater.*, vol. 221, 2000, pp. 132-136.

32. M. Yu, Y. Liu, A. Moser, D. Weller, D. J. Sellmyer, "Nanocomposite CoPt:C films for extremely high-density recording", *Appl. Phys. Lett.*, vol. 75, no. 25, 1999, pp. 3992-3994.

33. B.G. Demczyk, J.N. Zhou, G. Choe, E. Stach, E.C. Nelson, U. Dahmen, "Origin of the orientation ratio in sputtered longitudinal media", *J. Appl. Phys.*, vol. 93, no. 10, 2003. pp 7393-7395.

34. S. Iwasaki and K. Ouchi, "Co-Cr recording films with perpendicular magnetic anisotropy", *IEEE Trans. Magn.*, vol. 14, no. 5, 1978, pp. 849-851.

35. S. Iwasaki, "Perpendicular magnetic recording", *IEEE Trans. Magn.*, vol. 16, no. 1, 1980, pp. 71-76.

36. S. Iwasaki, "Guiding principle for research on perpendicular magnetic recording", *IEEE Trans. Magn.*, vol. 41, no. 2, 2005, pp 683-686.

37. R.L. White, R.M.H. New, and R.F.W. Pease, "Patterned media: a viable route to 50 Gbit/in[2] and up for magnetic recording?", *IEEE Trans. Magn.*, vol. 33, no. 1, 1997, pp 990-995.

38. M.R. Freeman, R.R. Ruf, and R.J. Gambino, "Picosecond pulsed magnetic fields for studies of ultrafast magnetic phenomena", *IEEE Trans. Magn.*, vol. 27, no. 6, 1991, pp. 4840-4842.

39. M.R. Freeman, M.J. Brady, and J. Smith, "Extremely high-frequency pulse magnetic resonance by picosecond magnetooptic sampling", *Appl. Phys. Lett.*, vol. 60, no. 20, 1992, pp. 2555-2557

40. M.R. Freeman, "Picosecond studies of nonequilibrium flux dynamics in a superconductor", *Phys. Rev. Lett.*, vol. 69, no. 11, 1992, pp. 1691-1694.

41. M.R. Freeman "Picosecond pulsed probes of magnetic systems", *J. Appl. Phys.*, vol. 75, no. 10, 1994, pp. 6194-6198.

42. L. He, W.D. Doyle, and H. Fujiwara, "High speed coherent switching below the Stoner-Wohlfarth limit", IEEE Trans. Magn., vol. 30, no. 6, 1994, pp. 4086-4088.

43. L. He and W.D. Doyle, "A theoretical description of magnetic switching experiments in picosecond field pulses", J. Appl. Phys., vol. 79, no. 8, 1996, pp. 6489-6491.

44. C.H. Back, D. Weller, J. Heidmann. D. Mauri, D. Guarisco, E.L. Garwin, and H.C. Siegmann, "Magnetization reversal in ultrashort magnetic field pulses", Phys. Rev. Lett., vol. 81, no. 15, 1998, pp. 3251-3254.

45. C.H. Back and H.C. Siegmann, "Ultrashort magnetic field pulses and the elementary process of magnetization reversal", *J. Magn. Magn. Mater.*, vol. 200, 1999, pp. 774-785.

46. T. Gerrits, H.A.M. van der Berg, J. Hohlfeld, L. Bar, and T. Rasing, "Ultradast precessional magnetization reversal by picosecond magnetic field pulse shaping", *Nature*, vol. 418, 2002, pp. 509-511.

47. H.W. Schumacher, C. Chapert, R.C. Sousa, P.P. Freitas, and J. Miltat, "Quasibalistic magnetization reversal", *Phys. Rev. Lett.*, vol. 90, no. 1, 2003, art. no. 017204.

48. S. Kaka and S.E. Russek, "Precessional switching of submicrometer spin valves", *Appl. Phys. Lett.*, vol. 80, no. 16, 2002, pp. 2958-2960.

49. A. Krichevsky and M.R. Freeman, "Precessional switching of a 3x1 micrometer elliptic element in a crossed-wire geometry", *J. Appl. Phys.*, vol. 95, no. 11, 2004, pp. 6601-6603.

50. J. Newman (ed.), "The world of mathematics", vol. 3, *Dover Publications*, New York, 2000.

51. D.C. Mattis, "The theory of ferromagnetism", *Harper and Row*, New York, 1965.

52. J. Miltat, G. Albuquerque, and A. Thiaville, "An introduction to micromagnetics in the dynamic regime", in Reference [12], pp. 1-31.

53. L. P. Levy, "Magnetism and superconductivity", *Springer*, Berlin, 2000. pp. 166-169.

54. A. H. Morrish, "The physical principles of magnetism", *John Wiley and Sons*, New York, 1965 pp. 27-29

55. M. Sparks, "Ferromagnetic relaxation theory", *McGraw-Hill Book Company*, New York, 1964.

56. A.G. Gurevich and G.A. Melkov, "Magnetization oscillations and waves", *CRC Press*, Boca Raton, 1996.

57. L. Landau and E. Lifshitz, "On the theory of the dispersion of magnetic permeability in ferromagnetic bodies", Phys. Z. Sowjet., vol. 8, 1935, pp. 135-148; reprinted in "Collected papers of L.D. Landau", *Gordon and Breach*, New York, 1965.

58. F. Bloch, "Nuclear inductions", *Phys Rev.*, vol. 70, no. 7, 1946, pp. 460-474.

59. T. L. Gilbert "Formulation, foundations and applications of the phenomenological theory of ferromagnetism", *PhD Thesis*, Illinois Institute of Technology, 1956; partially reprinted in *IEEE Trans. Magn.*, vol. 40, no. 6, 2004, pp. 3443-3449.

60. A. Bloch, P.S. Krishnaprasad, J.E. Marsden, and T.S. Ratiu, "The Euler-Poincare equations and double bracket dissipation", *Comm. Math. Phys.*, vol. 175, 1996, pp. 1-42.

61. G. Bertotti, I.D. Mayergoyz, and C. Serpico, "Identification of the damping coefficient in Landau-Lifshitz equation", Physica B, vol. 306, 2001, pp. 102-105.

62. D.C. Matis "The theory of magnetism", *Harper and Row*, New York, 1965.

63. C.S. Wang, R.E. Prange, and V. Korenman, "Magnetism in iron and nickel", *Phys. Rev. B*, vol. 25, no. 9, 1982, pp. 5766-5777.

64. M. van Schilfgaarde and V.P. Antropov, "First-principles exchange interactions in Fe, Ni, and Co", *J. Appl. Phys.*, vol. 85, no. 8, 1999, pp. 4827-4829.

65. S. Moran, C. Ederer, and M. Fahnle, "Ab initio electron theory for ferromagnetism in Fe: pressure dependence of spin-wave energies, exchange parameter, and Curie temperature", *Phys. Rev. B*, vol. 67, 2003, art. no. 012407.

66. N. Mori, "Calculation of ferromagnetic anisotropy for Ni and Fe metals", *J. Phys. Soc. Japan*, vol. 27, 1969, pp. 307-312.

67. Y. Xie and J. A. Blackman, "Magnetic anisotropy of nanoscale cobalt particles", *J. Phys.: Condens. Matter.*, vol. 16, 2004, pp. 3163-3172.

68. G. T. Rado and H. Suhl (eds.), "Magnetism (III)", *Academic Press*, New York, 1963.

69. http://www.ctcms.nist.gov/~rdm/mumag.org.html

70. G.M.B. de Albuquerque, "Magnetization precession in confined geometry: physical and numerical aspects", *PhD thesis*, University Paris XI, Orsay, France, 2002.

71. A. Spargo, "Finite element analysis of magnetization reversal in granular thin films", *PhD thesis*, University of Wales, Bangor, U.K., 2003.

72. W. Scholz, "Scalable parallel micromagnetic solvers for magnetic nanostructures", *PhD thesis*, Technical University Vienna, Austria, 2003.

73. J. Fidler and T. Schrefl, "Micromagnetic modeling – the current state of the art", *J. Phys. D: Appl. Phys.*, vol. 33, 2000, R135-R156.

74. P.S. Krishnaprasad and X. Tan, "Cayley transforms in micromagnetics", *Physica B*, vol. 306, 2001, pp. 195-199.

75. C. Serpico, I.D. Mayergoyz, and G. Bertotti, "Numerical technique for the Landau-Lifshitz equation", *J. Appl. Phys.*, vol. 89, no. 11, 2001, pp. 6991-6993.

76. M. d'Aquino, W. Scholz, T. Schrefl, C. Serpico, and J. Fidler, "Numerical and analytical study of fast precessional switching", *J. Appl. Phys.*, vol. 95, no. 11, 2004, pp. 7055-7057.

77. J. C. Maxwell, "A treatise on electricity and magnetism", vol. 2, *Dover*, New York, 1954.

78. L. Carroll, "Alice's adventures in Wonderland and through the looking glass", *Signet Classics*, 2000.

79. R. Kikuchi, "On the minimum of the magnetization reversal time", *J. Appl. Phys.*, vol. 27, no. 11, 1956, pp. 1352-1357.

80. J.C. Mallinson, "Damped gyromagnetic switching", *IEEE Trans. Magn.*, vol. 36, no. 4, 2000, pp. 1976-1981.

81. R.F.M. Thornley, "Pulse response of recording media", *IEEE Trans. Magn.*, vol. 11, no. 5, 1975, pp. 1197-1199.

82. M.H. Kryder and F.B. Humphrey, "Micromagnetic characteristics of transverse diffuse domain boundaries in permaloy thin films", IEEE Trans. Magn., vol. 7, no. 3, 1971, pp. 725-728.

83. W.D. Doyle, L. He, P.J. Flanders, "Measurement of the switching speed limit in high coercivity magnetic media", *IEEE Trans. Magn.*, vol. 29, no. 6, 1993, pp. 3634-3636.

84. N.D. Rizzo, T.J. Silva, A.B. Kos, "Nanosecond magnetization reversal in high coercivity thin films", *IEEE Trans. Magn.*, vol. 26, no. 1, 2000, pp.159-165.

85. M. Abramowitz and I.A. Stegun (eds), "Handbook of mathematical functions", *Dover*, New Yok, 1972.

86. P.F. Byrd and M.D. Friedman, "Handbook of elliptic integrals for engineers and scientists", *Springer*, New York, 1971.

87. D.G. Porter, "Analytical determination of the LLG zero-damping critical switching field", *IEEE Trans. Magn.*, vol. 34, no. 4, 1998, pp.1663-1665.

88. B. Spinoza, "The ethics", *Oxford University Press*, 2000.

89. I. Tudosa, C. Stamm, A.B. Kashuba, F. King, H.C. Siegmann, J. Stohr, G. Ju, B. Lu, and D. Weller, "The ultimate speed of magnetic switching in granular recording media", *Nature*, vol. 428, 2004, 831-833.

90. C. Serpico, I.D. Mayergoyz, G. Bertotti, "Analytical solutions of Landau-Lifshitz equation for precessional switching", *J. Appl. Phys.*, vol. 93, no. 10, 2003, pp. 6909-6911.

91. G. Bertotti, I.D. Mayergoyz, C. Serpico, and M. d'Aquino, "Geometrical analysis of precessional switching and relaxation in uniformly magnetized bodies", *IEEE Trans. Magn.*, vol. 39, no. 5, 2003, pp. 2501-2503.

92. G. Bertotti, I.D. Mayergoyz, and C. Serpico, "Critical fields and pulse durations for precessional switching in thin magnetic films", *IEEE Trans. Magn.*, vol. 39, no. 5, 2003, pp. 2504-2506.

93. G. Bertotti, I.D. Mayergoyz, and C. Serpico, "Analytical solutions of Landau-Lifshitz equation for precessional dynamics", *Physica B*, vol. 343, 2004, pp. 325-330.

94. G. Bertotti, I.D. Mayergoyz, and C. Serpico,, "Averaging technique for the analysis of magnetization relaxations", *J. Appl. Phys.*, vol. 95, no. 11, 2004, pp. 6598-6600.

95. T. Devolder and C. Chappert, "Precessional switching of thin nanomagnets: analytical study", *Eur. Phys. J. B*, vol. 36, 2003, pp. 57-64.

96. T. Devolder and C. Chappert, "Cell writing selection when using precessional switching in a magnetic random access memory," *J. Appl. Phys.*, vol. 95, no. 4, 2004, pp. 1933-1941.

97. T. Devolder and C. Chappert, "Spectral analysis of the precessional switching of the magnetization in an isotropic thin film", Solid State Commun., vol. 129, no. 2, 2004, pp. 97-101.

98. E. Ott, J.C. Alexander, I. Kan, J.C. Sommerer, J.A. Yorke, "The transition to chaotic attractors with riddled basins", *Physica D*, vol. 76, 1994, pp. 384-410.

99. E. Ott, "Chaos in dynamics systems", *Cambridge University Press*, Cambridge, 2002.

100. http://nobelprize.org/physics/laureates/1977/anderson-lecture.pdf

101. M. Jamet, W. Wernsdorfer, C. Thirion, V. Dupuis, P, Melinon, A. Perez, D. Mailly, "Magnetic anisotropy in single clusters", *Phys. Rev. B*, vol. 69, 2004, art. no. 0244001

102. J. Bansmann, S.H. Baker, C. Binns, J.A. Blackman, J.P. Bucher, J. Dorantes-Davila, V. Dupuis, L. Favre, D. Kechrakos, A. Kleibert, K.H. Meiwes-Broer, G.M. Pastor, A. Perez, O. Toulemonde, K.N. Trohidou, J. Tuaillon, Y. Xie, "Magnetic and structural properties of isolated and assembled clusters", *Surf. Sci. Rep.*, vol. 56, 2005, pp. 189-275.

103. D.A. Garanin and H. Kachkachi, "Surface contribution to the anisotropy of magnetic nanoparticles", *Phys. Rev. Lett.*, vol. 90, no. 6, 2003, art. no. 065504.

104. G.F. Goya, T.S. Berquo, F.C. Fonseca, M.P. Morales, "Static and dynamic properties of spherical magnetite particle", *J. Appl. Phys.*, vol. 94, no. 5, 2003, pp. 3520-3528.

105. D. Hinzke and U. Nowak, "Simulation of magnetization switching in nanoparticle systems", *Phys. Stat. Sol. (a)*, vol. 189, no. 2, 2002, pp. 475-480.

106. O. Iglesias and A. Labarta, "Finite-size and surface effects in maghemite nanoparticles: Monte Carlo simulations", Phys. Rev. B, vol. 63, 2001, art. no. 184416.

107. R.H. Kodama, "Magnetic nanoparticles", *J. Magn. Magn. Mater.*, vol. 200, 1999, 359-372.

108. R.H. Kodama and A.E. Berkowitz, "Atomic-scale modeling of oxide nanoparticles", *Phys. Rev. B*, vol. 59, no. 9, 1999, pp. 6321-6336.

109. M. Respaud, J. M. Broto, H. Rakoto, A.R. Fert, L. Thomas, B. Barbara, M. Verelst, E. Snoeck, P. Lecante, A. Mosset, J. Osuna, T.O. Ely, C. Amiens, B. Chaudret, "Surface effects on the magnetic properties of ultrafine cobalt particles", *Phys. Rev. B*, vol. 57, no. 5, 2925-2935.

110. D.A. Dimitrov and G.M. Wysin "Magnetic properties of spherical fcc clusters with radial surface anisotropy", *Phys. Rev. B*, vol. 51, no. 17, 1995, pp. 11947-11950.

111. J.P. Chen, C.M. Sorensen, K.J. Klabunde, and G.C. Hadjipanayis, "Enhanced magnetization of nanoscale colloidal cobalt particles", *Phys. Rev. B*, vol. 51, no. 17, 1995, pp. 11527-11532.

112. A. Hahn, "Theory of the Heisenberg superparamagnet", *Phys. Rev. B*, vol. 1, no. 7, 1970, pp. 3133-3142.

113. W. Scholz, D. Suess, T. Schrefl, and J. Fidler, "Micromagnetic simulation of magnetization reversal in small particles with surface anisotropy", *J. Appl. Phys.*, vol. 95, no. 11, 2004, pp. 6807-6809.

LIST OF JOURNAL PUBLICATIONS

The following list contains the record of my journal articles that were published during my doctoral studies:

1. I. Mayergoyz, M. Dimian, G. Bertotti, and C. Serpico, "Inverse problem approach to precessional switching in perpendicular media," to appear in *J. Appl. Phys.*, May 2005.

2. M. Dimian and I. Mayergoyz, "Influence of surface anisotropy on magnetization precessional switching in nanoparticles," to appear in *J. Appl. Phys.*, May 2005.

3. I. Mayergoyz, M. Dimian, G. Bertotti, and C. Serpico, "Critical fields and pulse durations for precessional switching of perpendicular media," to appear in *J. Appl. Phys.*, May 2005.

4. M. Dimian and I. Mayergoyz, "Spectral density analysis of nonlinear hysteretic systems," *Phys. Rev. E* **70** (4), 046124 (2004).

    This article has been selected for the November, 2004 issue of Virtual Journal of Applications of Superconductivity.

5. M. Dimian and I. Mayergoyz, "Spectral noise density of the Preisach model," *IEEE Trans. in Magn.* **40** (4), 2134 (2004).

6. I. Mayergoyz, M. Dimian, G. Bertotti and C. Serpico, "Inverse problem approach to the design of magnetic field pulses for precessional switching," *J. Appl. Phys.* **95** (11), 7004 (2004).

7. P. Andrei, M. Dimian, C. Krafft, I. D. Mayergoyz, D. I. Mircea, and R. Rojas, "Anisotropy characterization of garnet films by using VSM measurements," *J. Appl. Phys.* **93** (10), 7065 (2003).

8. I. Mayergoyz, P. Andrei, and M. Dimian, "Nonlinear magnetostatic calculations based on fast multipole method," *IEEE Trans. Magn.* **39** (3), 1103 (2003).

9. I. Mayergoyz and M. Dimian, "Analysis of spectral noise density of hysteretic systems driven by stochastic processes," *J. Appl. Phys.* **93** (10), 6826 (2003).

10. G. Bertotti, I. Mayergoyz, C. Serpico, and M. Dimian, "Comparison of analytical solutions of Landau-Lifshitz equation for damping and precessional switching," *J. Appl. Phys.* **93** (10), 6811 (2003).

11. H. Kachkachi and M. Dimian, "Hysteretic properties of a magnetic particle with strong surface anisotropy," *Phys. Rev. B*, **66** (17), 174419 (2002).

12. M. Dimian and H. Kachkachi, "Effect of surface anisotropy on the hysteretic properties of a magnetic particle" *J. Appl. Phys.* **91** (10), 7625 (2002).